NUMERICAL STUDY OF MIXED CONVECTION HEAT TRANSFER IN A VENTILATED CAVITY UNDER ACTIVE FLOW CONTROL

By

Md. Nazmul Hasan

A Thesis Submitted in Partial Fulfillment of the Requirements for the Degree of

MASTER OF SCIENCE IN MECHANICAL ENGINEERING

Department of Mechanical Engineering

BANGLADESH UNIVERSITY OF ENGINEERING AND TECHNOLOGY

Dhaka-1000, Bangladesh

August, 2017

RECOMMENDATIONS OF THE BOARD OF EXAMINAERS

The thesis titled "**NUMERICAL STUDY OF MIXED CONVECTION HEAT TRANSFER IN A VENTILATED CAVITY UNDER ACTIVE FLOW CONTROL",** submitted by **Md. Nazmul Hasan,** Student no: 0411102055P, Session: April, 2011 has been accepted as satisfactory in partial fulfillment of the requirement for the degree of MASTER OF SCIENCE IN MECHANICAL ENGINEERING on August 17, 2017.

BOARD OF EXAMINERS

1 ----------

Dr. Mohammad Nasim Hasan — Chairman
Associate Professor
Department of Mechanical Engineering
Bangladesh University of Engineering and Technology (BUET)
Dhaka-1000, Bangladesh.

2 ----------

Dr. Mohammad Ali — Member (Ex-officio)
Professor and Head
Department of Mechanical Engineering
Bangladesh University of Engineering and Technology (BUET)
Dhaka-1000, Bangladesh.

3 ----------

Dr. A.K.M. Monjur Morshed — Member
Associate Professor
Department of Mechanical Engineering
Bangladesh University of Engineering and Technology (BUET)
Dhaka-1000, Bangladesh.

4 ----------

Dr. Md. Abdur Razzaq Akhanda — Member (External)
Pro-Vice Chancellor, Sonargaon University,
Ex-Dean, Faculty of Mechanical Engineering
Bangladesh University of Engineering and Technology (BUET)
Dhaka-1000, Bangladesh.

CANDIDATE'S DECLARATION

It is here by declared that this thesis or any part of it has not been submitted elsewhere for any degree or diploma.

Md. Nazmul Hasan

CERTIFICATE OF RESEARCH

This is to certify that the work presented in this thesis is carried out by the author under the supervision of Dr. Mohammad Nasim Hasan, Associate Professor of Department of Mechanical Engineering, Bangladesh University of Engineering and Technology (BUET), Dhaka.

Dr. Mohammad Nasim Hasan

Md. Nazmul Hasan

ACKNOWLEDGEMENT

First of all, thanks to the Almighty for helping me to successfully complete this thesis. I would like to express my deep gratitude to my supervisor, Dr. Mohammad Nasim Hasan, Associate professor, Department of Mechanical Engineering, Bangladesh University of Engineering and Technology for enabling me to study and for the generous amount of guidance and support he provided me throughout my research. I am indebted to him for giving me invaluable support, for showing incredible patience with me and encouraging me at every step of this dissertation, which would not have been possible without guidance and help of him. His dedication and hard work towards the research will be a constant source of inspiration for me.

I would like to thank the members of my thesis evaluation committee, Professor Dr. Md. Abdur Razzaq Akhanda, Professor Dr. Mohammad Ali and Associate Professor Dr. A.K.M. Monjur Morshed for their valuable comments and suggestions.

ABSTRACT

The present work is carried out to investigate mixed convection heat transfer characteristic within a ventilated square cavity having a rotating circular conducting solid cylinder. Forced convection flow conditions are imposed by providing an inlet at the bottom of the left wall and an outlet vent at the top of the other side wall. Mixed convection is attained by keeping the right wall at constant heat flux condition and all other wall's thermal conditions are considered to be adiabatic. The heat transfer characteristics and performance are analyzed at different speed ratios, different vertical positions and different diameter of the cylinder. Finite element method is adapted to carry out the numerical solution of the present problem. Effect of cylinder size, different peripheral speed ratio and location are explored for various values of Richardson numbers ($0.1 < Ri < 10$), for different Reynolds numbers ($10 \sim 500$) and for a fixed Prandtl number ($Pr = 0.7$). Results are presented in terms of Streamlines, Isotherm contours, Heatlines and normalized average Nusselt number. The results indicate that the flow field and heat transfer characteristic inside the cavity are strongly dependent on the Richardson numbers and the position, size and speed of the rotating cylinder. It is found that the presence of a rotating cylinder enhances the heat transfer rate for all values of Reynolds number Maximum heat transfer enhancement is achieved at $Ri = 0.1$and for $D/L=0.1$, $\xi=1.0$, $X_c = 0.8$, $Y_c = 0.25$ at the expense of about 7.85% increase of pumping work at $Re= 500$ which corresponds to about 26% more heat transfer than no cylinder case.

Table of Contents

LIST OF FIGURES

LIST OF TABLES

ABBREVIATIONS

FEM	Finite Element Method
FVM	Finite Volume Method
FDM	Finite Difference Method
CFD	Computational Fluid Dynamics
CPU	Central Processing Unit

SYMBOLS

x	distance along x coordinate	m
y	distance along y coordinate	m
X	non-dimensional distance along x coordinate	
Y	non-dimensional distance along y coordinate	
u	x component of velocity	ms^{-1}
v	y component of velocity	ms^{-1}
U	x component of dimensionless velocity	
V	y component of dimensionless velocity	
p	dimensional pressure of fluid	Pa
P	dimensionless pressure	
g	gravitational acceleration	ms^{-2}
k_s	thermal conductivity of solid cylinder	$Wm^{-1}k^{-1}$
k_f	thermal conductivity of basefluid (air)	$Wm^{-1}k^{-1}$
K	cylinder thermal conductivity ratio	
C_p	constant pressure specific heat	$J\ Kg^{-1}\ K^{-1}$
L	length of the square enclosure	m
D	dimensional diameter of the cylinder	m
D/L	non-dimensional diameter of the cylinder	
T	temperature	K
T_c	temperature of the cold wall	K
H	heatfunction	
q	constant heat flux	Wm^{-2}
h	heat transfer coefficient	$W/m^2\ K$
Pr	Prandtl number	
Gr	Grashof number	
Ra	Rayleigh number	
Re	Reynolds number	
Nu	Nusselt number	
Ri	Richardson number, $Ri = Gr/Re^2$	

x_c x – coordinate of the center of the cylinder

y_c y – coordinate of the center of the cylinder

X_c X – coordinate of the center of the cylinder

Y_c Y – coordinate of the center of the cylinder

GREEK LETTERS

α	thermal diffusivity	m^2s^{-1}
β	volume expansion coefficient	K^{-1}
Θ	non-dimensional temperature	
ρ	density	Kgm^{-3}
μ	dynamic viscosity	Pa.s
ν	kinematic viscosity	m^2s^{-1}
ψ	non-dimensional stream function	
ε	dimensionless length of heat source	
ω	dimensional angular rotating velocity	rad s^{-1}
Ω	non-dimensional rotational velocity	

SUBSCRIPTS

s	solid cylinder
f	base fluid
l	local value
avg	average value
o	value at the center at the cylinder
c	cold wall

Chapter 1: Introduction

An important branch of engineering science is to study of thermal engineering. Importance of this field of study is interdisciplinary in nature. Heat transfer and related physics have numerous applications in electrical and electronic engineering (heat dissipation from microchips, effective heat removal from the electrical components etc.), computer engineering (cooling requirement of the circuit boards, minimizing the size of the device without affecting its performance etc.), aeronautical engineering (heat transfer in rocket nozzle and thermal shield in re-entry vehicles etc.), chemical engineering (evolution of heat in different reactions) and civil engineering (heat transfer to and from a conditioned space etc.) [1]. Scientists and researchers have investigated many problems involving heat transfer phenomena. In many cases, these problems are dealt with convection heat transfer. Both fluid mechanics and heat transfer phenomena render significant importance to study convection heat transfer phenomena. In most of the cases, analytical solution of such problems is very difficult to obtain as the complexities arise from the irregular geometries and boundary conditions of the problems. To solve these problems, numerical method is one of the most appropriate and useful technique. Development of new algorithms and advancement in computer science have made easier to yield reliable numerical solutions to many complicated problems.

1.1. Convection Heat Transfer

Heat is the form of energy that is transferred between two bodies or zones and that the condition is that two bodies or zones must be remained at different temperatures. Heat is always transported from a higher temperature region to a lower temperature region. There are three basic mechanisms of heat transfer: conduction, convection and radiation. Conduction heat transfer is defined as the transfer of thermal energy from the more energetic particles of a medium to the adjacent less energetic ones. Conduction can take place in liquids and gases as well as solids provided that there is no bulk motion involved. A cold canned drink in a warm room, for example, eventually warms up to the room temperature as a result of heat transfer from the room to the drink through the aluminium can by conduction. Radiation is the energy emitted by matter

in the form of electromagnetic waves as a result of the changes in the electronic configurations of the atoms or molecules. Unlike conduction and convection, the transfer of heat by radiation does not require the presence of an intervening medium. In fact, heat transfer by radiation is fastest (at the speed of light) and it suffers no attenuation in a vacuum. A familiar instance of thermal radiation is the transfer or heat from the sun to the earth.

Convection is the process of transferring heat and mass by the movement of molecules within fluids (e.g. liquids, gases) as a combination of two distinct mechanisms namely diffusion and advection. Convection heat transfer is complicated by the fact that it involves fluid motion as well as heat conduction. The fluid motion enhances heat transfer, since it brings warmer and cooler chunks of fluid into contact, initiating higher rates of conduction at a greater number of sites in a fluid. Therefore, the rate of heat transfer is higher by convection than it is by conduction. In fact, the higher the fluid velocity, the higher the heat transfer [2]. Generally, in fluid mechanics, convection means the motion of fluid regardless of cause [3]. In thermodynamics, convection always refers to only heat transfer [4]. At the interface between a solid surface and a fluid medium, the near wall fluid assumes the velocity of the surface with respect to fluid. This condition is termed as the no-slip condition. As a result, a velocity or hydrodynamic boundary layer is formed at the solid-fluid interface. Actually, convection mode of heat transfer is initiated by diffusion. After being energized, hot fluid molecules just near the heated solid surface keep vibrating and diffuse heat at microscopic level through diffusion. From this layer, energy is transported to the bulk fluid through advection. Although convection is often discussed as a distinct method of heat transfer, it involves the combined processes of conduction and advection [5]. So, it can be stated that convection is possible only in those media where both diffusion and advection are possible.

Convection heat transfer can be classified depending on different flow regimes, as laminar and turbulent flow. The highly ordered fluid motion characterized by smooth layers of fluid is termed as laminar flow. Laminar flow is layered and there is no interchange of particles between adjacent layers. The flow of high viscosity fluids such as oils at low velocities is typically laminar. The highly disordered fluid motion that typically occurs at high velocities and is characterized by velocity fluctuations is called turbulent flow. The flow of low viscosity fluids such as air at high velocities is typically turbulent. A flow that alternates between being laminar

and turbulent is called transitional flow [2]. Again, convective heat transfer can be classified as steady or unsteady depending on the time dependent properties of the fluid flow. The term steady implies that no change at a point with time. Unsteady flow is just the opposite of the steady flow with parameters being changed with time at any point in space. Also a flow is classified as being compressible and incompressible, depending on the level of variation of density during flow. A flow is said to be incompressible if the density remains nearly constant throughout. Gas flows can often be approximated as incompressible flow if the density changes are under about 5 percent, which is usually the case when Mach number, Ma < 0.3.

So, it can be concluded that convection heat transfer can be divided into three main categories on the basis of mechanism of sensible heat transfer as follows:

- Natural or free convection
- Forced convection
- Mixed convection or combined natural and forced convection

1.1.1. Natural Convection

Natural convection is a mechanism or type of heat transport, in which the fluid motion is not generated by any external source (e.g. fan, pump, suction device etc.) but only by density differences in the fluid occurring due to temperature gradients. Natural convection is initiated when the cold fluid comes in contact with the heated solid surface and when extraction of heat occurs. As a result, temperature of the moving fluid is increased and the volume also increases. The cold fluid has relatively higher density than the hot fluid. The lighter (hotter) portion of the fluid is acted upon by the buoyancy force generated as the density is low compared to the surroundings and rises upwards. As a result a void is created and that void is needed to be filled up. To fill the void, the currents of cold stream are generated. Thus the cold fluid sinks and the hot fluid gets to the top due to the buoyancy. Thus the hotter volume transfers heat towards the cooler volume of that fluid [6]. In a gravitational field, there is a net force that pushes upward a light fluid placed in a heavier fluid. The upward force exerted by a fluid on a body completely or partially immersed in it is called the buoyancy force. The magnitude of the buoyancy force is equal to the weight of the fluid displaced by the body. Natural convection occurs only if the buoyancy force is present. Convection under other types of the body forces such as force due to

magnetic field is also considered as natural convection as long as there is no provision to create an artificial pressure gradient by any external means (fans, blowers etc.).

1.1.2. Forced Convection

Forced convection is a mechanism in which bulk fluid motion is generated by an external source (e.g. pump, fan, suction device etc.) and the effect of natural force is negligible compared to the induced force. Forced convection can be classified on the basis of nature of flow into external and internal forced convection. When flow of an unbound fluid occurs over a heated surface such as a plate, a wire or a pipe, external forced convection takes place. Internal forced convection occurs when the flow of fluid during heat transfer is completely bounded by solid surfaces. Heat transfer inside pipe flow can be termed as internal forced convection. In forced convection high heat transfer rate can be achieved and this type of convection process is applied when high heat transfer rate is needed as extreme fluid mixing is involved in this process. Forced convection can take place as a byproduct of other process even when the objective is not to create forced convection, such as, the action of propeller in fluid or aerodynamic heating. Forced convection can also occur due to natural means, such as, expansion of bulk air due to fire or heat and the movement of bulk air due to this. Forced convection is often encountered by engineers designing or analyzing heat exchangers, pipe flow and flow over a plate at a different temperature than the stream.

1.1.3. Mixed Convection

Mixed convection is a combination of forced and free convections which is the general case of convection when a flow is determined simultaneously by both an outer forcing system (such as, outer energy supply to the fluid streamlined body system) and inner volumetric (mass) forces by the non-uniform density distribution of a fluid medium in a gravity field. Mixed convection can be found in much smaller scales system [7]. To study mixed convection, the involvement of wide range of variables is needed. For this reason, a comprehensive relation between variables is hard to obtain and if obtained, they are found under some limiting case of the problem [8]. In some cases of forced convection, however the effects of buoyancy forces are significant. Such convective heat transport is known as mixed convection heat transfer. Typical example of mixed convection heat transfer is heat transfer in a conditioned room of modern building. Air inventory

of each such room is replenished continuously or intermittently by a central air-conditioning system or by ventilation air. Hence at the vicinity of heated walls or windows, the room air is actually in motion. Now due to the heat given up by the heated walls or windows, air near those walls or windows floats upwards. Rate of heat transfer largely depends on relative dominance of flow regime.

1.2. Classification of Mixed Convection

Natural convection may help or hurt forced convection heat transfer, depending on the relative directions of buoyancy-induced and the forced convection motions. Mixed convection is primarily classified into three categories. These types of convection are termed as aiding flow, opposing flow and transverse flow mixed convection.

1.2.1. Aiding Mixed Convection

When the forced flow is such that it acts in the same direction as the buoyancy induced flow, the mechanism of heat transfer is termed as aiding flow mixed convection. In this case natural convection aids the effect of forced convection and thereby enhancing the total heat transfer. For example, Fan blowing upward on a hot plate falls under the aiding mixed convection.

1.2.2. Opposing Mixed Convection

If the forced and the buoyant flows act against each other, it is then identified as opposing flow mixed convection. This type of flow is observed when a fan is forcing air upward over a cold plate [2]. In this case, the cold air naturally falls due to the buoyancy force, but the air, being forced upward due to the force induced by the fan opposes this natural motion which keeps the cold air circulating around the cold plate. Thus heat transfer is hindered due to the two effects.

1.2.3. Transverse Mixed Convection

Another type of mixed convection is transverse mixed convection. In transverse mixed convection, the natural force action on the bulk fluid is perpendicular to the induced force on the same field. This increases the chance of fluid mixing and thereby enhances the heat transfer. This flow can be visualized when air is flowing horizontally over a hot or cold pipe. In transverse

mixed convection, phase change of fluid is encouraged which in turn increases heat transfer coefficient.

1.3. Mixed Convection in Cavity

Mixed convection can also be classified as internal flow and external flow. When a fluid is surrounded by a solid boundary, the flow can be termed as the internal flow. An example of internal flow is liquid flowing through a pipe. On the contrary, external flow is observed when a fluid is open to its surroundings and extends indefinitely without colliding a solid boundary. Now-a-days many investigations have been made on mixed convection in cavity both experimentally and numerically. In many cases, excellent and satisfactory agreement is obtained between the two results.

1.3.1. Closed Cavity Problems

When a system is comprised in such a way that it is closed and no mass transfer occurs from or to the cavity, and then these problems are termed as closed cavity problems. A conveyor belt removing heat from an enclosed area can be an effective practical application of closed cavity problems.

1.3.2. Open Cavity Problems

When the system remains open and the mass transfer occurs from or to the cavity, then these problems are termed as open cavity problems. So, these problems are just the opposite of closed cavity problems. In these problems, source of forced flow is external flow from inlet to outlet of an enclosure.

1.4. Heat Transfer Enhancement by Active Flow Control

"Active Flow Control" typically refers to the use of time-dependent (often periodic) disturbances that are introduced into the flow field by so-called "actuators". Examples for which active flow control proved to be most promising are control of separation, mixing, combustion etc. It is a special case where the heat is transferred in a controlled way. This can be achieved by controlling the flow and direction of fluid using external power. So, a control loop is required.

Active Flow Control is becoming more and more a viable tool for modifying flows for many practical applications

1.5. Heat Transfer Enhancement by Passive Flow Control

Passive control always involves geometrical modifications, such as vortex generators. This system requires no auxiliary power and such there is no control loop. Heat transfer can be enhanced by modifying the geometry in a positive manner that influences the fluid flow and thermal field.

1.6. Objectives

The present thesis has a goal to explore mixed convection heat transfer phenomena in a vented square enclosure in presence of a rotating circular cylinder. Thermally driven flow is encountered in numerous applications especially in some building service situations, when a pipe carrying a hot water passes through an enclosure formed by structural components of the building, rotating tube heat exchangers, drilling of oil wells etc. Relatively few works are done on investigation on rotating cylinder and isoflux heater about which particulars are described in Chapter 2 (Literature Review). In this case, basically non-dimensional rotational velocity of the cylinder has been taken into consideration mostly. Also, different non-dimensional vertical position of the rotating cylinder and non-dimensional cylinder diameter. Key objectives of the present work are mentioned below in the following points:

- To develop a generalized mathematical model for mixed convection in a vented square enclosure in presence of a rotating circular cylinder and discrete isoflux heater
- To derive the non-dimensional governing equations for the mathematical model and to co-relate the boundary conditions with the problem
- To solve the governing equations and boundary conditions using Finite Element Method
- To carry out the validation of the simulation algorithm by generating a previous research and comparing it with the original one and perform grid sensitivity test
- To study the effect of non- dimensional diameter and location of the cylinder on isotherm lines, streamlines and heatlines.

- To study the effect of speed ratio of the cylinder on isotherm lines, streamlines and heatlines.
- To study the normalized heat transfer performance (heat transfer rate) for different non-dimensional rotational speeds, diameter and location of the cylinder for different Richardson number and Reynolds number.
- To identify the optimum size, location and speed of the rotating cylinder for heat transfer enhancement inside the ventilated cavity for wide range of system governing parameters.

At present, technological improvement has been occurring rapidly and so increases the necessity of heat transfer. Different problems are investigated in order to secure a qualitative and quantitative understanding of free, forced and mixed convection flows in channels, duct and cavities having current engineering application. A survey on previous studies is presented in the Chapter 2. In this study, the aim is to numerically analyze the mixed convection flow and heat transfer characteristics in a ventilated square cavity with active flow control via a rotary heat conducting horizontal solid circular cylinder placed inside the cavity

Chapter 2: Literature Review

The improvement of device performance such as electronic component cooling systems, compact heat exchangers, solar energy systems, biomedical devices etc. is of great interest to researchers and is intensively studied recently. Indeed, the tendency for more compactness, economy in manufacturing and operating costs and energy consumptions, has become the major factor in the design of the above mentioned systems. To avoid temperature rises, which induce over heating of components that can be detrimental to electronic devices, better cooling allowing maximum heat dissipation is necessary. Therefore, in recent years many studies have been performed for the enhancement of heat transfer especially convective heat transfer in channel or cavities with obstacles, partitions and fins. But analytical solution of this problem is very difficult to obtain as the complexities arise from geometries and boundary conditions of the problems. Numerical method is the most useful technique to solve the problem. Therefore, now-a-days researchers analyzed heat transfer problem numerically.

2.1. Study of Natural convection Heat Transfer

Kim and Lee [9] studied natural convection numerically in a square enclosure with a circular cylinder at different vertical locations varying Rayleigh number in the range of 10^3-10^4. From this study the findings are, for all *Ra*, the flow and thermal fields eventually reach the steady state with the symmetric shape about the vertical center line through the center of the inner circular cylinder. It is also found that at high *Ra*, the effect of the inner cylinder position on heat transfer and fluid flow phenomena is significant.

Aminossadati and Ghasemi [10] focused on natural convection cooling considering a localized heat source at the bottom portion of a nanofluid-filled square enclosure. Several important concluding remarks are presented in his study. The increase of Rayleigh number strengthens the natural convection flows which results in the reduction of heat source temperature. It is also found out that the increase of heat source length increases the heat transfer to the nanofluid and therefore increases the surface temperature of the heat source and the strength of natural

convection circulating cells within the enclosure. Roslan *et al.* [11] considered a sinusoidally heated cylindrical source. His analysis concludes that, the cylinder temperature oscillation can drastically change the flow and temperature fields and also two inner vortices are found in the flow field and a warm chamber exists in the temperature field due to the effect of heated cylinder temperature oscillation. Heat transfer tends to increase by oscillating the source temperature signal.

Basak *et al.* [12] also studied natural convection in a square cavity filled with a porous medium and analyzed the effects of various boundary conditions. The study was adopted in a wide range of parameters $10^3 \leqslant Ra \leqslant 10^6$, Darcy number Da, $10^{-5} \leqslant Da \leqslant 10^{-3}$, $0.71 \leqslant Pr \leqslant 10$ with respect to continuous and discontinuous thermal boundary conditions. The results show that, non-uniform heating of the bottom wall produces greater heat transfer rate at the center of the bottom wall than uniform heating case for all *Ra* but average Nusselt number shows overall lower heat transfer rate for non-uniform heating case. As our main focus is on mixed convection, we mainly focused on mixed convection related recent works. Basak *et al.* [13] extended his research into mixed convection and made an analysis in the range of *Re* (1 - 100), *Gr* (10^3 - 10^5), *Pr* (0.015 - 10). The results indicated that, the effect of lid-driven flow is dominant for $Gr = 10^3$ and as the value of *Gr* increased, both the primary and secondary circulations appeared inside the cavity.

2.2. Study of Mixed Convection Heat Transfer inside a closed cavity

Studies of mixed convection heat transfer have been given special attention since the end of last century due to its ever increasing application in modern science and technology. Due to its vast application field in chemical processing technology, electronics cooling technology, glass and ceramic industries, solar thermal technology, space heating, food processing industries, mixed convection is becoming one of the key topics of research in the field of heat transfer now-a-days. Many researchers have investigated mixed convection related problems and the findings are quite significant in all cases and the effects of various parameters are also explained properly.

Oztop and Dagtekin [14] investigated mixed convection in two-sided lid-driven differentially heated square cavity. They found that, for $Ri > 1$, the average Nusselt number is relatively low

although the heat transfer is enhanced for the case of opposing buoyancy and shear forces and for *Ri* = 10. Moallemi and Jang [15] investigated the effects of Prandtl number on laminar mixed convection in lid driven cavity varying *Pr* in the range of 0.01-50 and *Re* in the range of 100-2200. The results of his research are stated as that, buoyancy effect and heat transfer in the cavity are greater for higher values of *Pr*, if *Re* and *Gr* are kept constant. It was also found that aiding natural convection effects were a function of both *Pr* and *Ri*. Aydin and Yang [16] also carried out an investigation numerically on mixed convection heat transfer in a two-dimensional square cavity having an aspect ratio of 1. In their configuration the isothermal sidewalls of the cavity were moving downwards with uniform velocity while the top wall was adiabatic. A symmetric isothermal heat source was placed at the otherwise adiabatic bottom wall. The effects of Richardson number and the length of the heat source on the fluid flow and heat transfer phenomena were investigated on their work. Guo and Sharif [17] also studied mixed convection numerically in rectangular cavities at various aspect ratios with moving isothermal sidewalls but in this case constant heat flux source was present on the bottom wall. The results indicate that the resulting flow consists of two counter-rotating vortices. As far as the temperature field is concerned, at low values of *Ri,* when forced convection is the dominant mechanism of heat transfer, the temperature is found to be more evenly distributed within the enclosure, and a relatively large region of the enclosure is affected by the heat source. As *Ri* increases and natural convection prevails, the temperature variation is restricted over a gradually diminishing region around the heat source. Billah *et al.*[18] studied mixed convection heat transfer enhancement of a heated circular hollow cylinder in a lid- driven rectangular enclosure or cavity. They revealed that the position of the circular heated hollow cylinder can be used as a control parameter for heat transfer, fluid flow and temperature distribution i.e. heat transfer and fluid flow are strongly affected by the location of the hollow cylinder.

2.2.1. Mixed Convection Heat Transfer inside a Vented Cavity

Bahlaoui *et al.*[19] studied the enhancement of heat transfer by using water based Al_2O_3 nano fluids in a vented vertical cavity heated from one side. They showed that the increase of volume fraction of nanoparticlescontributestoanenhancementofheattransfer.Theyalsorevealed that the heat transfer enhancement, using nanofluids, is more pronounced at shallow enclosures than at tall ones. Saedobin *et al.* [20] numerically investigated the mixed convection fluid flow and heat

transfer characteristics in an inclined ventilated square cavity containing two heated blocks which is subjected to an external Al_2O_3 - water nanofluid. They observed that at all values of Reynolds and Richardson numbers as well as all the aspect ratios, adding nanoparticles to the fluid causes temperature gradient to decrease, conduction heattransfer to increase and amount of heat transfer to considerably increase. Mehrizi *et al.*[21] used the lattice Boltzmann method to investigate the effect of suspension of nanoparticles on mixed convection in a square cavity with inlet and outlet ports and hot obstacle in the center of the cavity. Esfe *et al.*[22] analyzed the problem of mixed convection flow and heat transfer in a ventilated inclined cavity containing hot obstacles subjected to a nanofluid. They observed that for using obstacles and adding nanoparticles to the base fluid or increasing the volume fraction of the nano particles causes the Nusselt Number to increase. They also observed that heat transfer increases when Reynolds number increases. Saha *et al.*[23] studied the performance of mixed convection in a rectangular ventilated enclosure for different placement configurations of the inlet and outlet openings for a wide range of Richardson numbers, $0 < Ri < 10$. Raji *et al.*[24] studied similar type of problem. They studied a mixed convection flow in a ventilated cavity, heated from its vertical left wall with a constant heat flux and thermally insulated from its remaining boundaries. Mamun *et al.*[25] conducted numerical study on the effect of a heated hollow cylinder on mixed convection in a ventilated cavity. Heat transfer and air flow of a turbulent mixed convection in a ventilated cavity was analyzed and compared the results with experimental values by Hinojosa *et al.* [26]. The results show that the increasing of Rayleigh number significantly affects the temperature of the hot wall, butthevaluesofthetemperatureatthecenterofthecavityandtheregionnear isothermal wall maintain constant. It also revealed both the experimental and numerical results that the thickness of the boundary layers near the heated and isothermal walls is between 0.01m to 0.03m. Doghmi *et al.*[27] analyzed heat transfer characteristics in a three dimensional ventilated cavity whose side walls are kept at differentially heated condition. The results are presented in terms of streamlines, temperature distribution and average Nusselt number for two configurations (Cold to Hot and Hot to Cold).The obtained results show that injecting air through the cold wall is more effective in heat removal (Cold to Hot configuration),compared to the case of where the inlet opening is placed on the heated wall. This is due to the impinging effect of the cold air jet on the opposite hot wall. Chamkha *et al* .[28] studied mixed convection heat transfer characteristics of a vented cavity with a heated horizontal square cylinder. They

showed that the effects of the location of the inner square cylinder and the aspect ratio are found to play significant roles in the streamline and isotherm contour patterns. The average Nusselt number along the left cold wall of the square cavity increases almost linearly with Richardson number.

2.2.2. Mixed Convection Heat Transfer inside a Cavity using a rotating Cylinder

Elghnam *et al.* [29] performed both experimental and numerical investigation of heat transfer from a heated horizontal cylinder rotating in still air around its axis. They found that for a rotating cylinder, the difference between maximum and minimum values of the local Nusselt number decreases with increase of Reynolds number. For high values of Reynolds number, this difference tends to vanish and local *Nu* number distribution on cylinder circumference becomes uniform. Another noticeable finding from his research is that, for *Re* above 8000, the heat transfer rates were independent of the Grashof number and the dependence of Nusselt number on Grashof number decreases as the value of *Re* increases and for higher value of *Re* this dependence vanishes. Alam *et al.* [30] reported that, the presence of a rotating cylinder significantly affect the heat transfer characteristics of a heat source placed in a differentially heated cavity. The results indicate that the flow field, temperature distribution and heat transfer rate are dependent on rotating speeds and cylinder size. But the effect of conductivity ratio is not so prominent. Karimi *et al.* [30] studied the steady-state mixed convection around two heated horizontal cylinders in a square two-dimensional enclosure where the cylinders are located at the middle of the enclosure height and the walls of the cavity are adiabatic. The effects of cylinder diameter, Reynolds number, and Richardson number on the heat transfer characteristics are numerically analyzed. The results showed that both heat transfer rates from the heated cylinders and the dimensionless fluid temperature in the enclosure increased with increasing Richardson number and cylinder diameter. The average Nusselt number and non-dimensional temperature variation was completely opposite when Reynolds number increased. They also showed that increasing diameter of the cylinders and Richardson number, the left cylinder is less affected by the inlet flow than right one. Karimi *et al.*[31] studied the steady-state mixed convection around two heated horizontal cylinders in a square two-dimensional enclosure where the cylinders are located at the middle of the enclosure height and the walls of the cavity are adiabatic. The effects

of cylinder diameter, Reynolds number, and Richardson number on the heat transfer characteristics are numerically analyzed. The results show that both heat transfer rates from the heated cylinders and the dimensionless fluid temperature in the enclosure increase with increasing Richardson number and cylinder diameter. The average Nusselt number and non-dimensional temperature variation is completely opposite when Reynolds number increases. It also showed that increasing diameter of the cylinders and Richardson number, the left cylinder is less affected by the inlet flow than the right one. Selimefendigil *et al.* [32] studied mixed convection of ferrofluid flow in a lid driven cavity in the presence of two rotating cylinders with a magnetic dipole source. The results of this investigation revealed that cylinder angular velocities, ratio of the angular velocities and diameter ratios have profound effect on heat transfer enhancement within the cavity.

2.3. Motivation of the Present Study

Mixed convection heat transfer at steady state from a rotating cylinder to its surrounding enclosure is a subject of practical importance. In recent years, the flow around a rotating circular cylinder is considered a fundamental fluid mechanics problem of great interest. The analysis of flow pattern of isotherm lines and streamlines along with the heat transfer characteristics of different physics in today's engineering research works. Mixed convection heat transfer has a very promising sector in chemical vapor deposition and nuclear reactor technology. This thesis can definitely contribute to the further advancement of mixed convection as there are different types of discrete heaters like flat type heater, protrude type heater and slot type heater with iso-flux heat sources. The variation of heaters can help us a lot to know the best suited combination for an application.

Many investigations have been performed in the mixed convection heat transfer. Such as, Costa and Raimundo [33] studied mixed convection in a differentially heated square enclosure with an active rotating cylinder. Their configuration was a two-dimensional square enclosure with a fixed width and height and the cylinder was placed in the center of the enclosure. In his work, both the upper and lower horizontal walls were assumed perfectly insulated, left and right walls indicated isothermal hot and cold temperature respectively. Their study summarizes that, size of the cylinder has a strong influence on the resulting flow and heat transfer process and for high absolute values of the rotating velocity of the cylinder, the overall Nusselt number is strongly

dependent on the rotating velocity and only marginally related with the thermal conductivity and thermal capacity of the cylinder. It has been concluded that, cylinder rotation is benefic for the overall Nusselt number when enclosure geometrical aspect ratio is high and it is prejudicial when this parameter is small. Gupta *et al.* [34] analyzed mixed convection heat transfer inside a ventilated cavity with a stationary cylinder at the center of the cavity. They concluded that the flow and thermal fields are strongly influenced by the cylinder size inside the cavity. There also concluded that there is insignificant effect of thermal conductivity ratio on the flow field for purely forced convective case; however, for mixed convective cases the effects on both the flow and thermal fields are significant. The thermal conditions on the cavity walls are also having significant influences on the thermo-hydrodynamic feature and also showed that with increasing cylinder diameter, the heat transfer rate from the heated cavity wall increases for lower *Ri* and decreases for higher *Ri* for both cases; with increase in solid–fluid thermal conductivity ratio, the average Nusselt number on the hot plate reduces; however, the bulk fluid temperature is observed to increase for both cases. Hussain *et al.* [35] also carried out an investigation on mixed convection heat transfer in a differentially heated square enclosure with a conductive rotating circular cylinder but in this case, he took into consideration the effect of different vertical locations. The boundary conditions are exactly same as the Costa and Raimundo [33] but the different non-dimensional parameters are used and in this case the cylinder is moved vertically up and down. In this case, they also did not consider the presence of discrete isoflux heater. The conclusions drawn from his research work is that, when the Richardson number is small, major rotating vortices can be noticed around the rotating circular cylinder which is almost identical at $\boldsymbol{\delta} = 0$ and when the Richardson number is unity, no clear changes can be observed in the flow and thermal fields with the rotating circular cylinder locations. Further increases in the Richardson number causes the flow and thermal fields to be greatly affected. When *Re* increases the circulation of flow vortices increases dramatically and becomes stronger, which leads to make the forced convection effect more dominant for different values of *Ri* and $\boldsymbol{\delta}$. Similar type of work is conducted by Liao and Lin [36] considering the rotating cylinder as isothermal hot object. He found that, for $Ra = 10^4$, the conduction dominates the heat transfer within the enclosure and the variation of average Nusselt number for different *Ri* is small and for $Ra = 10^5$ and 10^6, average Nusselt number decreases in tandem with the decrease of *Ri*. All the researches mentioned above in this section do not consider the use of isoflux heater. Ghaddar and Thiele

[37] presented results of a constant heat flux rotating cylinder within an isothermal rectangular enclosure using spectral element method. The rotation was found to increase the heat transfer at low *Ra*, and on the contrary, noticeable decrease of the heat transfer was observed at high *Ra*.

Many researchers have performed many works on mixed convection heat transfer phenomena but very little attention has been paid to the problem of mixed convection in a vented square enclosure having a rotating cylinder and discrete isoflux heater together. It becomes a matter of great interest to study all the conditions such as, adiabatic surface, isoflux heater, effect of rotating cylinder and isothermal air inflow simultaneously and the objectives of this thesis are listed at the end of the previous chapter. Findings of this thesis can be of great help to reach the goal of producing more compact equipment in future and hopefully it will find its numerous applications.

Chapter 3: Mathematical Modeling

3.1. Physical Model

The goal of this section is to represent the physical model of the considered problem. The configuration of the two-dimensional square enclosure, of width L and height H (H/L = 1), with a rotating cylinder (diameter, d) placed inside the enclosure and with an inlet and an outlet in the left and right wall respectively, is sketched in Figure 3.1. The length of the inlet and outlet is $0.1L$ situated at (0, 0) and (1, 0.9) positions respectively. A discrete isoflux heater is placed at the right wall of the enclosure and the left wall is assumed to be adiabatic. Also the upper horizontal wall and the bottom horizontal wall of the enclosure are kept at perfectly insulated condition that means from this wall the net heat transfer is zero.

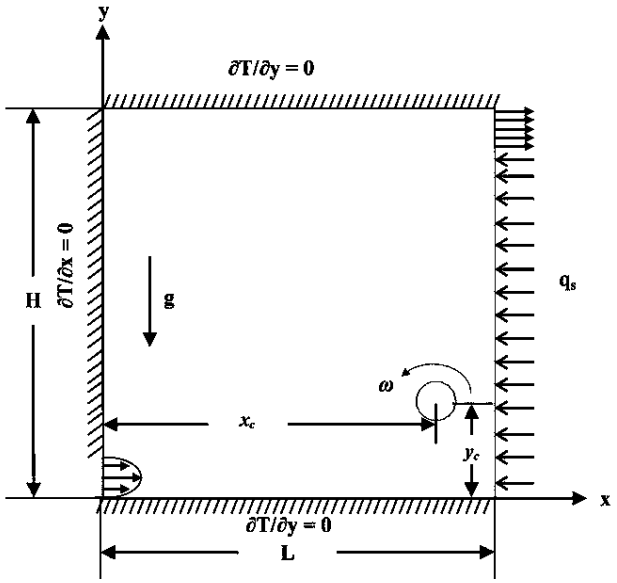

Figure 3.1: Schematic view of the dimensional physical model

At first the rotating cylinder is placed with its center at $x_c = 0.85L$ and $y_c = 0.25L$ and then it is moved vertically upwards or downwards direction. The rotating cylinder denotes the continuity condition that means the heat transfer medium is only conduction through the cylinder. Under the influence of the vertical gravitational field, the right wall thermal condition lead to a natural

convection problem. No-slip boundary condition exists for velocity on the surface of the square enclosure. The circular cylinder with a definite radius and thermal conductivity rotates with a fixed angular velocity in the counterclockwise (CCW) direction thus inducing a forced flow and thus overall the resulting problem becomes a mixed convection problem. The fluid entering the cavity through the inlet is assumed to be a Newton-Fourier fluid. Air is considered as the fluid flowing inside the enclosure with the fixed Pr = 0.7. In this work, rotational speeds of the cylinder are varied by varying the speed ratio (ξ = 0.0, 0.5, 1 and 2) of the cylinder Later different heat transfer and fluid flow phenomena are investigated by changing the diameter (d = 0.1L, 0.15L and 0.2L) and vertical position (y_c = 0.25L, 0.45L and 0.65L) of the cylinder.

3.2. Assumptions

Some assumptions have been made in our present work to simplify the modeling of the current problem. The assumptions are given below:

- The change of velocity component with flow has been assumed to be negligible that means it is a steady state problem.
- Heat and fluid flow has been assumed to be two dimensional.
- Thermal radiation heat radiation between the walls is negligible and the fluid is considered to be radiatively non-participating.
- Fluid is isotropic and fluid flow is assumed to be laminar flow.
- Density of fluid is not affected by pressure changes so that it can be staled as incompressible fluid.
- Density on the buoyancy term is temperature dependent and the Boussinesq approximation is used.
- No slip is condition for the outer surface of the square enclosure.

3.2.1. Boussinesq Approximation

In fluid dynamics, the boussincsq approximation is used in the field of buoyancy driven flow which is also known as natural convection. It ignores density differences except where they appear in terms g, the acceleration due to gravity. Actually the main theme of this approximation

is that the difference in inertia is negligible but gravity is sufficiently strong to make the specific weight appreciably different between the two fluids. Boussiaesq flows are common in nature (such as atmospheric fronts, oceanic circulation), industry (dense gas dispersion, fume cupboard ventilation), and the built environment (natural ventilation, central heating). This approximation is extremely accurate for many such flows and makes the physics simpler.

According to this approximation, the density difference between the inside and outside of the boundary layer that gives rise to buoyancy force and sustains flow. This approximation is useful when density *PI* and *Pl* need to be considered as a single density ρ and the difference ($\rho_1 - \rho_2$) is negligible. By performing dimensional analysis, it has been derived that the only way that acceleration due to gravity *g* should be used into the equations is in the reduced gravity *g'* where,

$$g' = \frac{\rho_1 - \rho_2}{\rho} \tag{3.1}$$

3.3. Dimensional Governing Equations

The two-dimensional steady state continuity, momentum and energy equations are considered to model tbe present problem for flow and thermal fields. From the above staled assumptions, the dimensional governing equations take the form as below:

For the square cavity the dimensional governing equations arc,

Continuity equation:

$$\frac{\partial u}{\partial x} + \frac{\partial v}{\partial y} = 0 \tag{3.2}$$

x–momentum equation:

$$\frac{\partial (uu)}{\partial x} + \frac{\partial (uv)}{\partial y} = -\frac{1}{\rho}\frac{\partial p}{\partial x} + \nu\left(\frac{\partial^2 u}{\partial x^2} + \frac{\partial^2 u}{\partial y^2}\right) \tag{3.3}$$

y–momentum equation:

$$\frac{\partial (uv)}{\partial x} + \frac{\partial (vv)}{\partial y} = -\frac{1}{\rho}\frac{\partial p}{\partial y} + \nu\left(\frac{\partial^2 v}{\partial x^2} + \frac{\partial^2 v}{\partial y^2}\right) + g\beta\left(T - T_c\right) \tag{3.4}$$

Energy equation:

$$\frac{\partial(uT)}{\partial x}+\frac{\partial(vT)}{\partial y}=\alpha\left(\frac{\partial^2 T}{\partial x^2}+\frac{\partial^2 T}{\partial y^2}\right). \tag{3.5}$$

For heat conducting rotating cylinder the energy equation is,

$$\left(\frac{\partial^2 T}{\partial x^2}+\frac{\partial^2 T}{\partial y^2}\right)=0 \tag{3.6}$$

Where x and y are the coordinates varying along the horizontal and vertical directions, respectively, u and v are the velocity components in the x and y directions, respectively, T is the dimensional temperature and p is the dimensional pressure.

3.4. Dimensional Boundary Conditions

The dimensional boundary conditions for both square enclosure and rotating cylinder are stated below,

At all solid boundaries of the square enclosure:

$$u=v=0 \tag{3.7}$$

And over the rotating cylinder velocity components are specified as:

$$u_c=-\omega(y-y_c);v_c=-\omega(x-x_c) \tag{3.8}$$

Where x_c and y_c denote the dimensional Cartesian coordinates at the center of the cylinder.

At any point of the cylinder, the absolute velocity can be expressed as,

$$\left|v_p\right|=\sqrt{\left(u_c{}^2+v_c{}^2\right)}=\sqrt{\left\{\omega^2\left(x-x_c\right)^2+\omega^2\left(y-y_c\right)^2\right\}}=\left|\omega\right|r \tag{3.9}$$

At the inlet a parabolic velocity inflow condition exists which is expressed as,

$$u=\frac{u_{\max}}{u_{mean}}=60y-600y^2 \tag{3.10}$$

Where, u_{max} is the maximum velocity of the parabolic velocity profile and u_{mean} is the mean velocity of the velocity profile.

At the outlet boundary, normal shear stress is assumed to be zero.

For rotating cylinder, the condition is continuity equation and for the square enclosure the conditions are specified such as:

Top wall, bottom wall and part of the left wall which is maintained at adiabatic condition:

For top wall and bottom wall: $\frac{\partial T}{\partial y} = 0$

For the left wall: $\frac{\partial T}{\partial x} = 0$

Heated right wall section: $-k_f \frac{\partial T}{\partial x} = q_s$

Where, k_f is the thermal conductivity of the fluid and q_s is the constant heat flux at the heater.

3.5. Dimensional Analysis

To solve the problem numerically, all the parameters arc non-dimensionalizcd. Dimensional analysis helps to qualitatively relate the beat transfer coefficient with fewer dimensional variables that are required to describe the above mentioned mixed convection problem, Actually all the equations and boundary conditions are non-dimensionalized by dividing all independent and dependent variables by relevant and meaningful constant quantities, The non-dimensional parameters are given below:

$$x = \frac{X}{L}; y = \frac{Y}{L}; u = \frac{U}{U_{ref}}; v = \frac{V}{U_{ref}}; p = \frac{P}{\rho_f U_{ref}^2}; \Theta = \frac{T - T_c}{\Delta T}; U_{ref} = u_{mean} \qquad (3.11)$$

3.6. Non-dimensional Governing Equations

After dimensional analysis, the non-dimensional equations are as follows:
For the square cavity:

Continuity equation:

$$\frac{\partial U}{\partial X}+\frac{\partial V}{\partial Y}=0 \tag{3.12}$$

X–momentum equation:

$$\frac{\partial (UU)}{\partial X}+\frac{\partial (UV)}{\partial Y}=-\frac{1}{\rho}\frac{\partial P}{\partial X}+\frac{1}{\mathrm{Re}}\left(\frac{\partial^2 U}{\partial X^2}+\frac{\partial^2 U}{\partial Y^2}\right) \tag{3.13}$$

Y–momentum equation:

$$\frac{\partial (UV)}{\partial X}+\frac{\partial (VV)}{\partial Y}=-\frac{1}{\rho}\frac{\partial P}{\partial Y}+\frac{1}{\mathrm{Re}}\left(\frac{\partial^2 V}{\partial X^2}+\frac{\partial^2 V}{\partial Y^2}\right)+Ri\Theta \tag{3.14}$$

Energy equation:

$$\frac{\partial (U\Theta)}{\partial X}+\frac{\partial (V\Theta)}{\partial Y}=\frac{1}{\mathrm{Re}\,\mathrm{Pr}}\left(\frac{\partial^2 \Theta}{\partial X^2}+\frac{\partial^2 \Theta}{\partial Y^2}\right). \tag{3.15}$$

For heat conducting rotating cylinder the energy equation is,

$$\left(\frac{\partial^2 \Theta}{\partial X^2}+\frac{\partial^2 \Theta}{\partial Y^2}\right)=0 \tag{3.16}$$

Where X and Y are the non-dimensional coordinates varying along the horizontal and vertical directions, respectively, U and V are the non-dimensional velocity components in the X and Y directions, respectively, while Θ and P are non-dimensional temperature and pressure respectively. In addition to the aforementioned non-dimensional variables, some other non-dimensional system parameters also appear during non-dimensional analysis such as Prandtl number (Pr), Reynolds number (Re), Richardson number (Ri) etc. Their significance in mixed convection analysis is summarized below:

- **Prandtl Number (*Pr*):** Prandtl number can be defined as the ratio of molecular diffusivity of momentum (ν) to molecular diffusivity of heat (α). The relative thickness of the velocity and the thermal boundary layer is best described by Prandtl number. It

represents the relative importance of momentum and energy transport by the diffusion process. The Prandtl numbers of gases are about 1, which means that both momentum and heat dissipate through the fluid at about the same rate. Heat diffuses very quickly in liquid metals ($Pr < 1$) and very slowly in oils ($Pr > 1$) relative to momentum.

$$\mathrm{Pr} = \frac{\mu C_p}{k} = \frac{\nu}{\alpha}$$

- **Reynolds Number (*Re*):** Reynolds number is the ratio of inertia force to viscous force. Re can be used as die criterion to determine the change from laminar to turbulent flow and thus predicts the flow type As the Reynolds number increases, the inertia forces become dominant and small disturbances in the fluid may be amplified to cause the transition from laminar to turbulent flow. Again, lower value of Re indicates the viscous force is dominant and in this case the flow is laminar.

$$\mathrm{Re} = \frac{U_{ref}\rho_f L}{\mu}$$

- **Richardson Number (*Ri*):** Richardson number is stated as the ratio or (the buoyancy term to the flow gradient term. In thermal convection problems, this number represents the importance of natural convection relative to the forced convection. In aviation, *Ri* is used as a rough measure of the expected air turbulence. A lower value indicates a higher value of turbulence.

$$Ri = \frac{g\beta\Delta TL}{\nu^2} = \frac{Gr}{\mathrm{Re}^2}$$

When *Ri* is much greater than 1, inertia forces are negligible and natural convection effects dominate and when it is much smaller than 1, buoyancy forces are negligible and forced convection effects dominate. When the value of Richardson number is almost equal to 1, both inertia and buoyancy forces are equally present and the flow is due to mixed convection. If the value of Richardson number is exactly to 1 then it is called pure mixed convection.

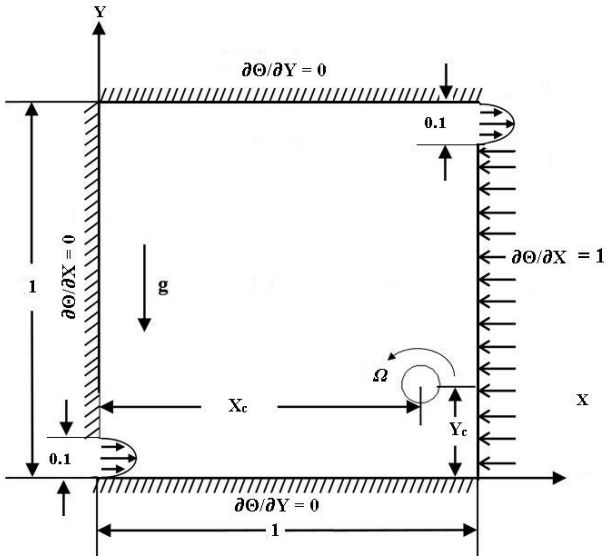

Figure 3.2: Schematic view of non-dimensional physical model.

3.7. Non-dimensional Boundary Conditions and System Parameters

The non-dimensional boundary conditions for both square enclosure and rotating cylinder are stated below,

At all solid boundaries of the square enclosure:

$$U = V = 0 \tag{3.17}$$

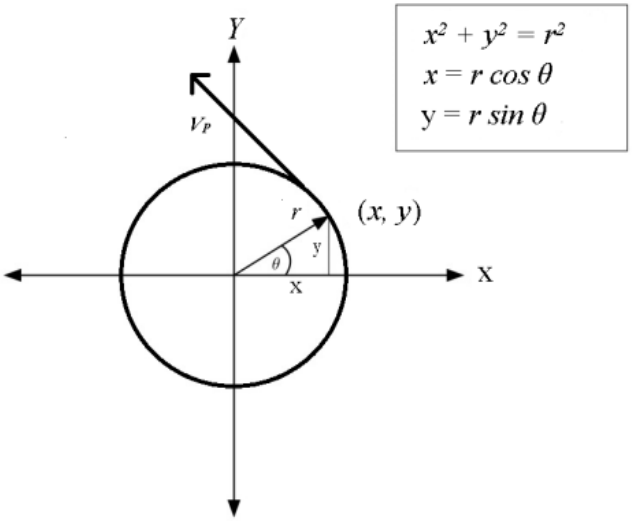

Figure 3.3: Graphical representation of the Peripheral Speed of the cylinder for any location on the circumference.

And over the rotating cylinder, velocity components are specified as in the non-dimensional form:

$$U_c = \frac{-\xi * (Y - Y_c)}{\sqrt{(X - X_c)^2 + (Y - Y_c)^2}} \tag{3.18}$$

$$V_c = \frac{-\xi * (X - X_c)}{\sqrt{(X - X_c)^2 + (Y - Y_c)^2}} \tag{3.19}$$

Where, X_c and Y_c denote the dimensionless Cartesian coordinates at the center of the cylinder and ξ denotes the speed ratio of the cylinder which is defined as,

$$\xi = \frac{V_P}{U_{mean}} \tag{3.20}$$

Where V_p is the absolute velocity over the surface of the cylinder and U_{mean} is the mean velocity of the inlet air. And, the absolute velocity is defined as, θ

$$V_p = \sqrt{U_c^{\,2} + V_c^{\,2}} \tag{3.21}$$

The non-dimensional velocity components at different location on the surface of the rotating cylinder for different speed ratios are shown below in Figure 3 to Figure 5.

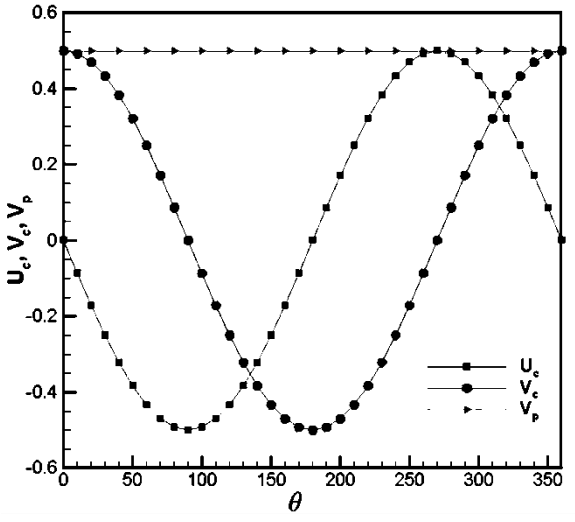

Figure 3.4: Boundary Conditions for the Rotating Cylinder (CCW) at speed ratios, ξ = 0.5.

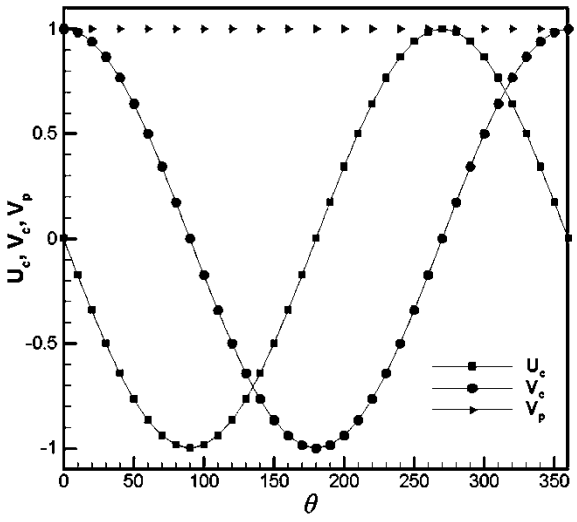

Figure 3.5: Boundary Conditions for the Rotating Cylinder (CCW) at speed ratios, $\xi = 1$.

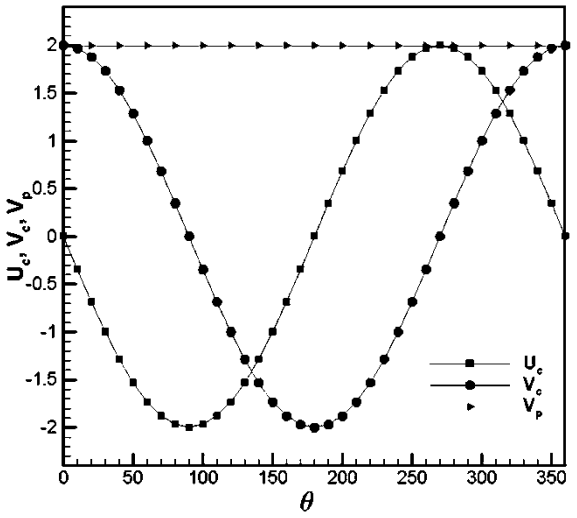

Figure 3.6: Boundary Conditions for the Rotating Cylinder (CCW) at speed ratios, $\xi = 2$.

At the inlet the non-dimensional velocity profile is expressed as,

$$U = \frac{U_{\max}}{U_{mean}} = 60Y - 600Y^2 \tag{3.22}$$

Where, U_{max} is the non-dimensional maximum velocity of the parabolic velocity profile and U_{mean} is the non-dimensional mean velocity of the velocity profile.

At the outlet boundary, normal shear stress is assumed to be zero.

Top wall, bottom wall and part of the left wall are maintained at adiabatic condition:

For the top wall and bottom wall, $\frac{\partial \Theta}{\partial Y} = 0$

For the left wall, $\frac{\partial \Theta}{\partial X} = 0$

Heated right wall section: $\frac{\partial \Theta}{\partial X} = 1$

At the solid-fluid vertical interfaces of the block:

$$\left(\frac{\partial \Theta}{\partial X}\right)_{fluid} = K\left(\frac{\partial \Theta}{\partial X}\right)_{solid}$$

At the solid-fluid horizontal interfaces or the block:

$$\left(\frac{\partial \Theta}{\partial Y}\right)_{fluid} = K\left(\frac{\partial \Theta}{\partial Y}\right)_{solid}$$

Here, K is the cylinder conductivity ratio which is defined as

$$K = \frac{k_s}{k_f}$$

In the present study K = 5.0.

Local Nusselt number can be defined as in the following way,

$$Nu_l = \frac{1}{\Theta(Y)} \tag{3.23}$$

Average Nusselt number is another one important parameter for the present work which is strongly analyzed to predict the heat transfer phenomena and this parameter is expressed as,

$$Nu_{avg} = \frac{1}{\varepsilon}\int_0^{\varepsilon} \frac{1}{\Theta(Y)} dY \tag{3.24}$$

Where, ε is the dimensionless length of the heat source i. e. ε = 0.9.

The visualization of the flow field is displayed by streamlines obtained from the velocity components U and V; the relationship between streamlines, ψ [40] and the velocity components for two dimensional flows are,

$$U = \frac{\partial \psi}{\partial Y}, V = -\frac{\partial \psi}{\partial X} \tag{3.25}$$

$$\frac{\partial^2 \psi}{\partial X^2} + \frac{\partial^2 \psi}{\partial Y^2} = \frac{\partial U}{\partial Y} - \frac{\partial V}{\partial X} \tag{3.26}$$

3.7.1. Heat function

Heat transfer visualization is performed through the dimensionless isotherms and through the dimensionless heat lines. The dimensionless heat function is another one important parameter which is used to analyze the heat flow within the enclosure. Heat function is obtained from the conductive heat fluxes $\left(-\frac{\partial\Theta}{\partial X},-\frac{\partial\Theta}{\partial Y}\right)$ as well as convective heat fluxes $\left(U\Theta,V\Theta\right)$. The heat function satisfies the energy balance equation in such a way,

$$\frac{\partial H}{\partial X}=-V\Theta+\frac{\partial\Theta}{\partial Y} \tag{3.27}$$

$$\frac{\partial H}{\partial Y}=U\Theta-\frac{\partial\Theta}{\partial X} \tag{3.28}$$

These two equations yield to a single non-dimensional heat function equation,

$$\frac{\partial^2 H}{\partial X^2}+\frac{\partial^2 H}{\partial Y^2}=U\frac{\partial\Theta}{\partial Y}+\Theta\frac{\partial U}{\partial Y}-V\frac{\partial\Theta}{\partial X}-\Theta\frac{\partial V}{\partial X} \tag{3.29}$$

Chapter 4: Numerical Methodology

Ordinary and partial differential equations are so powerful technique in mathematics that can represent any physical phenomena mathematically. These equations involve numerical or analytical investigation. In fluid mechanics and heat and mass transfer there is an involvement of a lot of partial differential equations but they are restricted to a limited number of flows. To obtain an approximate solution numerically, we have to approximate the partial differential equations by a system of algebraic equations, which can be solved on a computer. Actually numerical analysis is the study of algorithms that uses some approximations to simplify the analysis. The approximations are applied to small domains in space and the numerical solution provides results at discrete locations in space. For the whole result, it is needed to form a global matrix through the process of integrating the values of discrete locations. Discretization directly influences the accuracy of the numerical procedure and it should coincide with our desired results.

4.1. Advantages of Numerical Analysis

Many researchers have performed experimental investigation on the fluid flow, heat and mass transfer phenomena. But, the experimental approach is quite costly in many cases and time consuming which may not be desirable. To reduce the problem, numerical analysis becomes very attractive approach today. On the other hand, this technique provides accurate results with reduced time effort. The key advantages of the numerical analysis are mentioned below:

- This technique provides direct solution and results in an exact solution if exists.
- This technique usually requires less time to find out the solution.
- This is a useful and very powerful technique for functions that have moderately complex structures or geometry.
- This technique converts complex geometry into simpler ones.
- This technique discretizes the physical problem into small domains
- Lower cost is involved in the numerical procedure than experimental approach

4.2. Solution of Differential Equations

The mathematical model of complex geometry may be of very large shapes and limitations arise in this case for numerical modeling. So, scientists and researchers have sub-divided the complex system into smaller components or elements and thus the complex model can be analyzed easily. In many case, adequate accuracy of solution is obtained using a finite number of well-defined components (discrete problems), whereas, for other problems infinite number of sub-divisions or elements is possible (continuous problem). Since capacity of any computational machine is finite, continuous problems are solved using a finite number of elements. This results in an approximate solution rather than an exact one. Therefore, different computational methods are suggested so that entire problem domain can be subdivided into a number of elements or points or volumes that makes the approximation close to the exact solution. Based on the way of discretization different types of solution methods are available such as,

- Finite difference method (FDM),
- Finite element method (FEM),
- Finite volume method (FVM)

There are numerous other methods such as SEM, LBM etc. to solve a problem in CFD. And, many software packages such as ANSYS, COMSOL Multiphysics, MARC etc. are available now a days. In this work, we used COMSOL Multiphysics for simulation.

4.3. Finite Element Method

The Finite Element Method (FEM) is a numerical technique for finding approximate solutions to boundary value problems for partial differential equations. Finite element method considers that the solution region consists of many small, inter-connected sub-regions or elements and gives a piece-wise approximation to the governing equations [1].

Complex partial differential equations describing the system behavior are reduced to either linear or non-linear simultaneous equations. The continuum problem itself, over its domain, has infinite number of unknowns, since it is a continuous problem. Finite element method reduces such problem into a finite number of unknowns at specified points referred to as nodes.

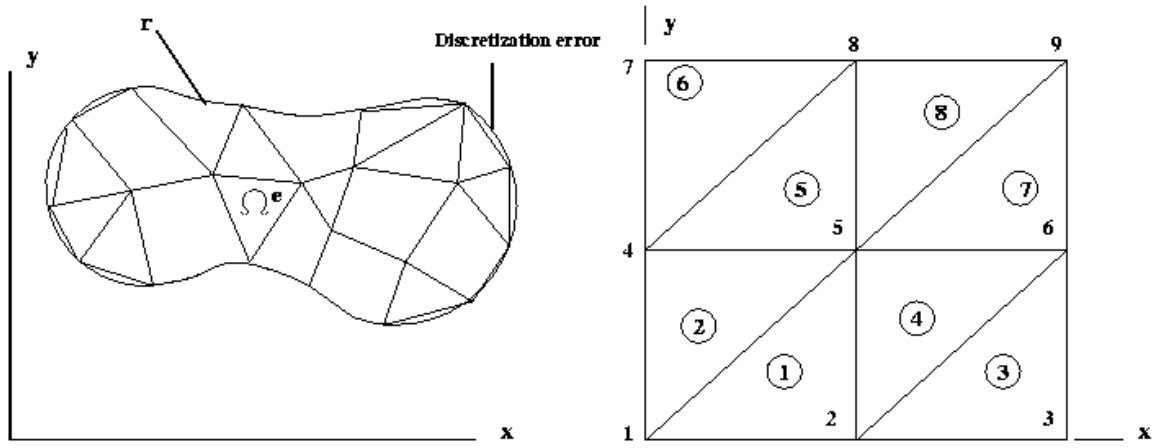

Figure 4.1: Finite element discretization of a domain

Basic steps required to solve a boundary value problem by Finite Element Method are given below,

- Discretization the original computational domain into a set of sub regions and numbering of element and nodes.
- Selection of interpolation functions and these functions are sometimes known as shape functions. Polynomial functions of lower order are chosen to express the variation of the dependent variable over an element.
- Derivation of element property equation or element characteristic equation. Usually these equations are derived in matrix form. This equation describes the characteristic of an element through a matrix, in terms of element nodal variables. Several mathematical models such as variational method, weighted residual method, direct approach method etc. are used in this case.
- Assembly of individual element characteristic matrix equation to form the global structural matrix equation that describes the behavior of the original boundary value problem.
- Applying the given boundary conditions to the problem
- Solution of the modified global structural matrix equation using a method such as iteration, elimination and inversion etc.
- Post-processing of the primary solution of FEMs. The presentation form may include graphical, contour, tabular form etc.

4.3.1. Advantages of Finite Element Method

Some advantages of the Finite Element method are mentioned below,

- This technique is well suited for boundary value problems with complex geometrical shapes.
- This technique can handle all class of complex boundary conditions.
- This method can be applied where the physical properties vary with the location.
- Time dependent as well as both linear and nonlinear boundary value problems can be handled.
- General structured computer programs can easily be developed for finite element calculation.
- Standard numerical techniques can be included to support FEM calculations.
- Higher order elements can be readily used to improve accuracy without complicating boundary conditions- a difficulty always arising with finite difference approximations of a higher order.

4.3.2. Galerkin Weighted Residual Method

Finite Element method is described in the previous section. In finite element method, there are various methods to obtain the approximate solution to the given problem. The methods are,

- Ritz method
- Rayleigh Ritz method
- Weighted Residual method

In the present work, problems are investigated using Galerkin weighted residual method which is the mostly used and most powerful technique used in FEM. So, main emphasis will be given on this method. This method is chosen because the global system matrix is decomposed into smaller matrices and then these sub-matrices are solved using a non-linear parametric solver. Six nodded non-uniform triangular mesh elements are used in this work as it results smooth non-linear variations of field variables and the used method ensures fast convergence and also the reliability.

Galerkin weighted residual method is an approximate analytical method suitable for direct solution to differential equations. This technique involves the principle of weighted residuals. It has wider scope of using as a tool to FEM formulation compared to Rayleigh-Ritz method. This method is very effective for practical applications as solutions can be directly obtained from the governing differential equation and boundary conditions and this method does not need to derive the functional compared to Rayleigh-Ritz method. Method of weighted residual actually takes cue from variation principle to solve problem for the entire domain. The philosophy behind this method is very straightforward. It is known that, for numerically solving a problem, an approximate solution is at first assumed. Now, if one puts the approximated value of solution into the governing equation, it will not satisfy the equation completely like an exact solution. There will always be a residue which is the difference between the values of dependent variable produced for exact solution and approximate solution. Mathematically,

$$y_{exact} - y_{approximate} = R \tag{4.1}$$

Here, R is the residual. As numerically calculated solution comes closer to the exact solution, value of R tends to zero. So, ultimate target of solution should be to minimize R essentially to zero. General weighted residual formulation is,

$$\int_{\Omega} w_i(x) R dx = 0 \tag{4.2}$$

Where i = 1, 2, 3, ……,n. Functions $w_i(x)$ are called the weighting functions. Purpose of this weighting function is to modify the values of residuals of each element in such way that when integrated over all the elements of a domain (Here, dx is element for one dimensional domain and Ω represents integral over entire domain), value of the integral is zero. This particular function is the unique feature of this method and it gets its name from this function. To solve a problem with weighted residual method, one is free to choose a weighting function. This can be a Dirac-Delta function or a simple polynomial function. However, some particular forms of the weighting function are found to be convenient in numerical calculation.

In Galerkin Weighted residual method, the weighting function is assumed to the trial function which is used to get the approximate solution of the equations over each element. Here “similar”

does not mean that the function must be exactly similar, rather, these should be of the same order and form. Therefore, for Galerkin weighted residual method the equation is,

$$\int_{\Omega} N_i(x) R dx = 0 \tag{4.3}$$

Where, $N_i(x)$ is the weighting function. Important properties of the weighting functions are mentioned below,

- Weighting function should satisfy homogeneous parts of essential boundary conditions of governing differential equations.
- Weighting function must be continuous.
- Value of shape functions N_i is 1 at node i, whereas, this value is dependent on the coordinates (x, y) for two dimensional element.
- $\sum_i^6 N_i = 1$For six-nodded triangular element.

4.4. Mesh Generation

The entire domain of square cavity is discretized into mesh elements of different sizes. Discretization is possible for variety of element shapes such as triangles, quadrilaterals etc. There is certain number of nodes at different points of the elements. The choice of interpolation function and the number of nodes determine the solution pattern. Suitable known functions, representing approximate solution, are assumed over each element. Order of the solution is dependent on the nodes of element.

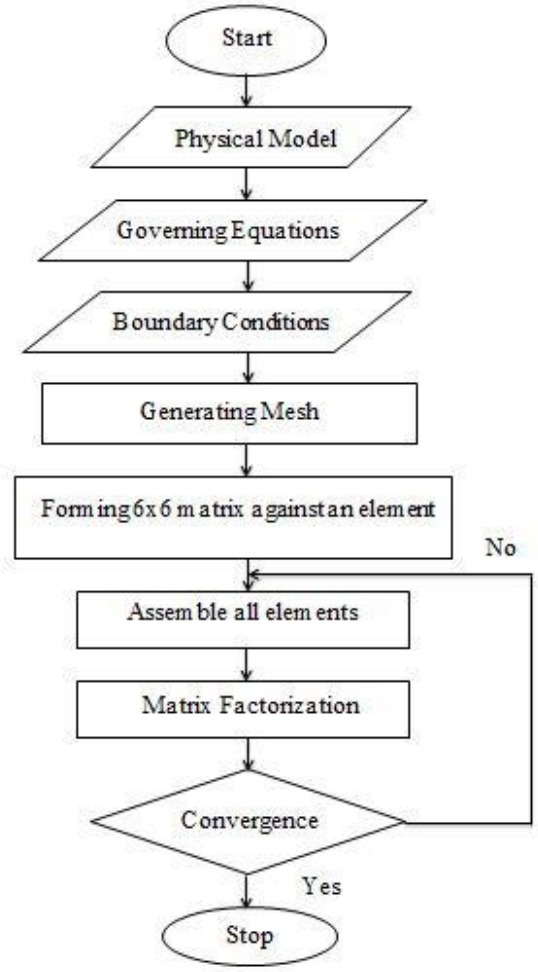

Figure 4.2: Flowchart of Finite Element Method

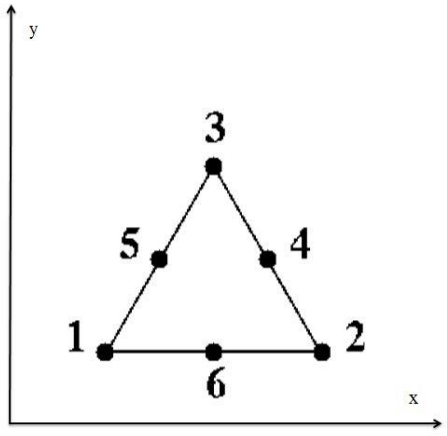

Figure 4.3: Six nodded triangular element

Consequently, number of nodes in each element and subsequently, in the entire domain governs the accuracy of CFD solution. Six nodded triangular element were used in this work to discretize the domain. An example of each element is presented in Fig. 4. The process is called linear triangular element when only corner nodes of such element is considered during solution. A linear triangular element signifies a linear approximation of the variable of interest over each sub-domain. It is also known as simplex element. A two-dimensional linear triangular element is modeled by the following equation,

$$T(x,y) = \alpha_1 + \alpha_2 x + \alpha_3 y \tag{4.4}$$

Where the polynomial is linear in *x* and *y* co-ordinates, *T(x, y)* is the general dependent variable and polynomial contains three coefficients. Since a linear triangle (simplex element) has three nodes, values of the constants α_1, α_2 and α_3 are determined from three linear equations one at each node resembling the above equation. Now, in case of quadratic triangular element we write,

$$T(x,y) = \alpha_1 + \alpha_2 x_1 + \alpha_3 y_1 + \alpha_4 x_1^2 + \alpha_5 y_1^2 + \alpha_6 x_1 y_1 \tag{4.5}$$

There are six arbitrary constants in this case, so the quadratic element will have six nodes. In the similar manner of simplex element, six constants can be evaluated by writing the above equation for six nodes of the element. If we know the values of the constants, it is possible to write the same equation for all the nodes of domain and then evaluate the unknown variable *T(x, y)*. Although exactly same principle is not strictly followed in different numerical codes, this is the best structure.

Structured, unstructured and hybrid grid are the three types of grid or mesh in finite element analysis. The structured grid has the characteristic of having regular connectivity of the vertices. In two-dimensional analysis, chosen element type is quadrilateral while in 3D, hexahedra. This type of grid is highly space efficient as the neighborhood relationship is defined by storage arrangement. Higher resolution and better convergence is provided by structured grid. However, construction of structured grid is tedious for complex geometries. An unstructured grid is identified by irregular connectivity. In complex geometries, it is logical to use a large number of blocks or elements which leads to unstructured grid. In CFD, unstructured grid is widely used to solve different problems. This type of grid has far more flexibility and computational resources are also efficiently used. Two-dimensional unstructured mesh uses triangular elements, while

three-dimensional unstructured mesh uses tetrahedral elements. In reality, unstructured mesh consists of structured meshes that are arranged in an irregular manner. Advantage of this type of grid is that mesh can be refined wherever needed. For this thesis, unstructured mesh is used as shown in the Fig. 5 given below. In mesh distribution, particular importance should be given on boundary meshes. At boundaries, especially at connecting points of different boundaries, condition may be Dirichlet or Neumann or a combination of both types. Hence to capture sudden change of dependent variables along boundaries and avoid singularity, very fine mesh is applied at boundaries. Mesh density is gradually reduced to the center of domain. A hybrid grid is nothing but a mixture of structured and unstructured grid portions.

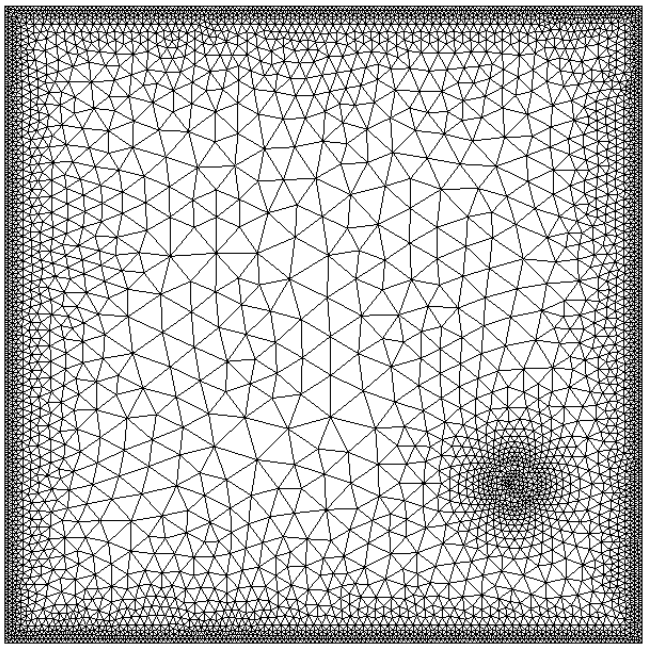

Figure 4.4: Finite element mesh generation inside the computational domain of square enclosure

4.5. Grid Sensitivity Test

In numerical solution of different heat transfer related problems, grid sensitivity test is performed to reduce the cost of computation. Discretization method and density of elements in computational grid dictate the accuracy of numerical solution. Higher number of elements generally provides more accurate solution. However, there is a limit up to which accuracy can be improved only by increasing the element number inside a computational domain. Value of any particular derived parameter becomes constant once that limit is reached and further refinement

of the grid is futile. Coupled to the accuracy of the solution is the question of cost. Computational cost is a function of number of calculations performed to solve the problem and for high number of elements in the computational domain, number of calculations is also high resulting in unnecessary cost of computation. To avoid this, a particular derived parameter is selected and change in its value is observed for alteration of number of elements or nodes in the domain keeping all other variables constant at any convenient value. Once number of element in a domain reaches optimum value (sufficiently high for satisfactory solution), implementing a finer mesh does not change the value of the derived parameter under observation significantly. This particular grid is considered as standard and reproduced for all subsequent calculations.

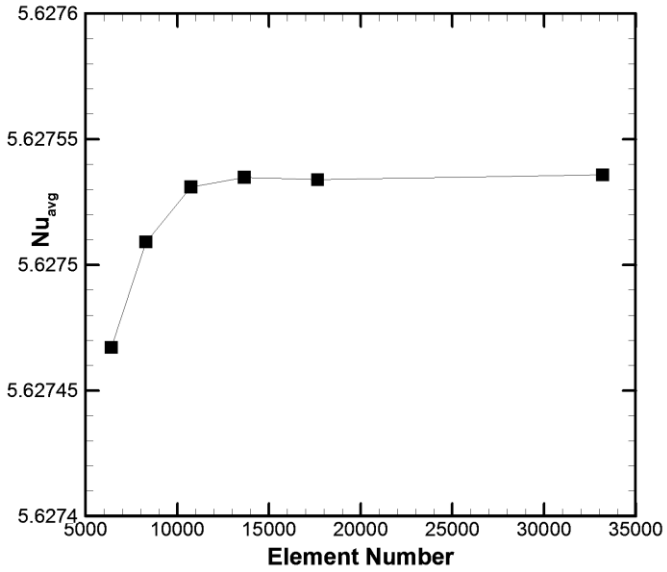

Figure 4.5: Variation of average Nusselt number with different mesh size for Re = 100, D/L = 0.1, ξ = 1.0, K = 5, Ri = 10 and Pr = 0.7.

The results of grid sensitivity test performed for mixed convection heat transfer inside a square enclosure is shown in the Fig. 4.5. The test is performed for Reynolds number, Re = 100; cylinder diameater, D/L = 0.1; cylinder speed ratio, ξ = 1.0, conductivity ratio, K = 5 and Richardson number, Ri = 10 by considering air as the fluid which has Prandlt number, Pr = *0.7*. The figure shows that for large number of elements the average Nusselt number Nu_{avg} is high with a value of 5.6275. It is also evident from the figure that as the number of element increases the value of average Nu also increases. However , from about 13652 elements the average nusselt number becomes almost constant at 5.62753. Further increment of nodes does not cause a

significant change of *Nu*. Hence , for all subsequent numerical simulations of the problem , a node number of 13652 is selected as the optimum mesh size.

4.6. Validation of the Model

One of the major parts of CFD analysis is the proper validation of the model that is under study. Accuracy of the code used for simulation has to be verified with respect to some other previously validated numerical models. In this work, validation is checked for the isotherm lines, streamlines, heatlines and Nusselt number for the specified conditions.

4.6.1. Validation of the present model with Costa and Raimundo [33]

Validation check of isotherm lines and streamlines is performed for the case of mixed convection in a differentially heated square enclosure with an active rotating cylinder with reported by Costa and Raimundo [33].

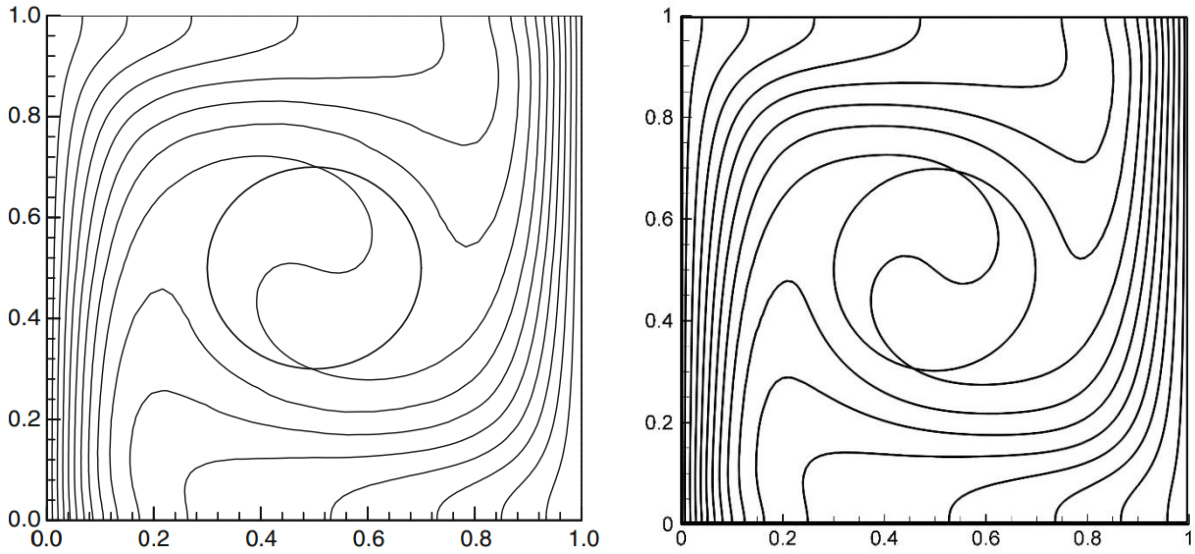

Figure 4.6: Comparison of isotherm lines with Costa and Raimundo [33] (left) and present work (right) for Ω = -500, K = 1, R_c = 1 and R = 0.2

For checking the validation we consider the case Ω = -500, K = 1, R_c = 1 and R = 0.2. From the two figures, we can conclude that, isotherm contours show good agreement with the reported results and both the results are almost identical.

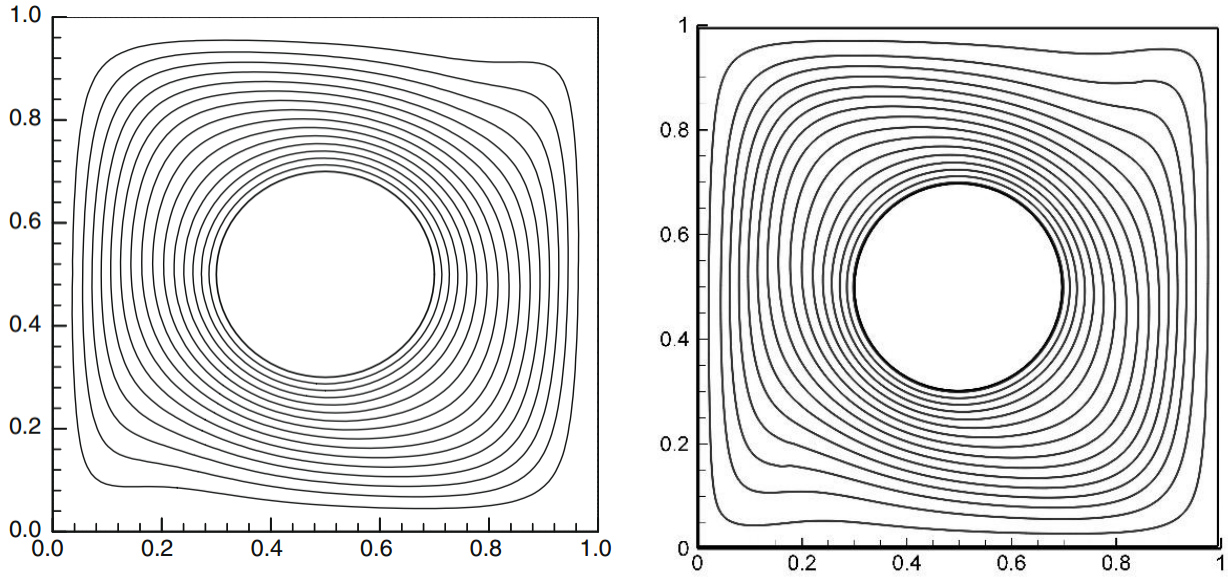

Figure 4.7: Comparison of streamlines with Costa [33] (left) and present work (right) for Ω = -500, K = 1, R_c = 1 and R = 0.2

For streamlines validation, we reproduced the work of Costa and Raimundo [33] and compared with his work. The left box above indicates the work of Costa and Raimundo [33] and the right box indicates the present work. From the comparison between two results, it can be said that the numerical method applied in the present work is trustworthy.

	Nu_{avg}			
R	0.1	0.2	0.3	0.4
Present model	4.45	4.26	4.35	4.7
Costa and Raimundo [33]	4.48	4.35	4.4	4.9
% Difference	0.67	2.07	1.14	4.08

Table 1: Comparison of average Nusselt number between the present model and Costa and Raimundo [33] for Ω = -500, K = 1 and Rc = 1 and radius R is varied in the range from 0.1 to 0.4.

Average Nusselt number is also validated with Costa and Raimundo [33] for the same conditions stated above but in this case the radius is not constant, it is varied in the range from 0.1 to 0.4. From the table we see that, in all cases, the difference between two results is very negligible and the error percentage is within tolerance level. So, it is evident that present model closely agrees with the reported results of Costa and Raimundo [33].

4.6.2. Validation of the present model with Gupta *et al.* [34]

Validation check of isotherm lines and streamlines is performed for the case of mixed convection in a differentially heated vented square enclosure with a stationary cylinder with reported by Gupta *et al.* [34].

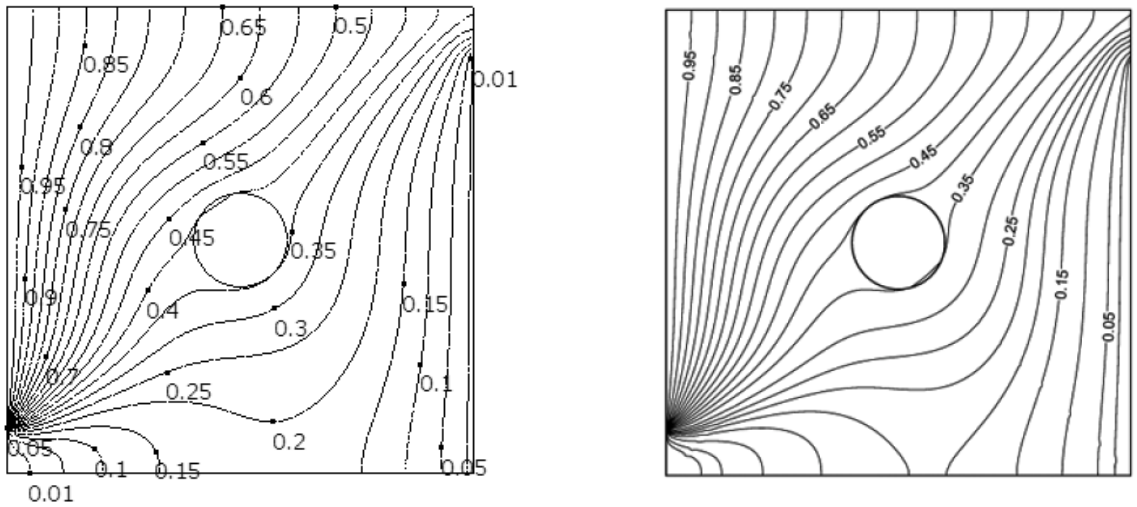

Figure 4. 8: Comparison of isotherm lines with Gupta *et al.* [34] (right) and present work (left) for D/L = 0.2, Re = 100, K = 5 and Ri = 0.

For checking the validation we consider the case D/L = 0.2, Re = 100, K = 5 and Ri = 0 and D/L = 0.2, Re = 100, K = 5 and Ri = 1.From Figure 4.5 and Figure 4.7, we can conclude that, isotherm contours show good agreement with the reported results and both the results are almost identical.

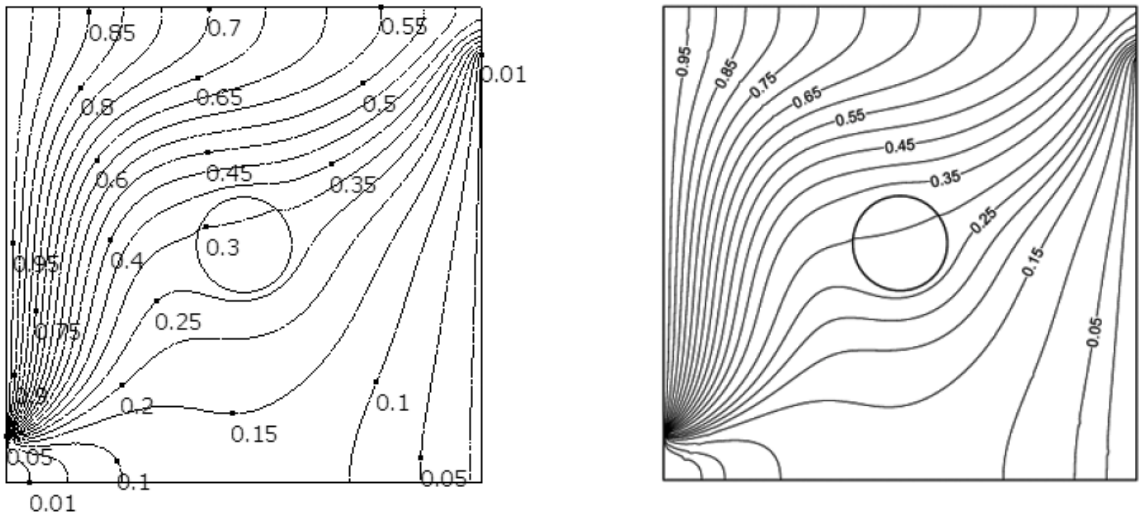

Figure 4.9: Comparison of isotherm lines with Gupta *et al.* [34] (right box) and present work (left box) for D/L = 0.2, Re = 100, K = 5 and Ri = 1.

	Nu_{avg}		
Ri	0	1	5
Present model	3.83	4.68	6.32
Gupta *et al.*[34]	3.66	4.52	6.18
% Difference	4.64	3.54	2.27

Table 2: Comparison of average Nusselt number between the present model and Gupta *et al.* [37] for $D/L = 0.2$, $Re = 100$, $K = 5$ and Ri is varied in the range from 0 to 5.

Average Nusselt number (Nu_{avg}) is also validated with Gupta *et al.* [34] for the same conditions stated above but in this case the Richardson number is not constant, it is varied in the range from 0 to 5. Table 1 indicates that, in all cases, the difference between the results of Gupta *et al.* [34] and present study is very negligible and the error percentage is within tolerance level. So, it is evident that present model closely agrees with the reported results of Gupta *et al.* [34].

4.7. Summary

The purpose of this chapter was to represent and elaborate on the numerical background of the solutions provided in this thesis. The aim was to provide the reader a concise and resourceful sense of different numerical schemes involved to solve problems in CFD. Despite maximum effort, the limited scope of thesis has compelled to present only brief idea about numerical formulation and theory behind it. After a brief introduction to different numerical methods to solve a set of differential equations, fundamentals of Galerkin method along with discretization of governing equations are provided. Mathematical definitions of computed parameters are presented afterwards. The following section consists of grid sensitivity test of the problem. In the last part of this chapter the details of code validation tests are provided to establish validity of numerical scheme used for present analysis.

Chapter 5: Results and Discussion

In this chapter the different features of mixed convection heat transfer inside a ventilated and heated square enclosure in presence of a heat conducting rotating cylinder are studied. In the analysis the Reynolds number and the Richardson number is varied in finite range and the Prandlt number is kept constant at 0.7. Firstly, the effect of presence of the cylinder either stationary or rotational on the heat transfer and fluid flow phenomena are focused. Then the effect of different speed ratio of the cylinder is also investigated. Further, the effect of different diameter is studied and finally the effect of the location of the cylinder on the fluid flow and heat transfer phenomena is investigated. The qualitative analysis that is the analysis of temperature field, flow field and heat transfer process is developed by the use of isotherm lines, streamlines and heatlines. The quantitative analysis that is the analysis of heat transfer rate is done by average Nusselt number (Nu_{avg}) at the isoflux portion. The thermal conductivity ratio is kept constant at 5 for all the cases. The effect of the speed ratio of the rotating cylinder is investigated by varying it from 0 to 2. The diameter of the cylinder is varied from $0.1L$ to $0.2L$ to observe the effect of cylinder size. Then the location of the cylinder for a specific cylinder speed ratio and diameter is varied. The cylinder is moved up and down with y - coordinate varying from $0.25L$ to $0.65L$ at a fixed x - coordinate of $0.8L$. The Reynolds number is varied in the range of 10 to 500 and the Richardson number is varied in the range of 0.1 to 10. The average Nusselt number is plotted against Richardson number for all the cases and the percent increase in pumping work is plotted against Richardson number for only in the case of different diameter of the cylinder.

5.1. Effect of presence of a cylinder inside ventilated cavity

5.1.1. Effect of presence of cylinder (Stationary / Rotating) on streamlines

The streamline pattern inside a ventilated cavity for different cylinder configurations (stationary / Rotating) at different Richardson number (*Ri* =0.1, 1 and 10) for different Reynolds number (*Re* = 10, 100 and 500) are shown in Figure 5.1.1 to Figure 5.1.3.

In Figure 5.1.1, streamline patterns for different *Re* and three different cylinder configurations such as, No Cylinder (NC), Stationary Cylinder (SC) and Rotating Cylinder (RC) with unity speed ratio (ξ=1.0) at *Ri* = 0.1 is shown. The flow in the ventilated cavity when there is no cylinder at *Re* = 10 is mostly streamline flow. Most of the air entering through the inlet into the cavity is directly exiting through the outlet without much distortion or change of direction in the flow field. However, in case of presence of a cylinder either stationary or rotating at unity speed ratio the flow field distortion takes place as a certain amount of air gets trapped and rotates around the cylinder, and a certain amount exits the cavity after flowing around the cylinder tangentially which may be occurring due to the inertia force acting on the adjacent fluids around the cylinder. Also, most of the air is flowing directly from the inlet to the outlet without any disruption in the flow field, in this case. For, *Re* =100 there is a presence of counter clockwise circulation along with fine streamline flow. It is observed that, in case of the presence of stationary cylinder in the cavity the streamline flow does not distort like it did previously for *Re* =10 whilst for rotating cylinder the streamline flow distorts around the cylinder tangentially due to the inertia force generated due to the rotation of the cylinder.

In case of higher *Re* (*Re* = 500) the span of the vortex increases and pushes the streamline flow towards the right sidewall for all cylinder configuration, although the strength of the vortex reduces for the presence of the cylinder and in case of no cylinder the vortex strengthens on the outer regions. However, in case of stationary cylinder configuration the cylinder works as an obstruction in the streamline flow path whereas for rotational cylinder configuration the vortex strength increases again and pushes the streamline flow towards the bottom right corner of the cavity and the cylinder acts as a driving force for the streamline flow.

In Figure 5.1.2, streamline patterns for different *Re* and three different cylinder configurations at *Ri* = 1 is shown. For *Re* = 10 the flow in the ventilated cavity when there is no cylinder is mostly streamline flow. Most of the air entering through the inlet into the cavity is directly exiting through the outlet without any distortion or change of direction in the flow and in case of presence of a cylinder either stationary or rotating at unity speed ratio the flow field distortion takes place as a certain amount of air gets trapped and rotates around the cylinder, and a certain amount exits the cavity after flowing around the cylinder tangentially field which is very much likely to *Ri* = 0.1. For, *Re* =100, like before, there is also a presence of counter clockwise circulation along with fine streamline flow. It is also observed that, in case of the presence of stationary cylinder in the cavity only a small portion of the streamline flow distorts whilst for rotating cylinder a larger portion of the streamline flow distorts around the cylinder tangentially than in case of stationary cylinder. In case of higher *Re* (*Re* = 500) similar trend of flow pattern is observed like that of in case of *Ri* = 0.1 is evident which is, the span of the vortex increases and pushes the streamline flow towards the right sidewall for all cylinder configuration. And also, in case of stationary cylinder configuration the cylinder works as an obstruction in the streamline flow path whereas for rotational cylinder configuration the vortex strength increases again and pushes the streamline flow towards the bottom right corner of the cavity and the cylinder acts as a driving force for the streamline flow.

In Figure 5.1.3, streamline patterns for different *Re* and three different cylinder configurations at *Ri* = 10 is shown. It is evident from the figure that for *Ri* = 10 at low *Re* (*Re* = 10) there is a presence of counterclockwise vortex in the cavity for all cylinder configuration. The vortex strength increases with higher *Re* and the presence of the cylinder influences the flow field similarly like it did for the cases of lower *Ri.*

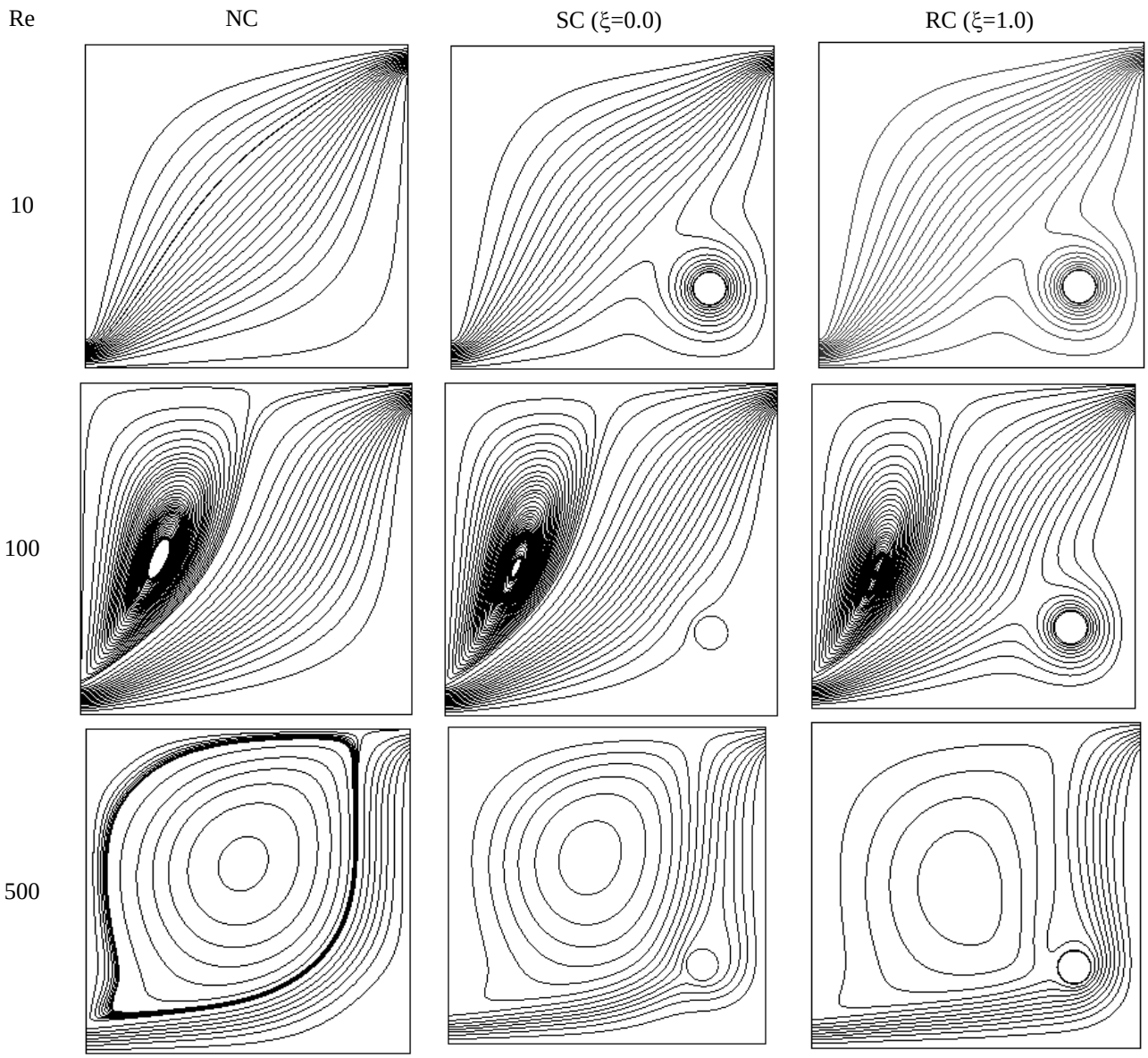

Figure 5.1.1: Flow Field inside ventilated cavity for different cylinder configurations at Ri = 0.1

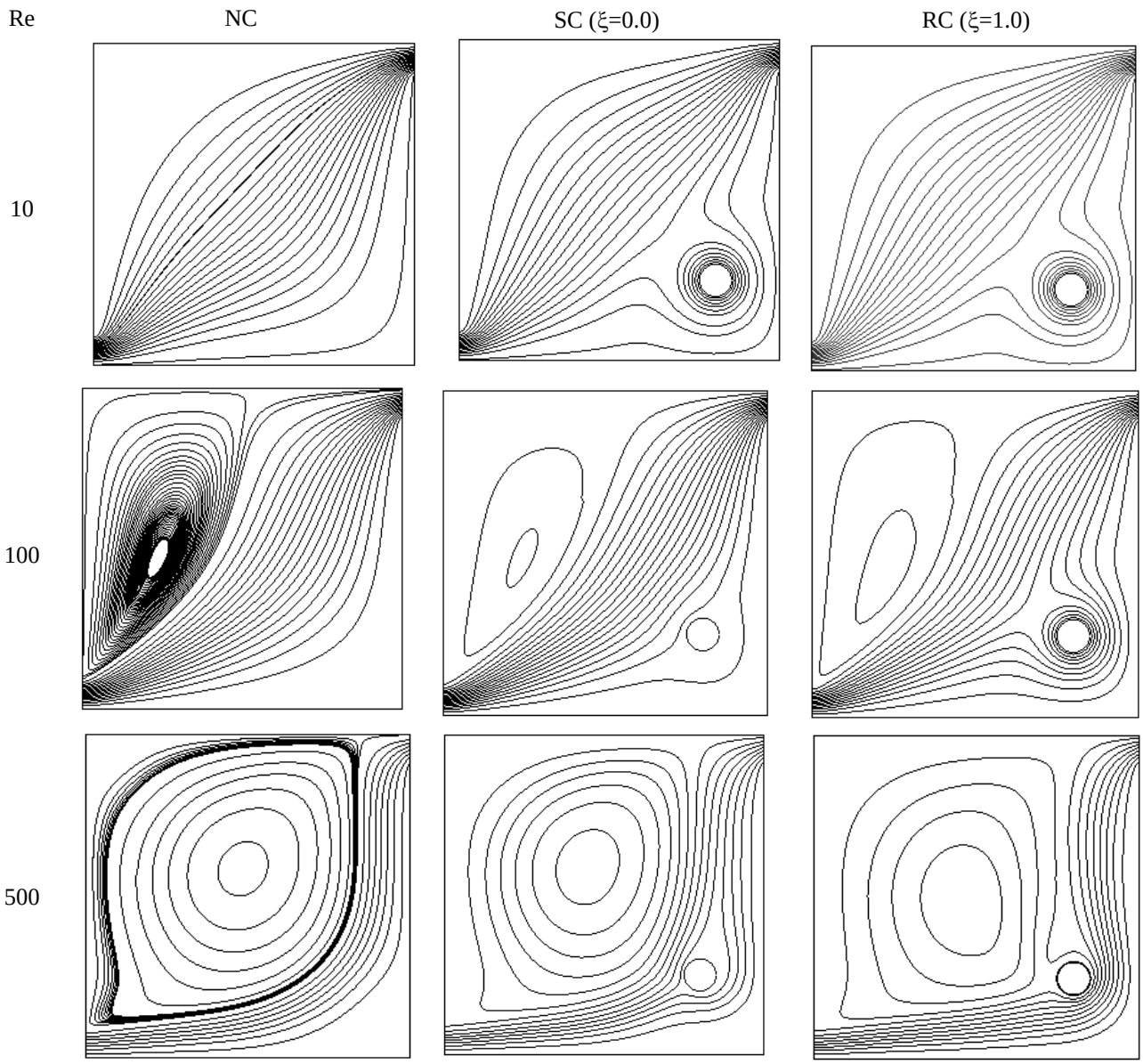

Figure 5.1.2: Flow Field inside ventilated cavity for different cylinder configurations at Ri = 1.0

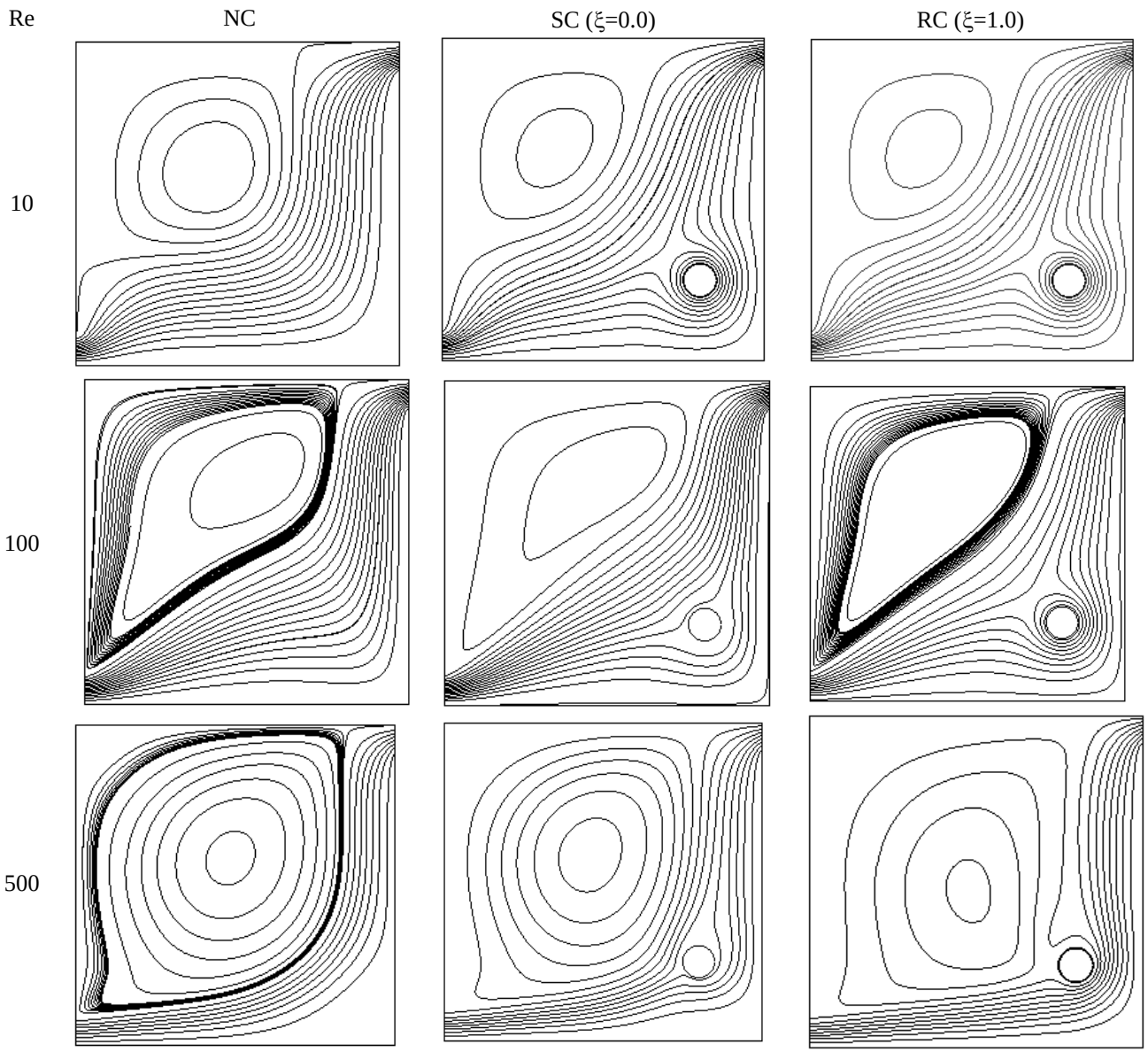

Figure 5.1.3: Flow Field inside ventilated cavity for different cylinder configurations at Ri = 10.0

5.1.2. Effect of presence of cylinder on isotherm contours

Figure 5.1.4 to Figure 5.1.6 show the isotherm contours inside a ventilated cavity for different cylinder configurations at different Richardson number (*Ri* =0.1, 1 and 10) for different Reynolds number (*Re* = 10, 100 and 500). In Figure 5.1.4, isotherm contours for different *Re* and three different cylinder configurations at *Ri* = 0.1 is shown. It is evident from the Figure 5.1.4 that at *Ri* = 0.1 for low *Re*, the isothermal contours are distributed throughout the cavity for all cylinder configuration. However, with increase in *Re* the isotherms are densely distributed in the right side of the cavity which indicates that most of the cavity is cold. The presence of the cylinder only distorts the isotherms locally where the cylinder is located which is more rigorous for rotating cylinder. For *Re* = 500, the isotherms are more densely distributed near the right hot wall and the presence of cylinder pushes the isotherms more to right, where in case of rotating cylinder the isotherms are denser.

It is evident from the Figure 5.1.5 and 5.1.6 that at *Ri* = 1 and 10 for low *Re* the isothermal contours are distributed throughout the cavity for all cylinder configuration which is similar to the case of *Ri* = 0.1. Also similar to *Ri* = 0.1, with increase in *Re* the isotherms are densely distributed in the right side of the cavity which indicates that most of the cavity is cold and the presence of the cylinder only distorts the isotherms locally where the cylinder is located which is more rigorous for rotating cylinder. Similarly, for *Re* = 500, the isotherms are also more densely distributed near the right hot wall and the presence of cylinder pushes the isotherms more to right, where in case of rotating cylinder the isotherms are dense.

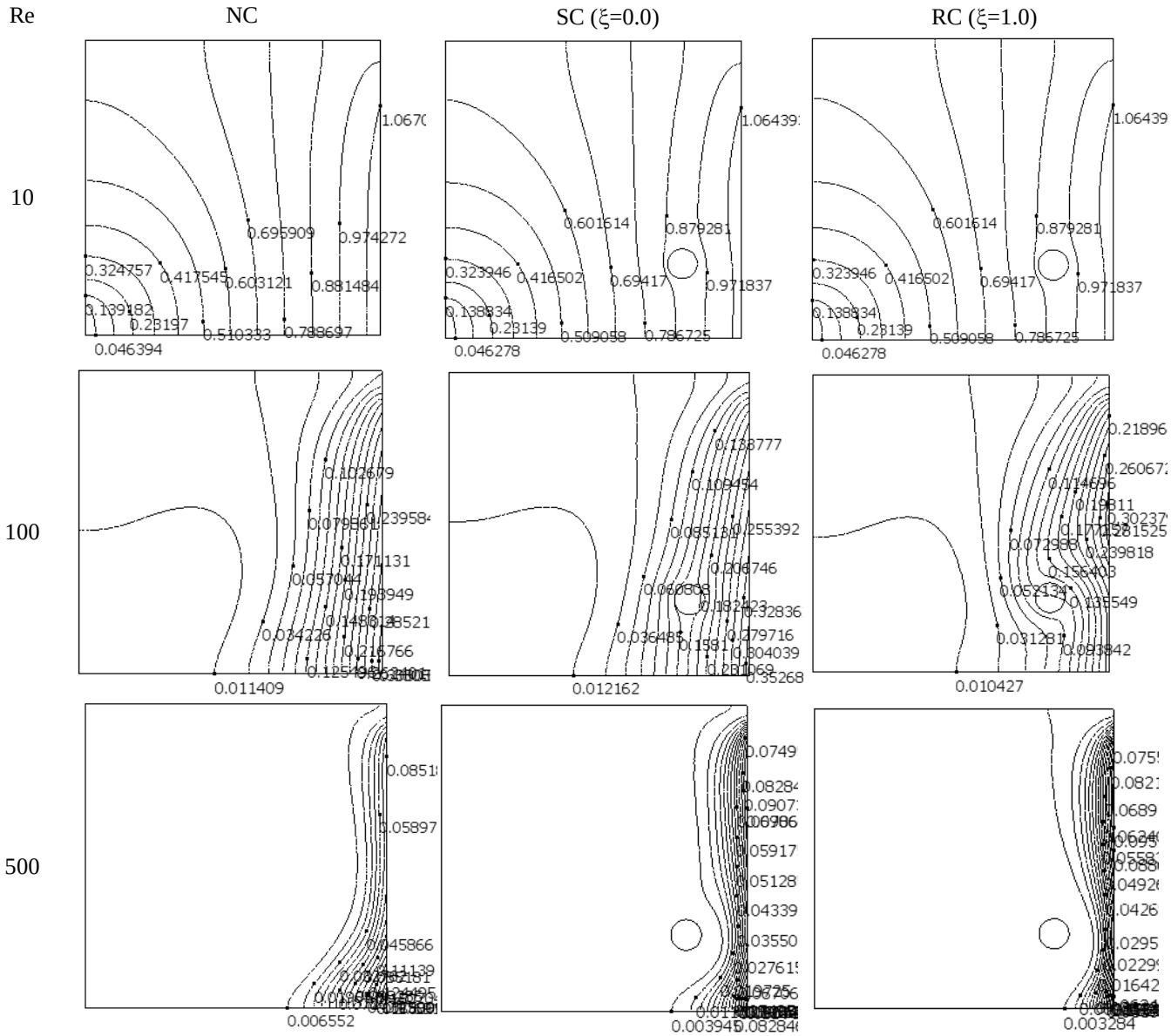

Figure 5.1.4: Thermal Field inside ventilated cavity for different cylinder configurations at Ri = 0.1

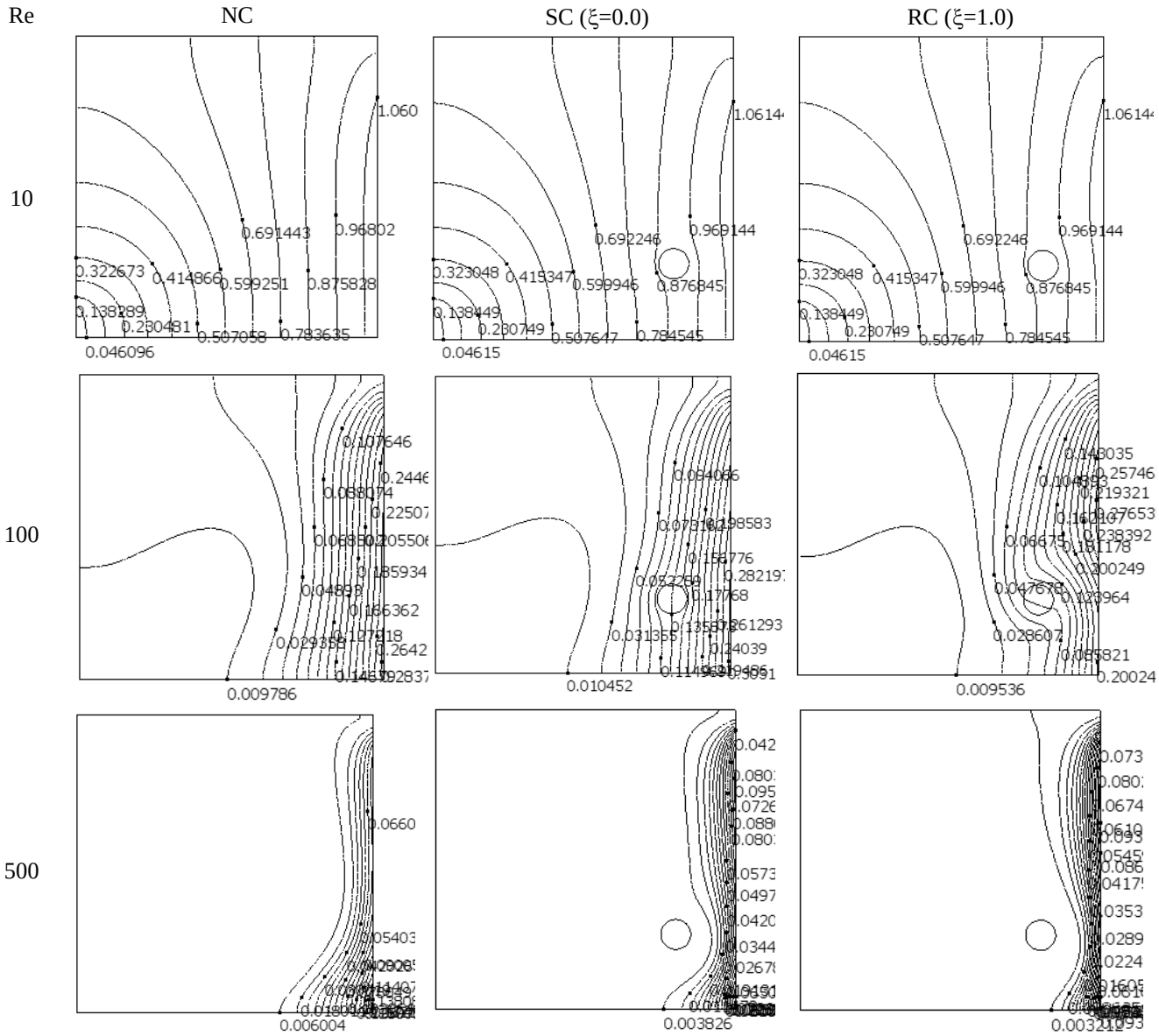

Figure 5.1.5: Thermal Field inside ventilated cavity for different cylinder configurations at Ri = 1.0

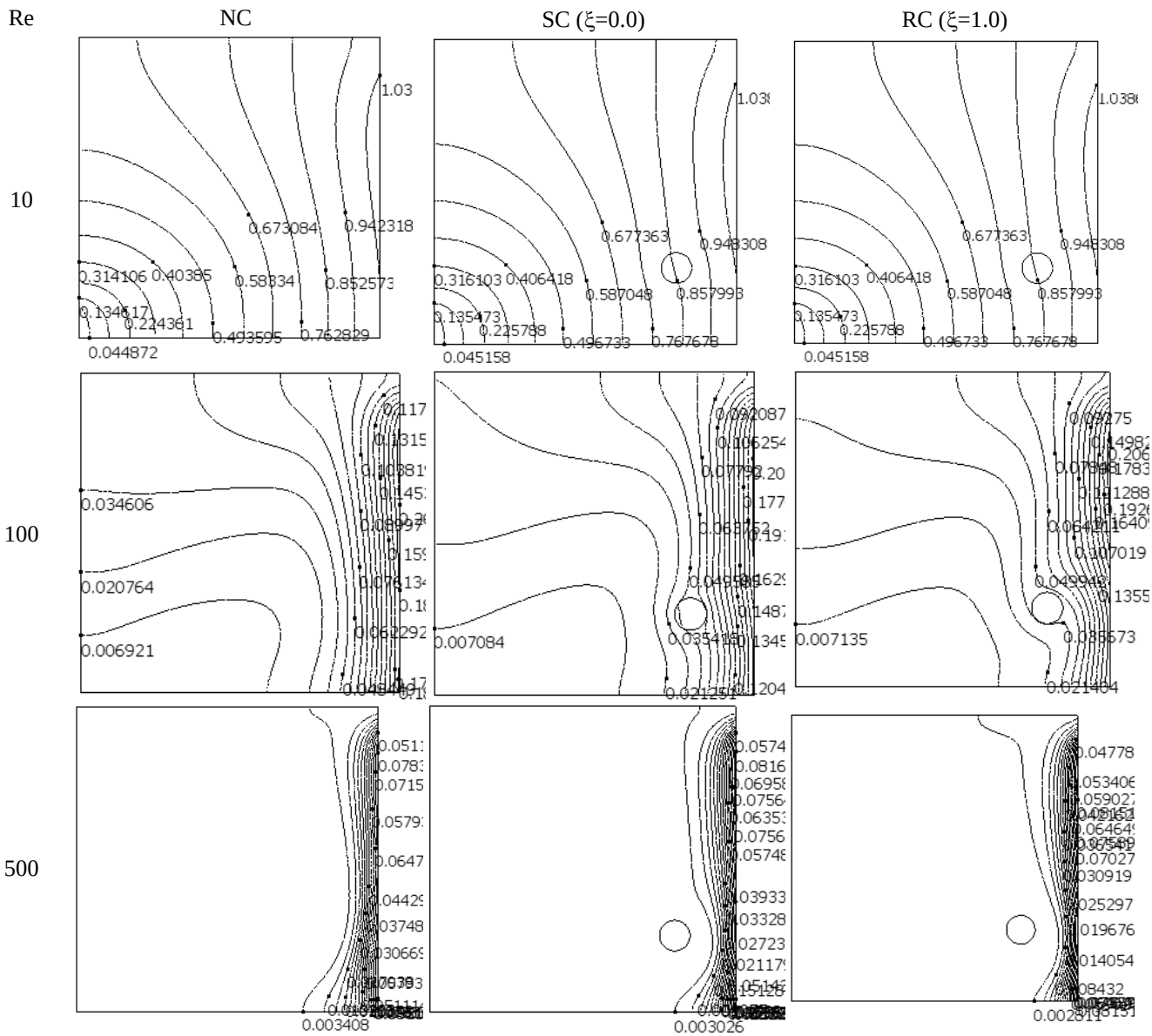

Figure 5.1.6: Thermal Field inside ventilated cavity for different cylinder configurations at Ri = 10.0

5.1.3. Effect of presence of cylinder on Heatlines

Figure 5.1.7 to Figure 5.1.9 show the heat line distribution inside a ventilated cavity for different cylinder configurations at different Richardson number (*Ri* =0.1, 1 and 10) for different Reynolds number (*Re* = 10, 100 and 500).

In Figure 5.1.7, heat line distributions for different *Re* and three different cylinder configurations (such as, no cylinder, stationary cylinder and rotating cylinder with unity speed ratio (ξ=1.0)) at *Ri* = 0.1 is shown. The heat lines in the ventilated cavity, when there is no cylinder, at *Re* = 10 is mostly diagonal straight lines. Most of the air entering through the inlet into the cavity is directly exiting through the outlet without any distortion or change of direction in the flow field and meanwhile undergoing through temperature change due to hot surface. However, presence of a cylinder either stationary or rotating the heat lines get distorted and as a certain amount of air gets trapped and rotates around the cylinder, heat line is also distributed circumferentially around the cylinder and a certain amount of heat lines is distributed around the cylinder tangentially which may be occurring due to the inertia force acting on the adjacent fluids around the cylinder. For *Re* =100, there is a presence of counter clockwise circulation along with finely distributed heat lines from the inlet to the outlet. It is observed that, in case of the presence of stationary cylinder in the cavity, the heat lines does not distort like it did previously for *Re* =10 whilst for rotating cylinder the heat lines distorts around the cylinder tangentially like before and a counterclockwise heat circulation is also visible. In case of higher *Re* (*Re* = 500), the strength of the vortex increases and pushes the streamline flow towards the right sidewall for all cylinder configurations. However, in case of no cylinder configuration there is also another vortex is visible near the bottom right corner whose strength decreased in stationary cylinder configuration and which is diminished in rotating cylinder configuration.

In Figure 5.1.8, heat line distributions for different *Re* and three different cylinder configurations at *Ri* = 1 is shown. For *Re* = 10 the flow in the ventilated cavity for all cylinder configuration is mostly same except for in case of stationary cylinder configuration there was a vortex of low strength when *Ri* = 0.1 which is not present for *Ri* = 1. For, *Re* =100, like before, there is also a presence of counter clockwise heat circulation along with finely distributed heat lines. It is also observed that, in case of the presence of stationary cylinder in the cavity only a small portion of the heat lines distorts whilst for rotating cylinder a larger portion of the heat lines distorts around

the cylinder tangentially. In case of higher *Re* (*Re* = 500) similar trend of flow pattern observed in case of *Ri* = 0.1 is evident which is, the strength of the vortex increases and pushes the heat lines towards the right sidewall for all cylinder configuration. In Figure 5.1.9, heat line distributions for different *Re* and three different cylinder configurations at *Ri* = 10 is shown. It is evident from the figure that for *Ri* = 10 at low *Re* (*Re* = 10), there is a presence of counterclockwise vortex in the cavity for all cylinder configuration which is very much unlikely for lower *Ri*. The vortex strength increases with higher *Re* and the presence of the cylinder influences the flow field similarly like it did for the cases of lower *Ri.* However, for rotating cylinder configuration the vortex strength decreased for *Re* = 500.

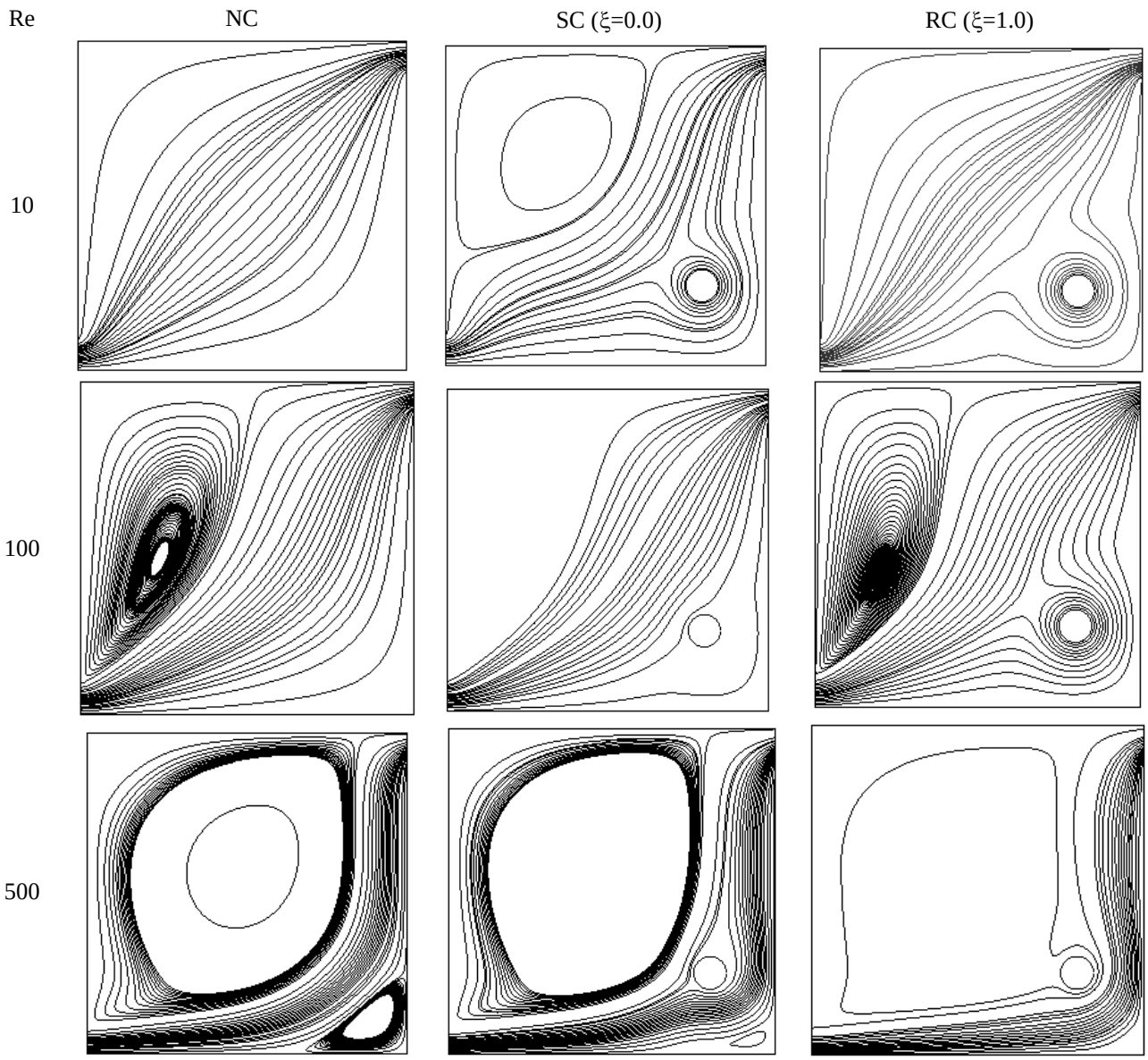

Figure 5.1.7: Heat Line distribution inside ventilated cavity for different cylinder configurations at Ri = 0.1

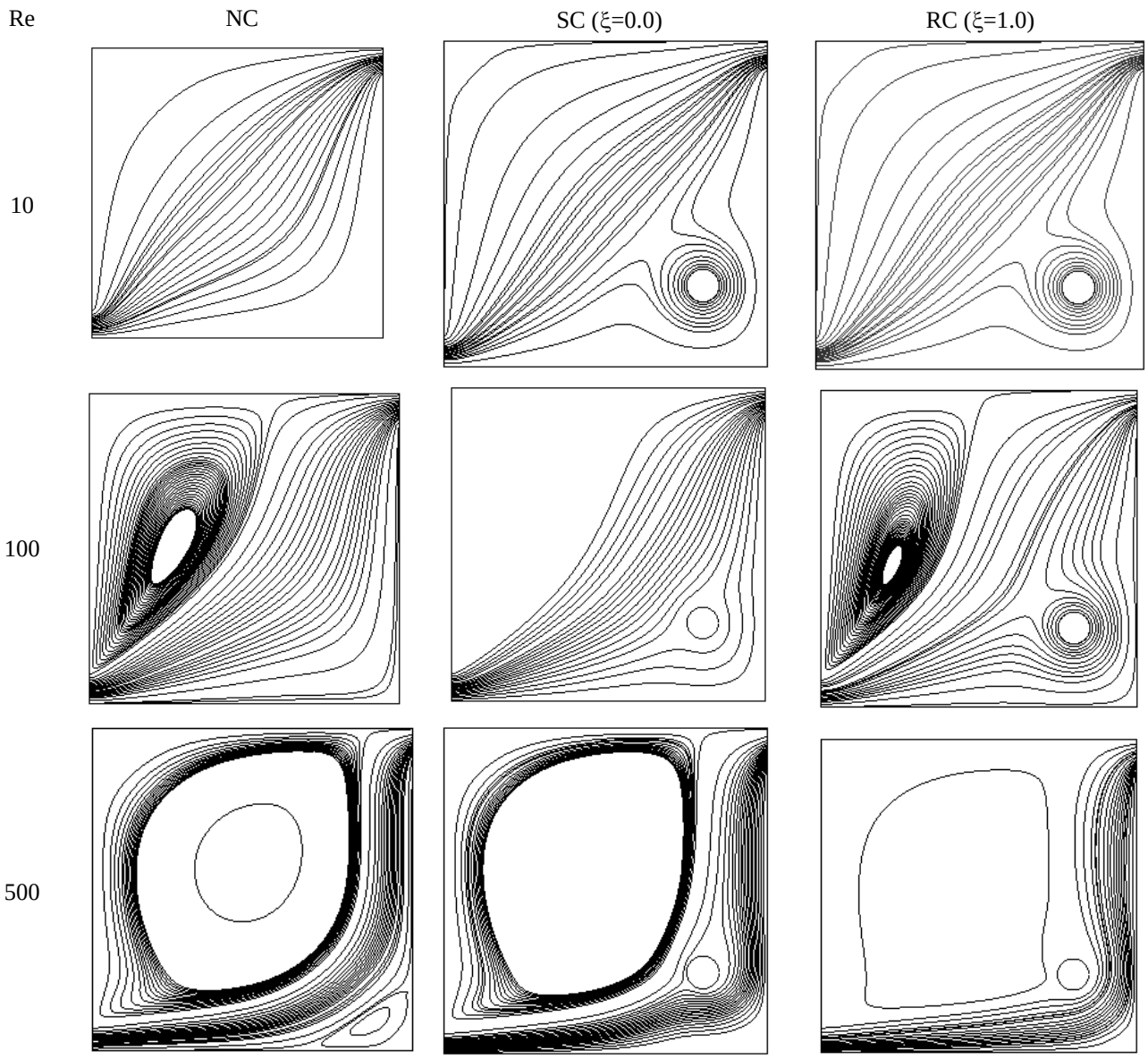

Figure 5.1.8: Heat Line distribution inside ventilated cavity for different cylinder configurations at Ri = 1.0

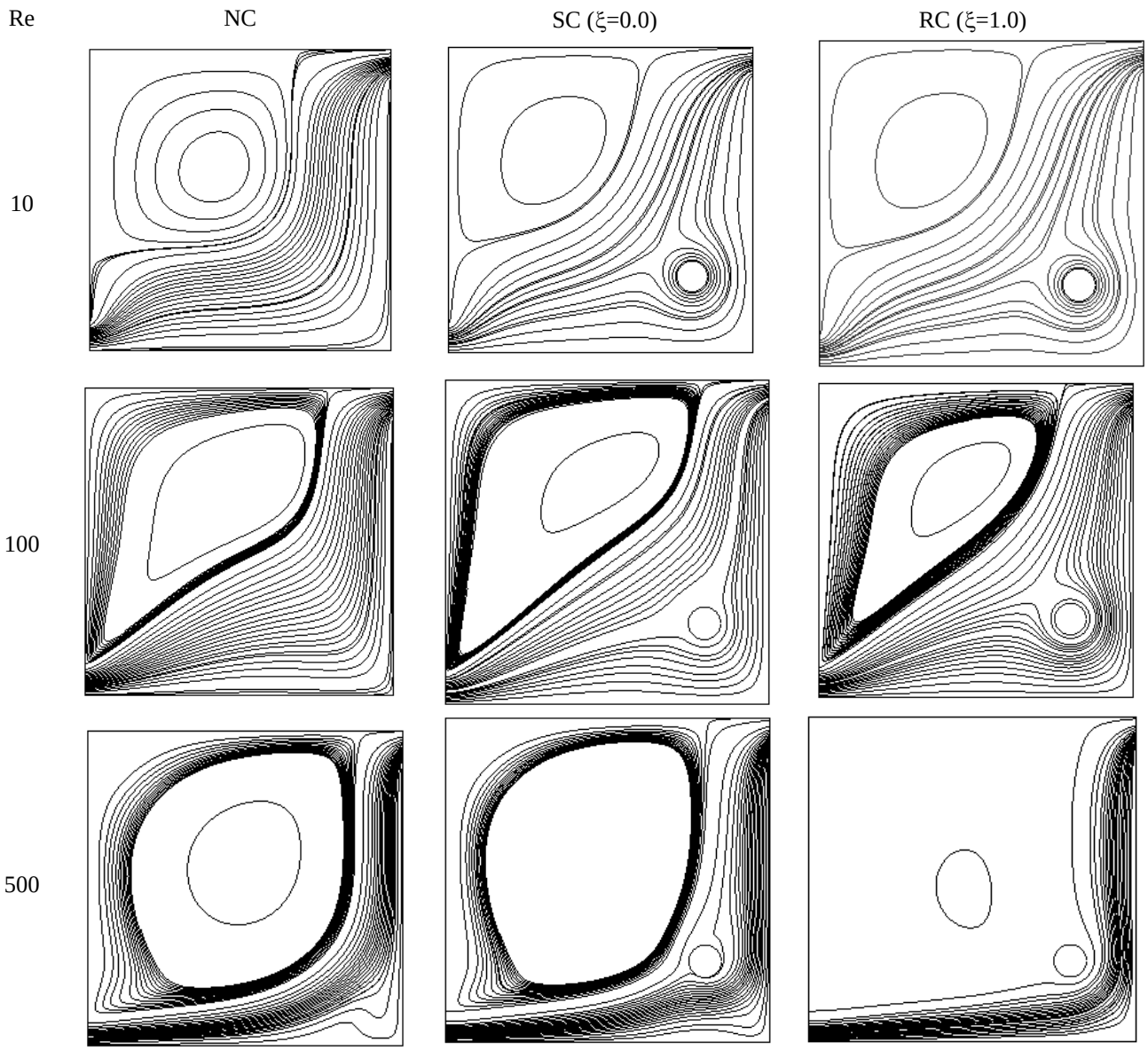

Figure 5.1.9: Heat Line distribution inside ventilated cavity for different cylinder configurations at Ri = 10.0

5.1.4. Effect of presence of cylinder on the heat transfer rate

Figure 5.1.10 shows the variation of normalized heat transfer rate for different Reynolds number with different Richardson number for stationary cylinder configuration. It is obvious from the figure that for *Re* = 50 and 100, the heat transfer rate is less than that of when there is no cylinder. Heat transfer rate is decreasing with increasing *Ri* and after achieving a minimum the heat transfer performance increases with further increase in *Ri* though the performance is still less than that of in case of no cylinder. For *Re* = 10, at lower *Ri* the heat transfer rate is slightly better. However, with increasing *Ri* it also decreases and for *Ri* > 2.5 the heat transfer performance is less than that of in the case of no cylinder. For *Re* = 250, the heat transfer rate is higher for all *Ri* and with increasing *Ri* heat transfer rate increases, though for lower *Ri* the rate is low. For *Re* = 500, the heat transfer rate is also higher and it increases with increase in *Ri*, however, after reaching a maximum of it starts to decrease with further increase in *Ri*, although the heat transfer rate is still higher than that of the case of no cylinder.

Figure 5.1.11 shows the variation of normalized heat transfer rate for different Reynolds number with different Richardson number for rotational cylinder configuration. It is evident from the figure that for all *Re* the heat transfer rate is higher than that of in the case of no cylinder for all *Ri* except for *Re* = 10, for which the heat transfer rate is lower for *Ri* > 2.5. Heat transfer rate at all other *Re* shows some variation with *Ri*, though the value is still larger than that in no cylinder configuration. Highest heat transfer rate is achieved at *Re* = 500 for low Richardson numbers.

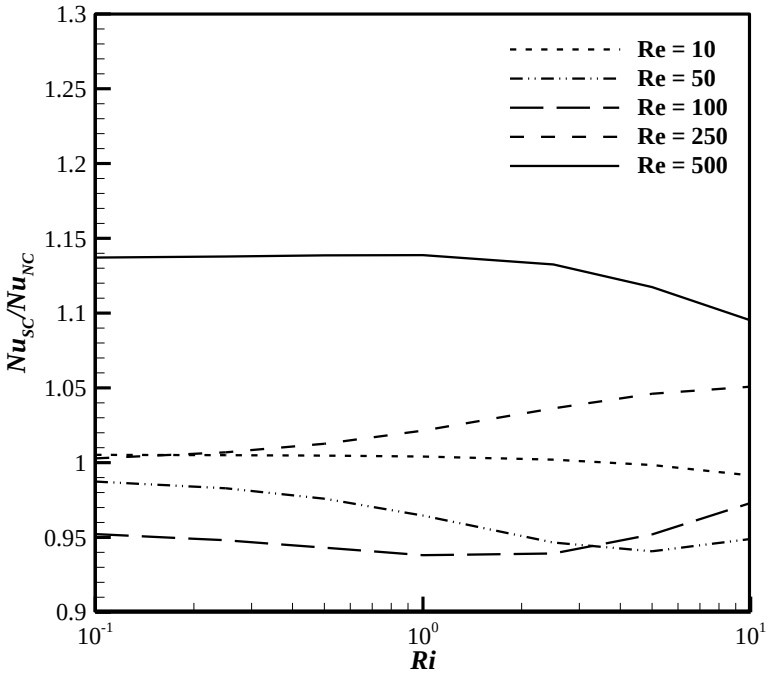

Figure 5.1.10: Normalized Heat Transfer Rate against *Ri* with stationary cylinder placed inside ventilated cavity for different *Re*.

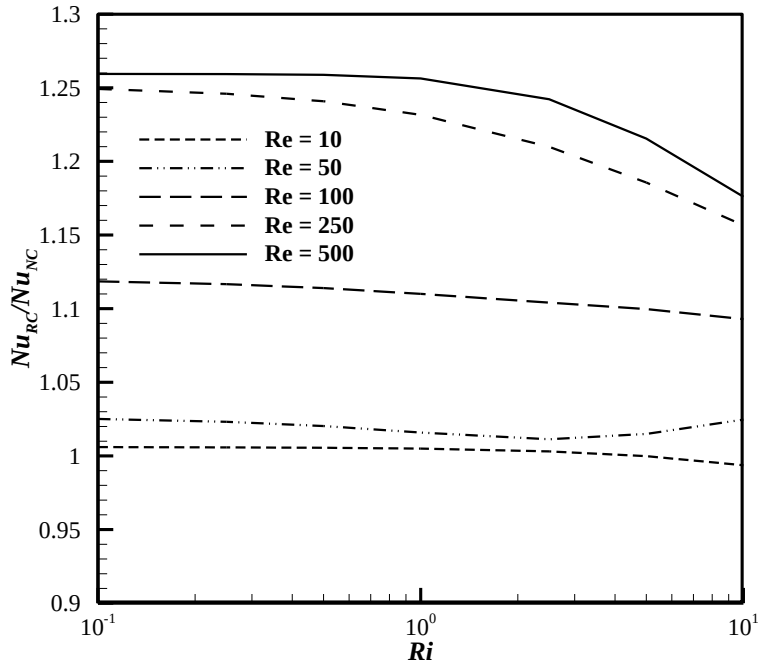

Figure 5.1.11: Normalized Heat Transfer Rate against *Ri* with Rotating cylinder placed inside ventilated cavity for different *Re*.

5.2. Effect of speed ratios of the rotational cylinder inside ventilated cavity

5.2.1. Effect of speed ratios of the cylinder on streamlines

The streamline pattern inside a ventilated cavity for different speed ratios (ξ) of the rotating cylinder (D/L = 0.1; X_c = 0.80, Y_c = 0.25) at different Richardson number (Ri =0.1, 1 and 10) for different Reynolds number (Re = 10, 100 and 500) are shown in Figure 5.2.1 to Figure 5.2.3.

In Figure 5.2.1, streamline patterns for different Re and different speed ratios at Ri = 0.1 is shown. The flow in the ventilated cavity, at Re = 10 for all speed ratios, is mostly diagonal streamline flow meaning most of the air entering through the inlet into the cavity is directly exiting through the outlet without any distortion or small change of direction in the flow field. However, presence of the rotating cylinder distorts the flow and directs along its boundary tangentially and a certain amount of air gets trapped and rotates around the cylinder which is occurring due to the inertia force acting on the adjacent fluids around the cylinder. With increasing speed ratio the inertia force is more dominant and the streamlines gets more distorted around the cylinder. In some local places the flow is separating, generally near the bottom wall and right wall. For, Re =100, there is a presence of counter clockwise circulation which is more strong at the center of the vortex. It is also observed that, for all speed ratios a portion of the streamlines also distorts around the cylinder tangentially which increases with increase in speed ratio due to large inertia force for large speed ratio. In this case, the flow is also separating in the bottom and right wall, however for speed ratio 2 the flow is only separating at the right wall due to large inertia force. In case of higher Re (Re = 500), the span of the vortex increases and pushes the streamline flow towards the right sidewall for all speed ratios, though the strength of the vortex minimizes. However, in case of stationary cylinder configuration the cylinder works as an obstruction in the streamline flow path whereas for rotational cylinder configuration the vortex strength increases again and pushes the streamline flow towards the bottom right corner of the cavity and the cylinder acts as a driving force for the streamline flow.

In Figure 5.2.2, streamline patterns for different Re and different speed ratios of the rotating cylinder at Ri = 1 is shown. For Re = 10, the flow in the ventilated cavity is almost same as it was for Ri =0.1 except in this case the fluid flows covering the entire bottom and right wall of the

cavity. For, *Re* =100, like before, there is also a presence of counter clockwise circulation along with fine streamline flow, however the vortex for speed ratio 1 and *Re* = 100 has less strength. From the figure it is evident that flow separation is taking place for all speed ratios and *Re* = 100. In case of higher *Re* (*Re* = 500), similar trend of flow pattern observed that of in case of *Ri* = 0.1 is evident which is, the span of the vortex increases and pushes the streamline flow towards the right sidewall for all speed ratios. And, the span of the vortex increases again and pushes the streamline flow towards the bottom right corner of the cavity and the cylinder acts as a driving force for the streamline flow and flow separation only occur for speed ratio 2.

In Figure 5.2.3, streamline patterns for different *Re* and different speed ratio of the rotating cylinder at *Ri* = 10 is shown. It is evident from the figure that for *Ri* = 10 at low *Re* (*Re* = 10) there is a presence of counterclockwise vortex in the cavity for all speed ratios. The vortex strength increases with higher *Re* and the presence of the cylinder influences the flow field similarly like it did for the cases of lower *Ri*, however for *Re* = 100, the vortices have less strength for speed ratio 0.5 and 2 and for speed ratio 1 the boundary region of the vortex has more strength than its core. At *Re* = 500, for *Ri* = 10 the streamlines follows similar trends as it was for lower *Ri*, however the inertia force of the cylinder is less dominant.

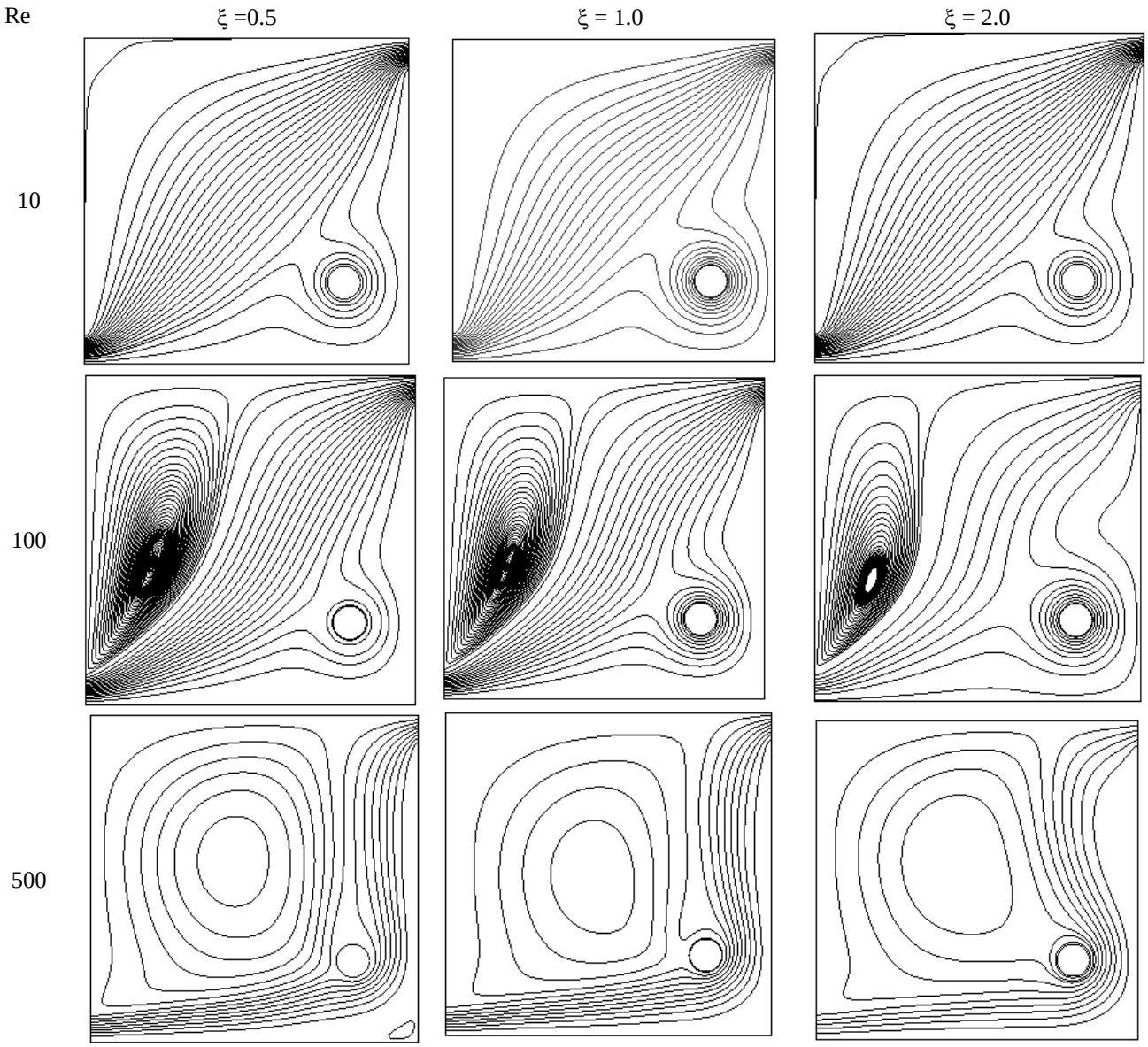

Figure 5.2.1: Streamline distribution inside ventilated cavity for different speed ratios of the rotating cylinder (D/L = 0.1; X_c = 0.80, Y_c = 0.25) at Ri = 0.1.

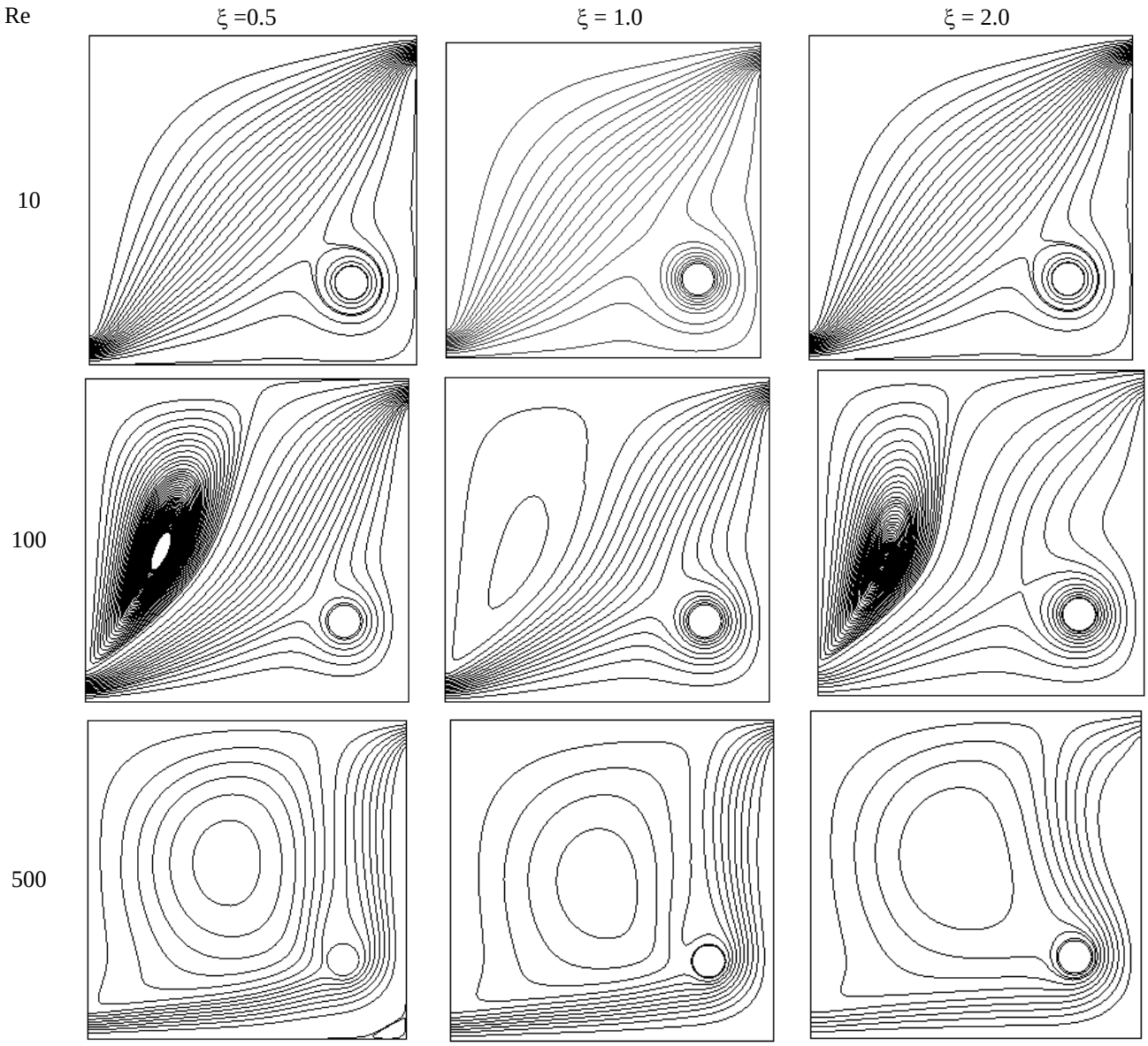

Figure 5.2.2: Streamline distribution inside ventilated cavity for different speed ratios of the rotating cylinder (D/L = 0.1; X_c = 0.80, Y_c = 0.25) at Ri = 1.0.

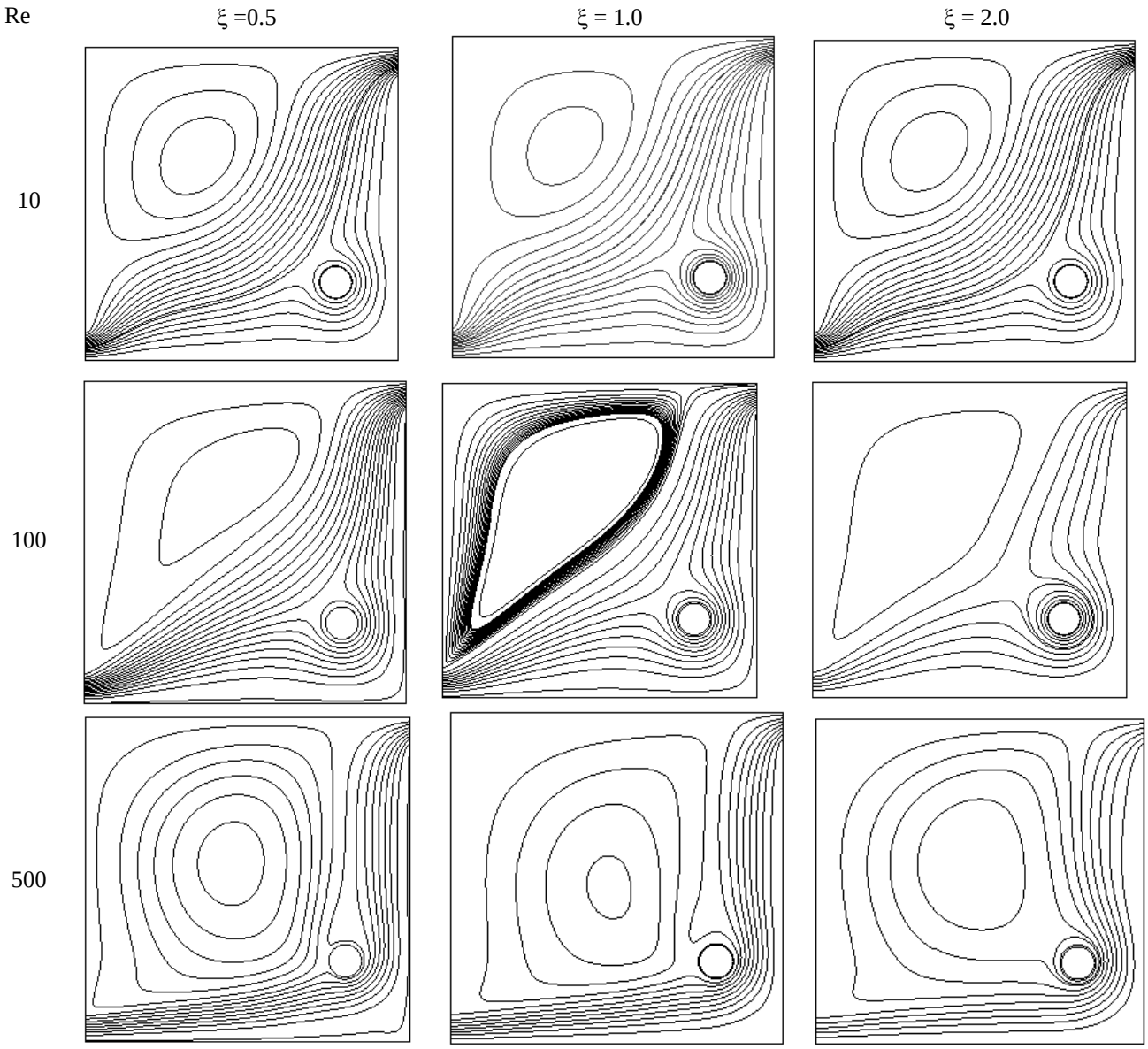

Figure 5.2.3: Streamline distribution inside ventilated cavity for different speed ratios of the rotating cylinder (D/L = 0.1; X_c = 0.80, Y_c = 0.25) at Ri = 10.0.

5.2.2. Effect of speed ratios of the cylinder on isotherm contours

Figure 5.2.4 to Figure 5.2.6 show the isotherm contours inside a ventilated cavity for different speed ratios of the rotating cylinder at different Richardson number (*Ri* =0.1, 1 and 10) for different Reynolds number (*Re* = 10, 100 and 500). In Figure 5.2.4, isotherm contours for different *Re* and speed ratios at *Ri* = 0.1 is shown. It is evident from the Figure 5.2.4 that at *Ri* = 0.1 for low *Re,* the isothermal contours are distributed throughout the cavity for all speed ratios. However, with increase in *Re* the isotherms are pushed to the right side of the cavity which indicates that most of the cavity is cold. Due to the presence of rotating cylinder the isotherms near the cylinder distorts and where the scale of distortion increases with increasing speed ratio. For *Re* = 500, the isotherms are more densely distributed near the right hot wall and with increase in the speed ratio the isotherms are pushed more to right, where in case of speed ratio 2 the isotherms are denser.

It is evident from the Figure 5.2.5 and 5.2.6 that at *Ri* = 1 and 10 for low *Re* the isothermal contours are distributed throughout the cavity for all speed ratios and the speed ratio has next to no influence of the isotherms which is similar to the case of *Ri* = 0.1. Also, similar to *Ri* = 0.1, with increase in *Re* the isotherms are densely distributed in the right side of the cavity which indicates that most of the cavity is cold and with increase in speed ratio the isotherms near the cylinder distorts more than lower speed ratios. Similarly, for *Re* = 500, the isotherms are also more densely distributed near the right hot wall like that in case of *Ri* = 0.1.

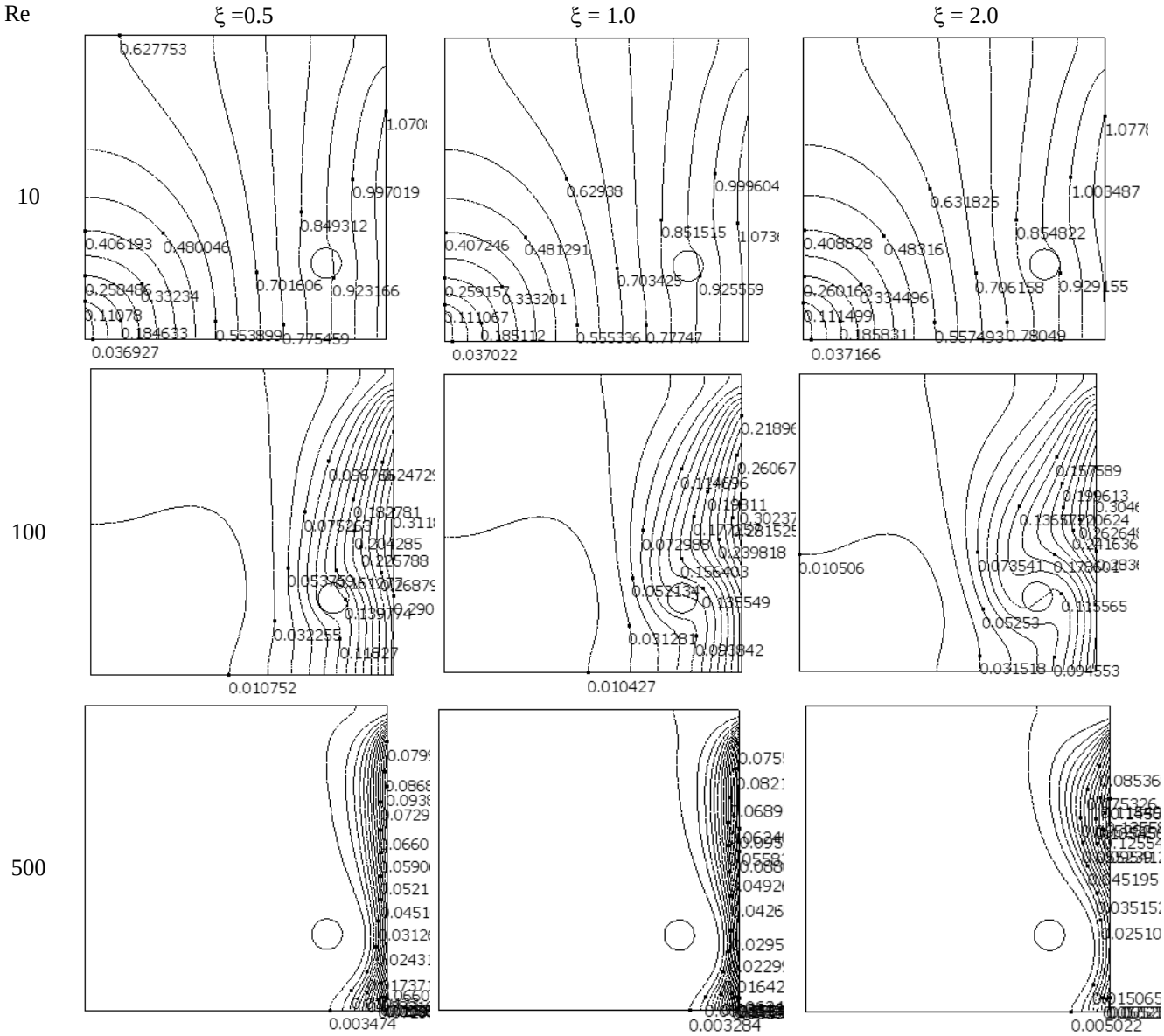

Figure 5.2.4: Thermal field inside ventilated cavity for different speed ratios of the rotating cylinder (D/L = 0.1; X_c = 0.80, Y_c = 0.25) at Ri = 0.1.

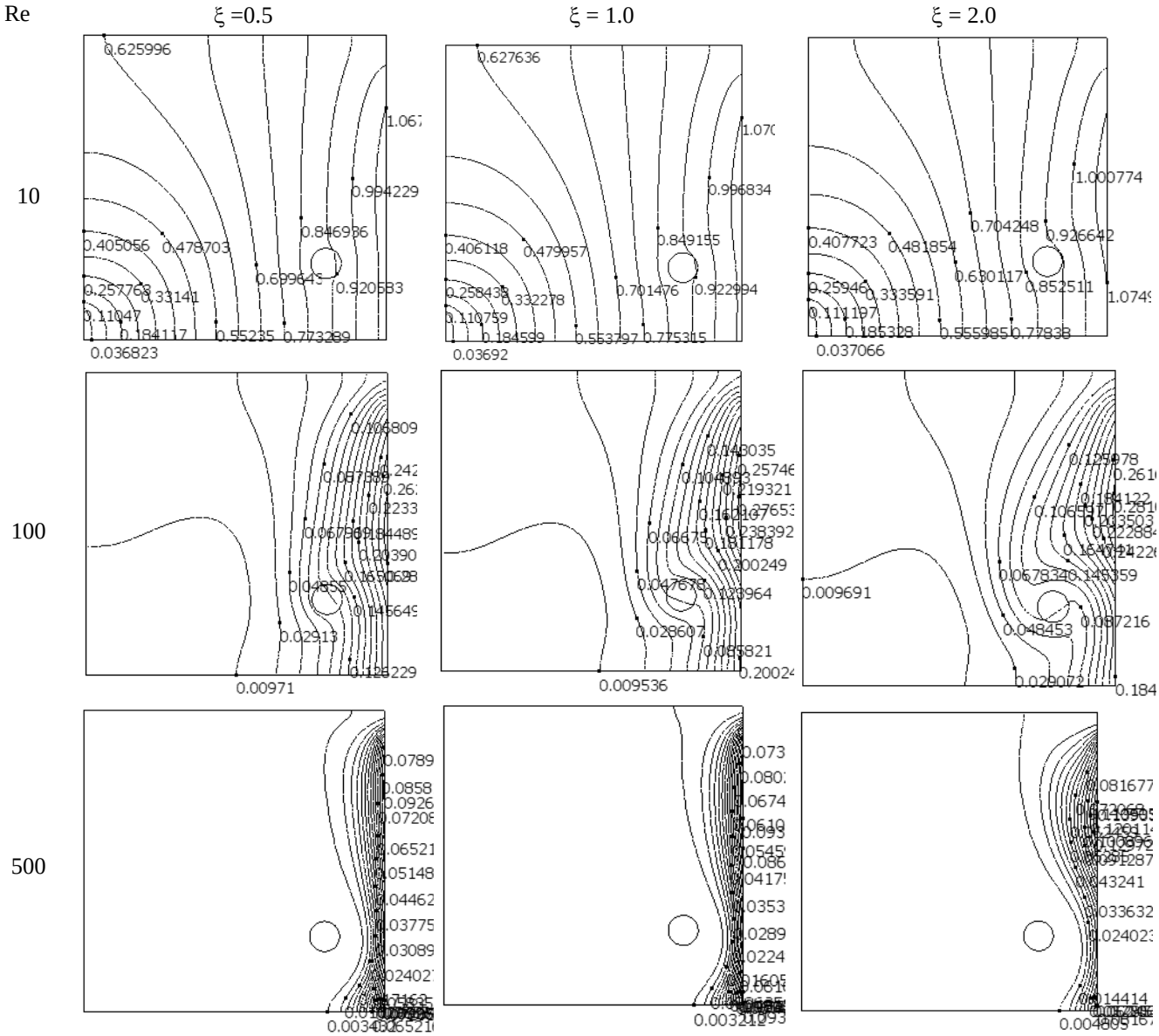

Figure 5.2.5: Thermal field inside ventilated cavity for different speed ratios of the rotating cylinder (D/L = 0.1; X_c = 0.80, Y_c = 0.25) at Ri = 1.0.

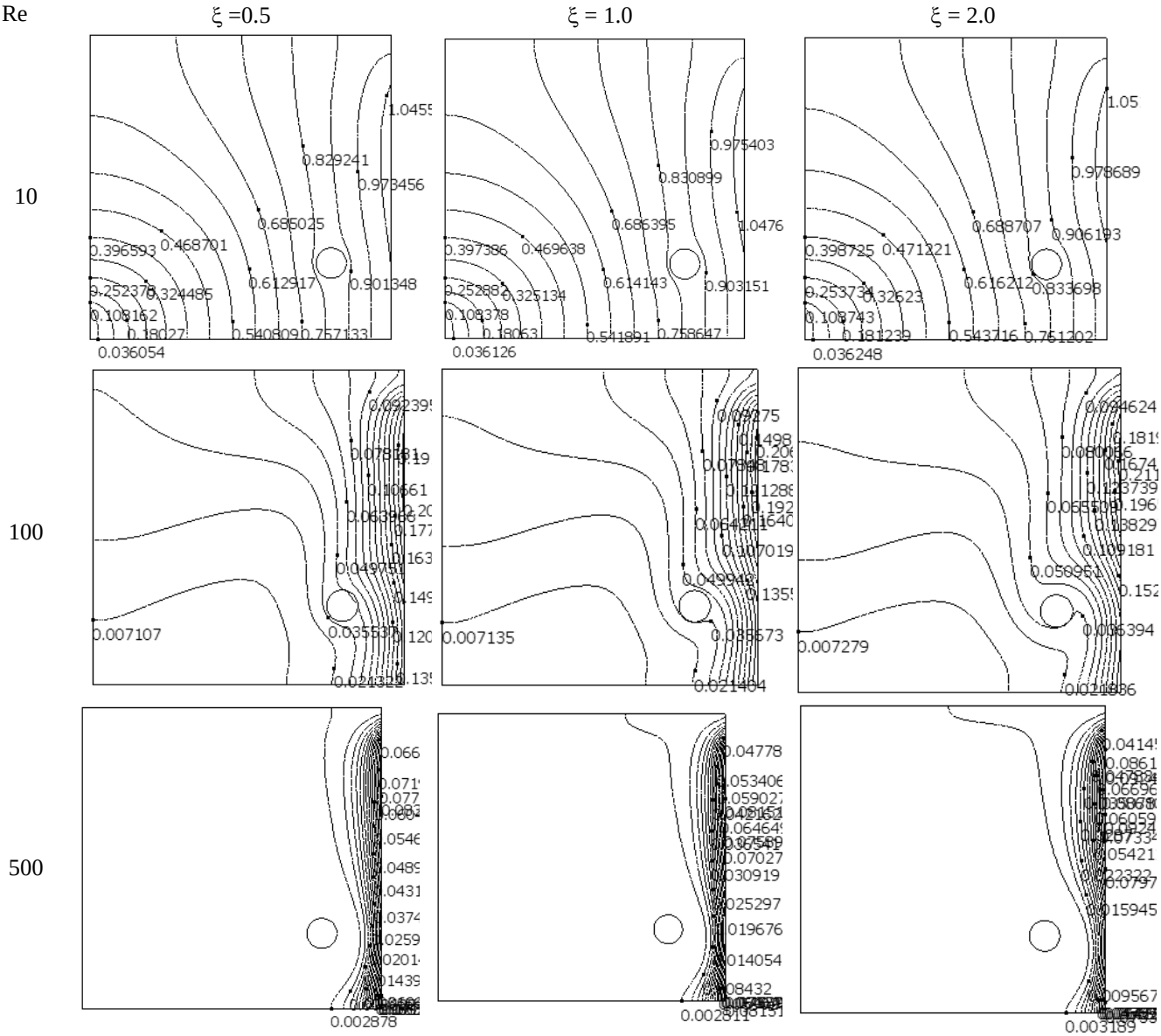

Figure 5.2.6: Thermal field inside ventilated cavity for different speed ratios of the rotating cylinder (D/L = 0.1; X_c = 0.80, Y_c = 0.25) at Ri = 10.0.

5.2.3. Effect of speed ratios of the cylinder on heatlines

Figure 5.2.7 to Figure 5.2.9 show the heat line distribution inside a ventilated cavity for different speed ratios of the rotating cylinder at different Richardson number (*Ri* =0.1, 1 and 10) for different Reynolds number (*Re* = 10, 100 and 500). In Figure 5.2.7, heat line distributions for different *Re* and different speed ratios of the rotating cylinder at *Ri* = 0.1 is shown. The heat lines in the ventilated cavity, for all speed ratios, at *Re* = 10 is mostly diagonal straight lines which indicates that most of the heat flows in this diagonally, although distortions in the heat flow is visible in the upper triangle of the cavity and near the rotating cylinder.

As the cylinder is rotating counterclockwise so the heat is flowing along the circumference of the cylinder and flowing from left to the top of the cavity for all speed ratios. For, *Re* =100, there is a presence of counter clockwise circulation along with finely distributed heat lines from the inlet to the outlet and like before distorted heat lines near the rotating cylinder. It is evident that, for all speed ratios the vortex has the maximum strength near its core except when the speed ratio is equal to unity the vortex has the maximum strength at its core. Flow separation at the right wall is evident for higher speed ratios and found maximum when speed ratio is equal to 2 due to larger inertia force due to the rotation of the cylinder. In case of higher *Re* (*Re* = 500), the strength of the vortex decreases although the span increases and pushes the heat lines towards the bottom and right sidewalls for all speed ratios. However, the strength of the vortex is higher for high speed ratio and at speed ratio equal to 2 flow separation at the right hot wall is visible.

In Figure 5.2.8, heat line distributions for different *Re* and different speed ratios of the rotating cylinder at *Ri* = 1 is shown. For *Re* = 10 the flow in the ventilated cavity for all speed ratio is mostly same and flow separation is present which is not the case for *Ri* = 1. For, *Re* =100, like before, there is also a presence of counter clockwise circulation along with finely distributed heat lines. However, for speed ratio equal to 0.5 the strength of the vortex is low which for higher speed ratios is higher. In case of higher *Re* (*Re* = 500), similar trend of heat flow pattern is observed like that is in case of *Ri* = 0.1 which is, the span of the vortex increases at the cost of its strength and pushes the heat lines towards the bottom and right sidewalls for all speed ratios.

In Figure 5.2.9, heat line distributions for different *Re* and for different speed ratios of the rotating cylinder at *Ri* = 10 is shown. It is evident from the figure that for *Ri* = 10 at low *Re* (*Re* =

10), there is a presence of counterclockwise vortex in the cavity for all speed ratios which is very much unlikely for lower *Ri*. At *Re* = 100, the strength of the vortex is higher at the outer region for speed ratio 0.5 and 1 and for speed ratio 2 the vortex strength is seem to be lowered. However, at *Re* = 500, the strength of the vortex increased in the outer region of the vortex whilst the strength of the vortices for lower speed ratios decreased. Majority of the heat line is similar to that of at lower *Ri*.

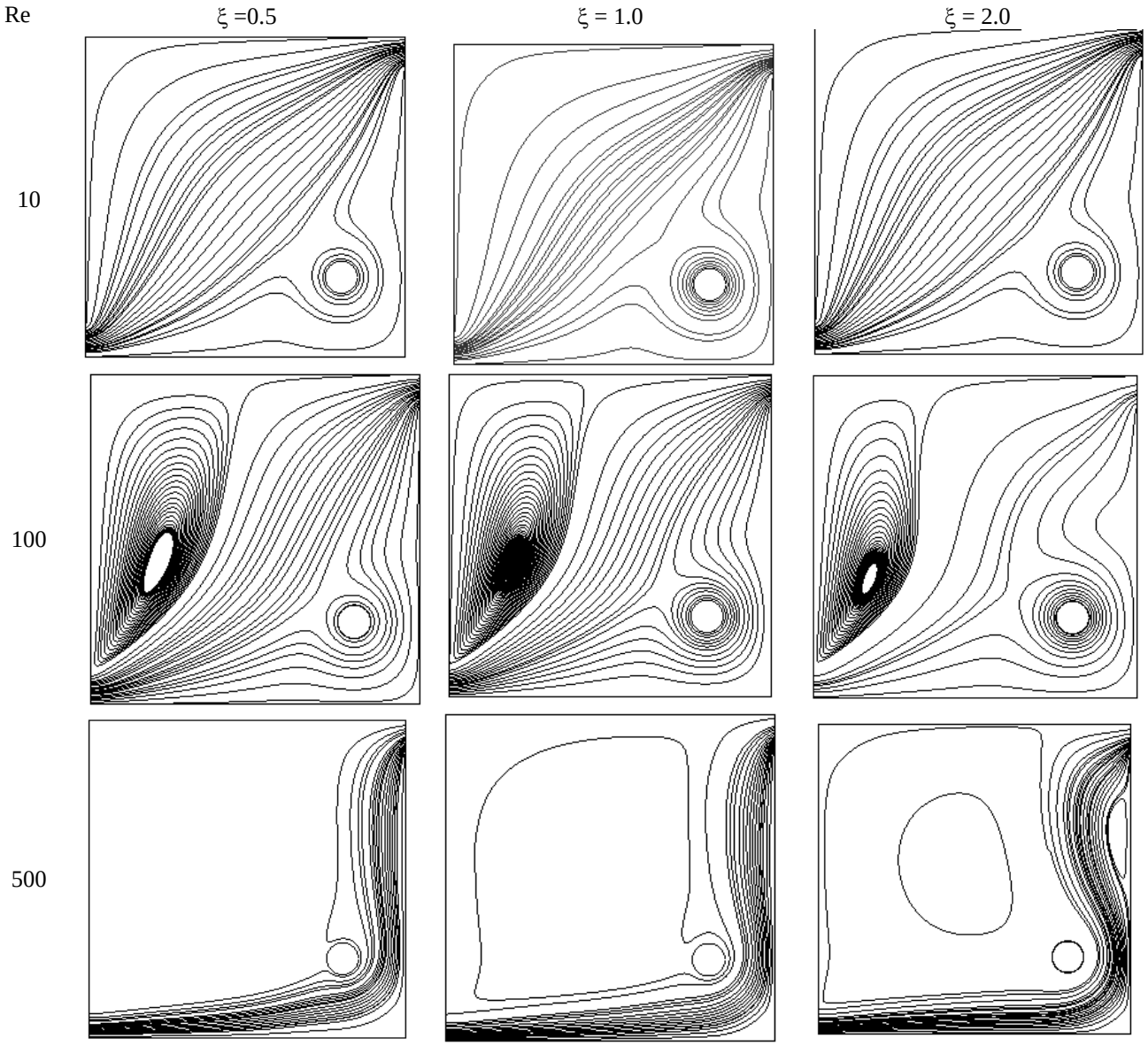

Figure 5.2.7: Heat lines inside ventilated cavity for different speed ratios of the rotating cylinder (D/L = 0.1; X_c = 0.80, Y_c = 0.25) at Ri = 0.1.

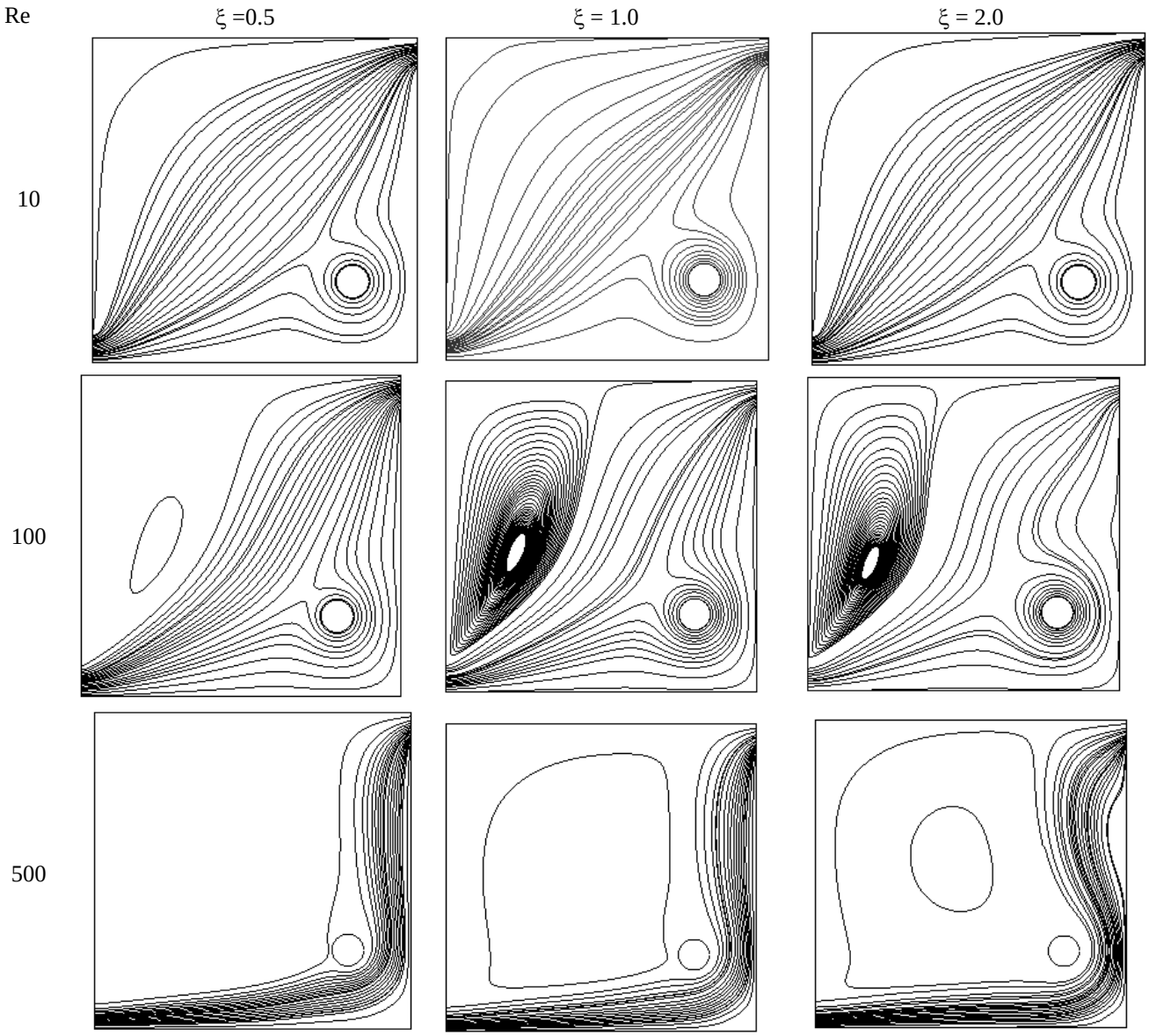

Figure 5.2.8: Heat lines inside ventilated cavity for different speed ratios of the rotating cylinder (D/L = 0.1; X_c = 0.80, Y_c = 0.25) at Ri = 1.0.

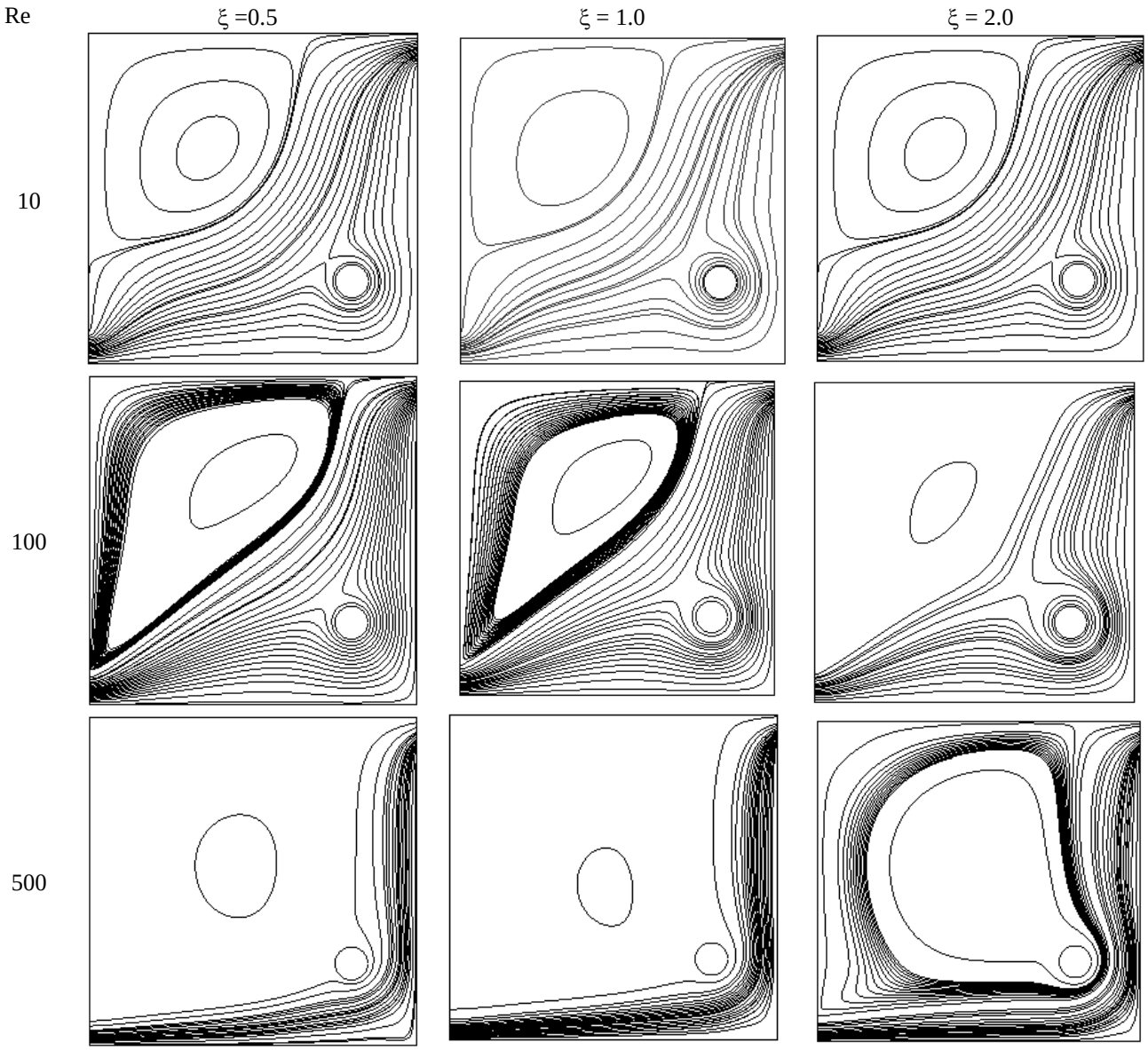

Figure 5.2.9: Heat lines inside ventilated cavity for different speed ratios of the rotating cylinder (D/L = 0.1; X_c = 0.80, Y_c = 0.25) at Ri = 10.0.

5.2.4. Effect of speed ratios of the cylinder on the heat transfer rate

Figure 5.2.10 shows the variation of normalized heat transfer rate at *Re* = 10 with different Richardson number for different speed ratios. It is obvious from the figure that for all speed ratios the heat transfer rate at this *Re* is similar and slightly better than when there is no cylinder. However, after about *Ri* = 2.5 the heat transfer rate decreased from that of when there is no cylinder for all speed ratios.

Figure 5.2.11 shows the variation of normalized heat transfer rate at *Re* = 50 with different Richardson number for different speed ratios. From the figure it is obvious that when the speed ratio is equal to 1 and 2 the heat transfer rate is better than when there is no cylinder in the cavity for all *Ri*, although there is a variation for different *Ri*. The highest heat transfer is found for both the cases at *Ri* = 10. When the speed ratio is zero, the cylinder is stationary, the heat transfer rate is lower than when there is no cylinder for all *Ri* and the lowest value is found at about *Ri* = 5. And in case of speed ratio equal to 0.5 the rate is slightly better at low *Ri*, however with increasing *Ri* the heat transfer rate decreases. At this *Re* the highest rate is found at speed ratio 2 and at *Ri* = 10.

Figure 5.2.12 shows the variation of normalized heat transfer rate at *Re* = 100 with different Richardson number for different speed ratios. It is obvious from the figure that for all rotating cylinders the heat transfer is better than when there is no cylinder whilst stationary cylinder has lower rate for all *Ri* though there is variation of performance with increasing *Ri*. The highest heat transfer rate is found at about *Ri* = 2.5 when the speed ratio equal to 2 at this *Re*.

Figure 5.2.13 shows the variation of normalized heat transfer rate at *Re* = 250 with different Richardson number for different speed ratios. It is obvious from the figure that for all speed ratios the heat transfer rate is better for all *Ri*. However, at this *Re* the highest heat transfer rate is evident at *Ri* = 0.1 when the speed ratio is 1.

Figure 5.2.14 shows the variation of normalized heat transfer rate at *Re* = 500 with different Richardson number for different speed ratios. It is obvious from the figure that at this *Re* for all speed ratios the heat transfer rate is better and the highest value is found at *Ri* = 0.1 for speed ratio 2.

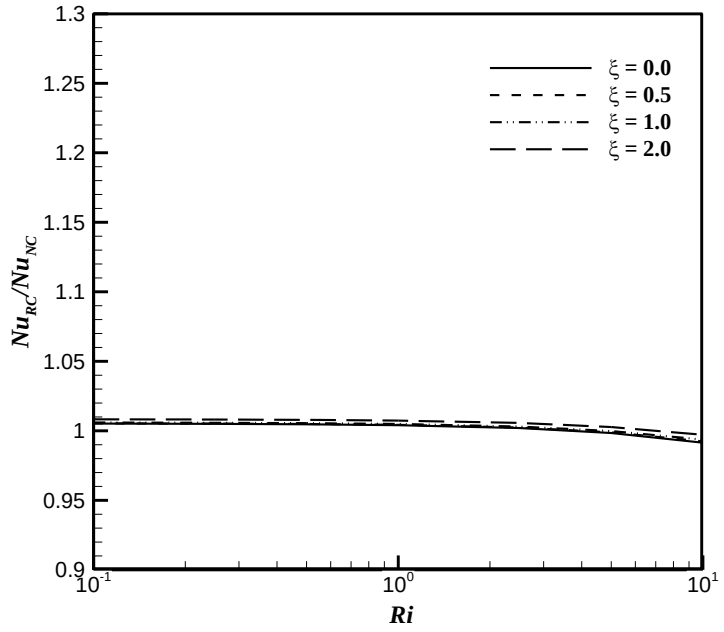

Figure 5.2.10: Normalized Nusselt No. variation with Richardson number (*Ri*) for different speed ratios of the rotating cylinder (ξ) at *Re* = 10

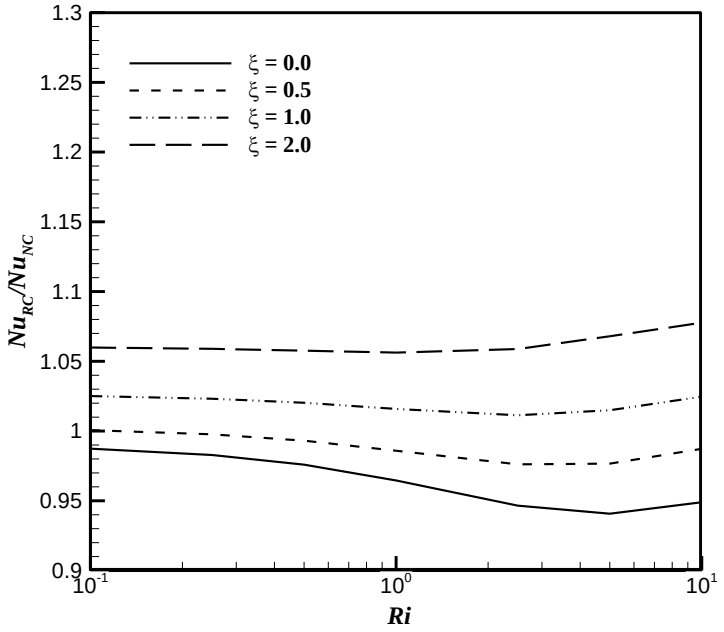

Figure 5.2.11: Normalized Nusselt No. variation with Richardson number (*Ri*) for different speed ratios of rotating cylinder (ξ) at *Re* = 50

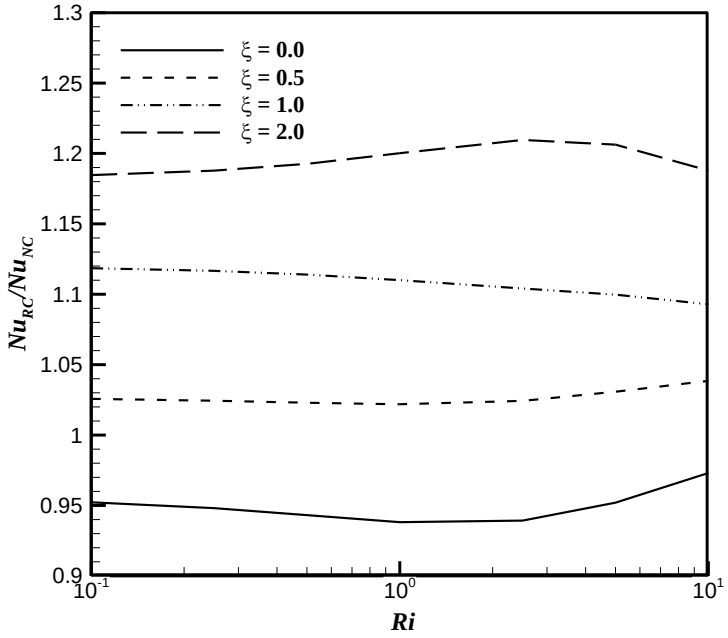

Figure 5.2.12: Normalized Nusselt No. variation with Richardson number (*Ri*) for different speed ratios of rotating cylinder (ξ) at *Re* = 100

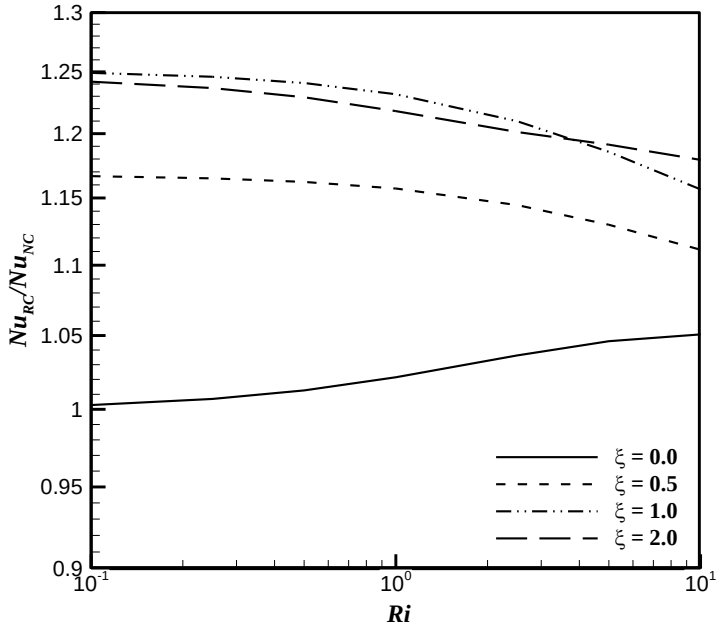

Figure 5.2.13: Normalized Nusselt No. variation with Richardson number (*Ri*) for different speed ratios of rotating cylinder (ξ) at *Re* = 250

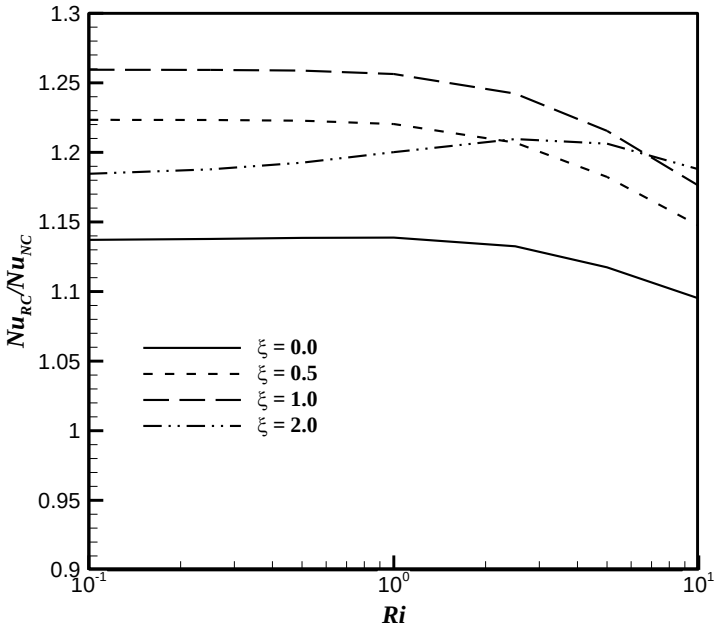

Figure 5.2.14: Normalized Nusselt No. variation with Richardson number (*Ri*) for different speed ratios of rotating cylinder (ξ) at *Re* = 500

5.3. Effect of size of the rotating cylinder inside ventilated cavity

5.3.1. Effect of size of the cylinder on streamlines

The streamline pattern inside a ventilated cavity for different non-dimensional diameters (*D/L*) of the rotating cylinder(ξ=1.0; X_c = 0.8, Y_c = 0.25) at different Richardson number (*Ri* =0.1, 1 and 10) for different Reynolds number (*Re* = 10, 100 and 500) are shown in Figure 5.3.1 to Figure 5.3.3.

In Figure 5.3.1, streamline patterns for different *Re* and different non-dimensional diameters at *Ri* = 0.1 is shown. The flow in the ventilated cavity, at *Re* = 10 for all non-dimensional diameters, is mostly diagonal streamline flow. However, presence of the rotating cylinder distorts the flow and directs the flow along its boundary tangentially. With increasing diameter the inertia force is more dominant and the streamlines gets more distorted around the cylinder. For *D/L* = 0.15 there is a counterclockwise vortex in the cavity which is not present for other diameters whereas for *D/L* = 0.2, flow separation is taking place. For, *Re* =100, there is a presence of counter clockwise circulation which is more strong at the center of the vortex. It is also observed that, for all non-dimensional diameters a portion of the streamlines also distorts around the cylinder tangentially which increases with increase in diameter due to large inertia force for large diameter. In this case, the flow is also separating in the bottom and right wall.

In case of higher *Re* (*Re* = 500), the span of the vortex increases and pushes the streamline flow towards the right sidewall for all non-dimensional diameters, though the strength of the vortex minimizes. However, in case of stationary cylinder configuration the cylinder works as an obstruction in the streamline flow path whereas for rotational cylinder configuration the vortex strength increases again and pushes the streamline flow towards the bottom right corner of the cavity and the cylinder acts as a driving force for the streamline flow which is evident in the figure, however at *Re* =500 for *D/L* = 0.2 the distortion is a maximum and hence flow separation at the right wall.

In Figure 5.3.2, streamline patterns for different *Re* and different non-dimensional diameters of the rotating cylinder at *Ri* = 1 is shown. For *Re* = 10 the flow in the ventilated cavity is almost

same as it was for *Ri* =0.1. For, *Re* =100, like before, there is also a presence of counter clockwise circulation along with fine streamline flow, however the vortex for *D/L* = 0.1 and *Re* = 100 has less strength. From the figure it is evident that flow separation is taking place for all non-dimensional diameters and *Re* = 100. In case of higher *Re* (*Re* = 500), similar trend of flow pattern observed that of in case of *Ri* = 0.1 is evident which is, the span of the vortex increases again and pushes the streamline flow towards the bottom right corner of the cavity and the cylinder acts as a driving force for the streamline flow and flow separation is also occurring.

In Figure 5.3.3, streamline patterns for different *Re* and different diameters of the rotating cylinder at *Ri* = 10 is shown. It is evident from the figure that for *Ri* = 10 at low *Re* (*Re* = 10) there is a presence of counterclockwise vortex in the cavity for all non-dimensional diameters. The vortex strength increases with higher *Re* and the presence of the cylinder influences the flow field similarly like it did for the cases of lower *Ri*, however for *Re* = 100 the vortices have less strength for *D/L* = 0.5 and 2 and for *D/L* = 1 the boundary region of the vortex has more strength than its core. At *Re* = 500, for *Ri* = 10 the streamlines follows similar trends as it was for lower *Ri*, however the inertia force of the cylinder is less dominant and flow separation does not occur for any diameter.

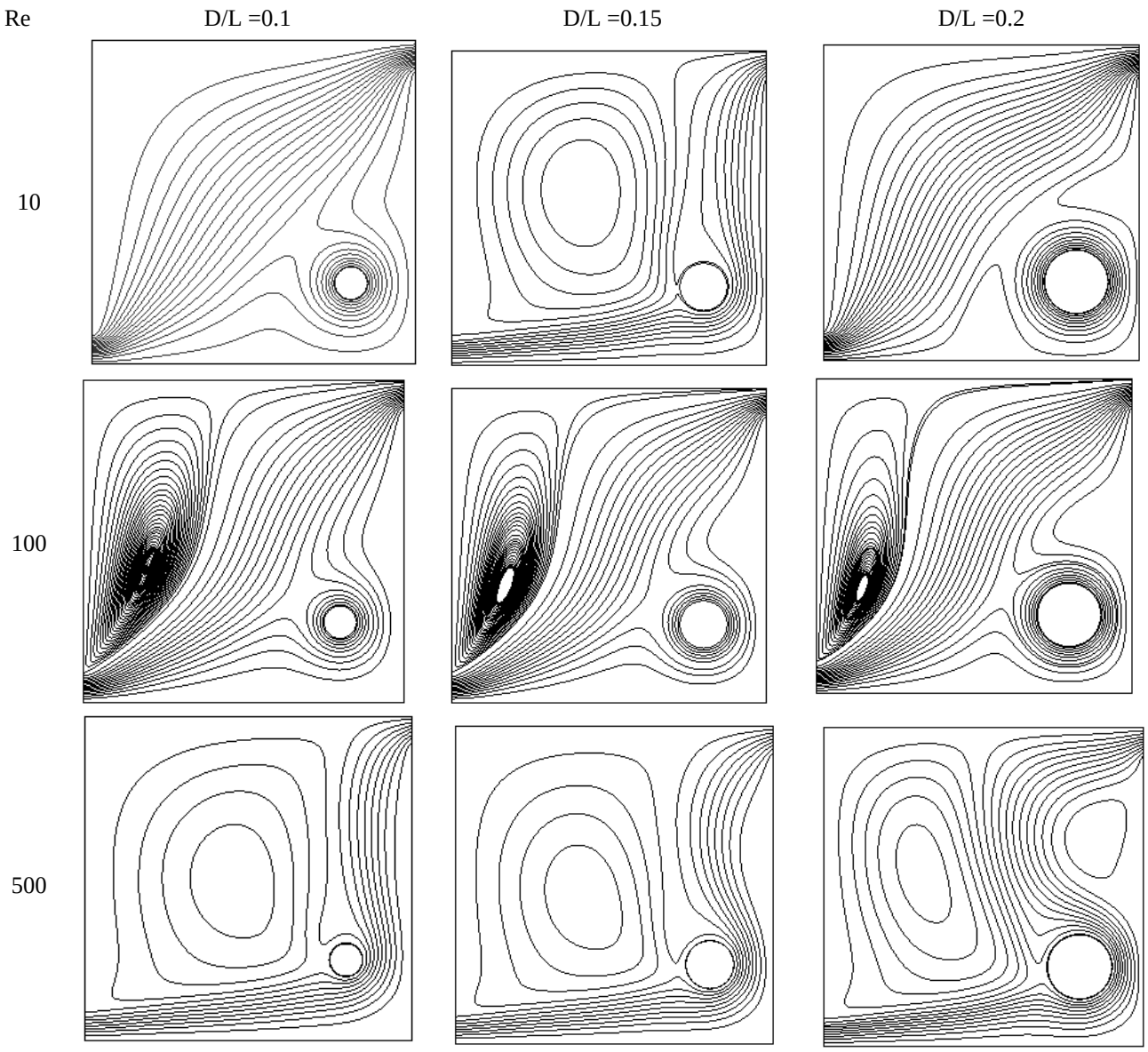

Figure 5.3.1: Streamline distribution inside ventilated cavity for different non-dimensional cylinder diameter of the rotating cylinder (ξ =1.0; X_c = 0.8, Y_c = 0.25) at Ri = 0.1.

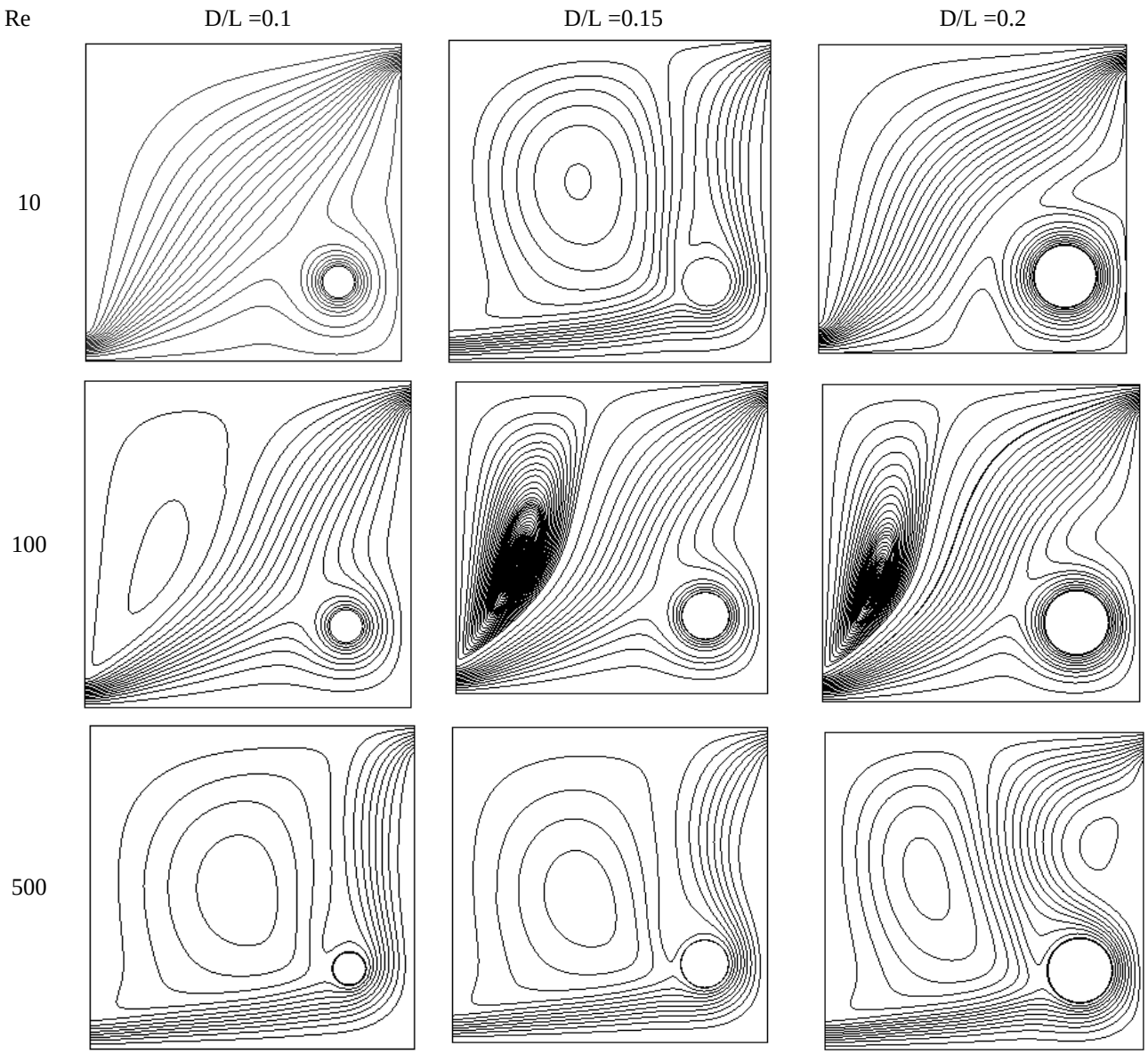

Figure 5.3.2: Streamline distribution inside ventilated cavity for different non-dimensional cylinder diameter of the rotating cylinder (ξ =1.0; X_c = 0.8, Y_c = 0.25) at Ri = 1.0.

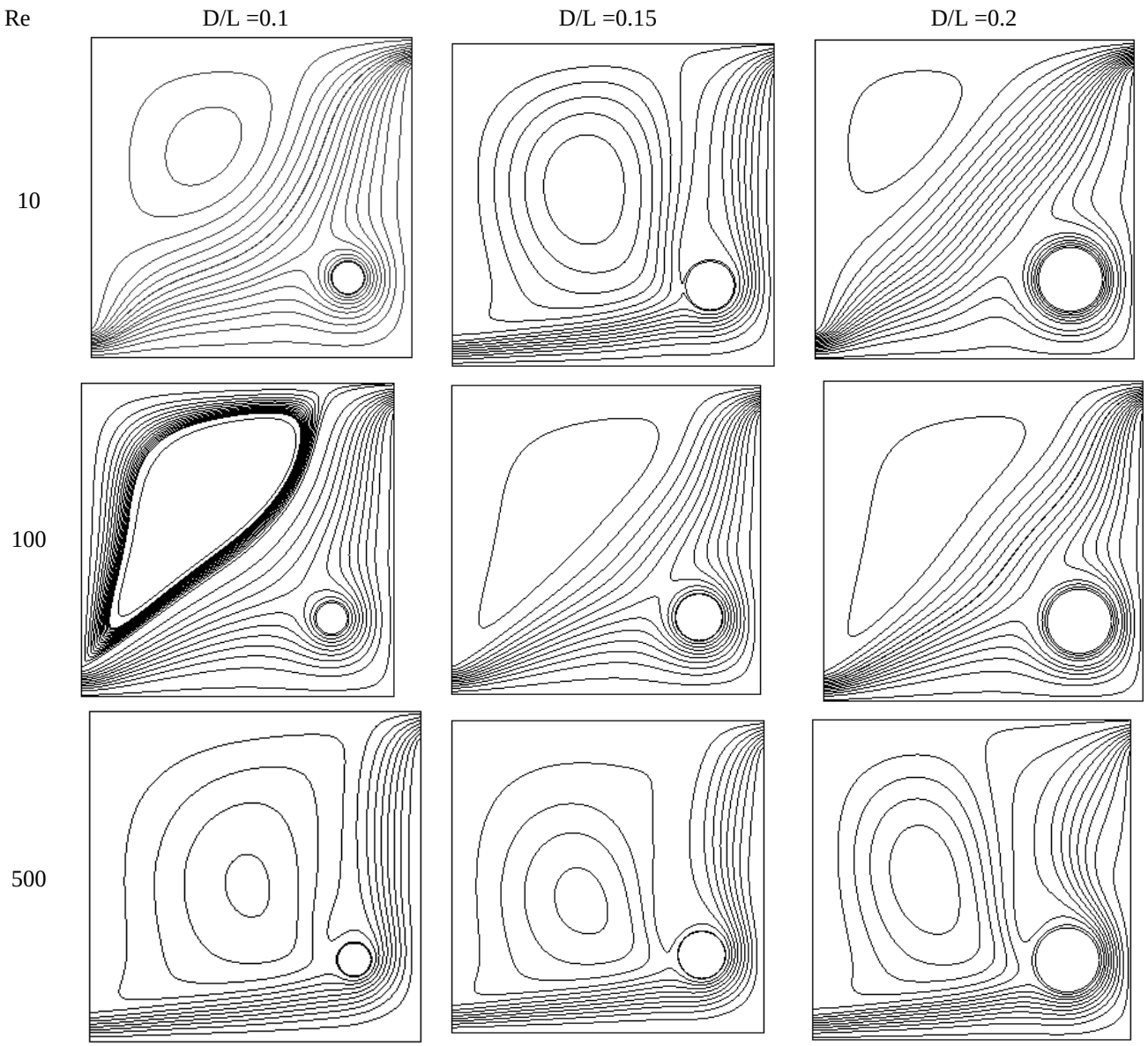

Figure 5.3.3: Streamline distribution inside ventilated cavity for different non-dimensional cylinder diameter of the rotating cylinder (ξ =1.0; X_c = 0.8, Y_c = 0.25) at Ri = 10.0.

5.3.2. Effect of size of the cylinder on isotherm contours

Figure 5.3.4 to Figure 5.3.6 show the isotherm contours inside a ventilated cavity for different non-dimensional diameters of the rotating cylinder at different Richardson number (*Ri* =0.1, 1 and 10) for different Reynolds number (*Re* = 10, 100 and 500). In Figure 5.3.4, isotherm contours for different *Re* and non-dimensional diameters at *Ri* = 0.1 is shown. It is evident from the Figure 5.2.4 that at *Ri* = 0.1 for low *Re* the isothermal contours are distributed throughout the cavity for all non-dimensional diameters. However, with increase in *Re* the isotherms are pushed to the right side of the cavity which indicates that most of the cavity is cold. Due to the presence of rotating cylinder the isotherms near the cylinder distorts and where the scale of distortion increases with increasing diameter. For *Re* = 500, the isotherms are more densely distributed near the right hot wall and with increase in the diameter the isotherms gets more distorted, where in case of *D/L* = 0.2 the isotherms are more distorted due to large inertia force.

It is evident from the Figure 5.3.5 and 5.3.6 that at *Ri* = 1 and 10 for low *Re* the isothermal contours are distributed throughout the cavity for all non-dimensional diameters which is similar to the case of *Ri* = 0.1. Also similar to *Ri* = 0.1, with increase in *Re* the isotherms are densely distributed in the right side of the cavity which indicates that most of the cavity is cold and with increase in the diameter the isotherms near the cylinder distorts more than lower diameters of the cylinder. Similarly, for *Re* = 500, the isotherms are also more densely distributed near the right hot wall and more distorted for *D/L* = 0.2 like that in case of *Ri* = 0.1.

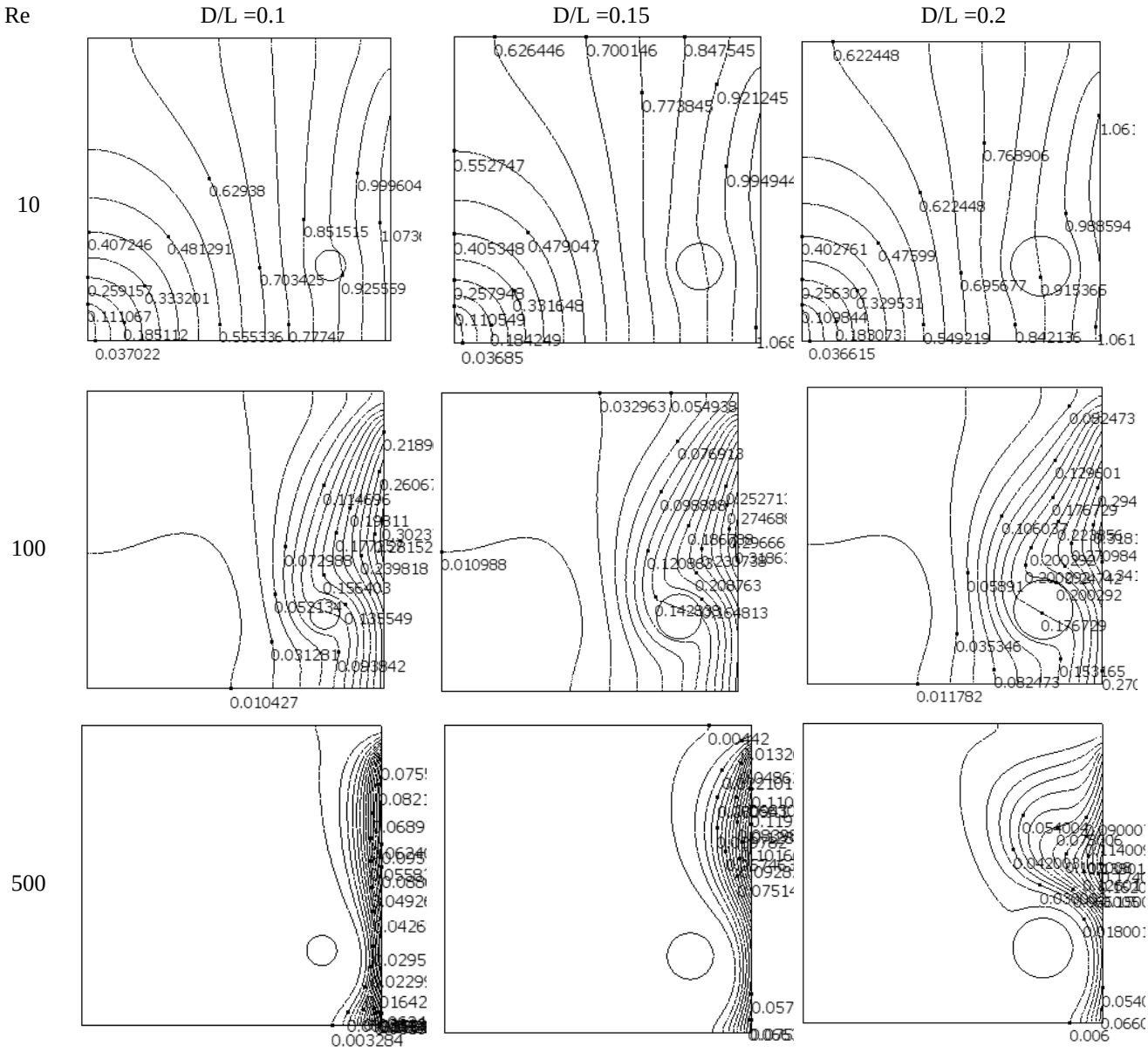

Figure 5.3.4: Thermal field inside ventilated cavity for different non-dimensional cylinder diameter of the rotating cylinder (ξ =1.0; X_c = 0.8, Y_c = 0.25) at Ri = 0.1.

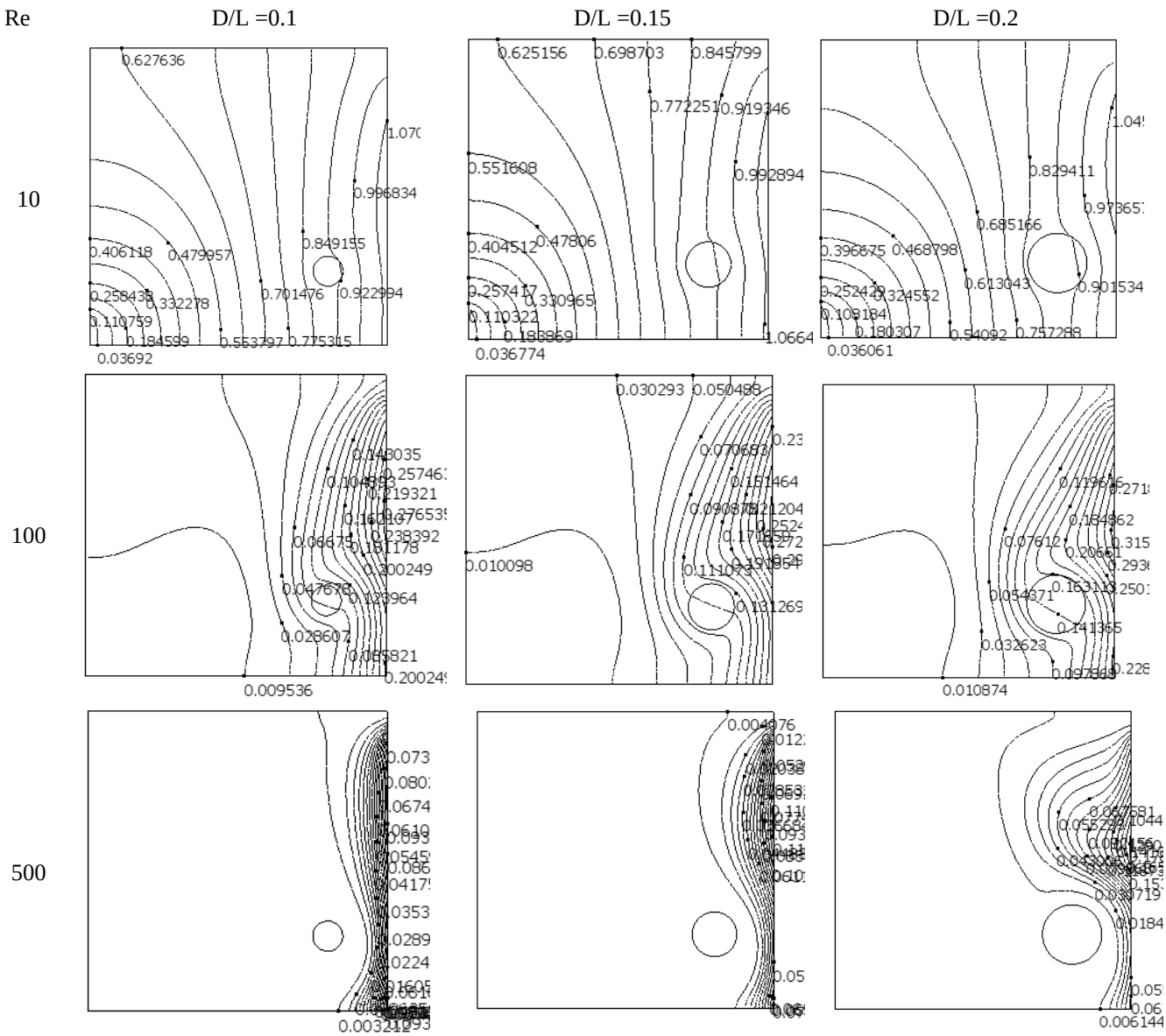

Figure 5.3.5: Thermal field inside ventilated cavity for different non-dimensional cylinder diameter of the rotating cylinder (ξ =1.0; X_c = 0.8, Y_c = 0.25) at Ri = 1.0.

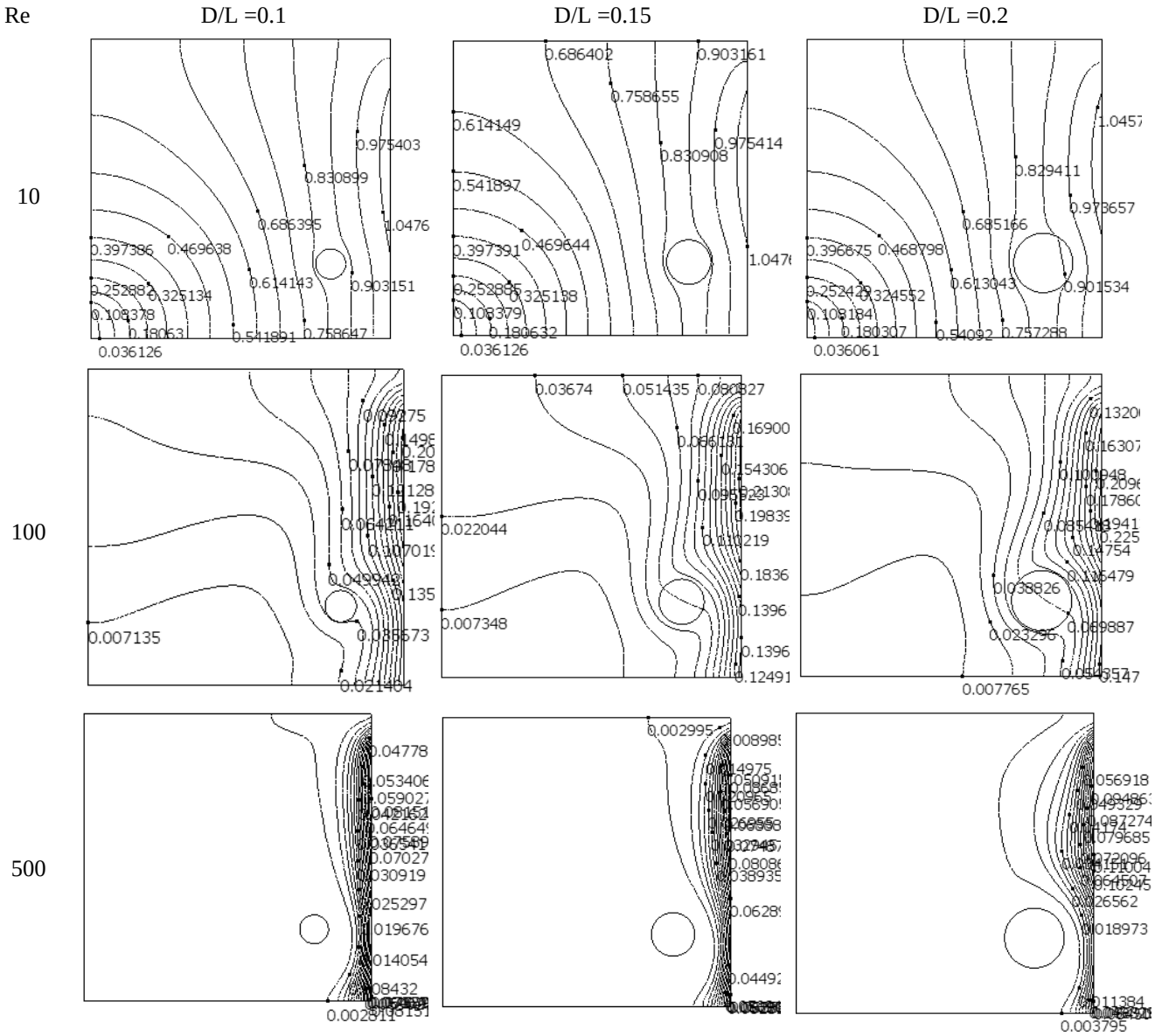

Figure 5.3.6: Thermal field inside ventilated cavity for different non-dimensional cylinder diameter of the rotating cylinder (ξ =1.0; X_c = 0.8, Y_c = 0.25) at Ri = 10.0.

5.3.3. Effect of size of the cylinder on heatlines

Figure 5.3.7 to Figure 5.3.9 show the heat line distribution inside a ventilated cavity for different non-dimensional diameters of the rotating cylinder at different Richardson number (*Ri* =0.1, 1 and 10) for different Reynolds number (*Re* = 10, 100 and 500). In Figure 5.3.7, heat line distributions for different *Re* and different diameters of the rotating cylinder at *Ri* = 0.1 is shown. The heat lines in the ventilated cavity, for all non-dimensional diameters, at *Re* = 10 is mostly diagonal straight lines which indicates that most of the heat flows diagonally, although distortions in the heat flow is visible in the upper triangle of the cavity and near the rotating cylinder.

In Figure 5.3.8, heat line distributions for different *Re* and different non-dimensional diameters of the rotating cylinder at *Ri* = 1 is shown. For *Re* = 10, the flow in the ventilated cavity for all diameters is mostly same and flow separation is present which is not the case for *Ri* = 1. For, *Re* =100, like before, there is also a presence of counter clockwise circulation along with finely distributed heat lines. In case of higher *Re* (*Re* = 500), similar trend of heat flow pattern is observed like that is in case of *Ri* = 0.1 which is, the span of the vortex increases at the cost of its strength and pushes the heat lines towards the bottom and right sidewalls for *D/L* = 0.1 and 0.2 and for *D/L* = 0.15 the vortex is strong at its boundary.

In Figure 5.3.9, heat line distributions for different *Re* and for different non-dimensional diameters of the rotating cylinder at *Ri* = 10 is shown. It is evident from the figure that for *Ri* = 10 at low *Re* (*Re* = 10) there is a presence of counterclockwise vortex in the cavity for all non-dimensional diameters which is very much unlikely for lower *Ri*. At *Re* = 100 the strength of the vortex is higher at the outer region for *D/L* = 0.1 and 0.15 and for *D/L* = 0.2 the vortex is diminished. However, at *Re* = 500 the strength of the vortices for lower non-dimensional diameters decreased. Majority of the heat line is similar to that of at lower *Ri*.

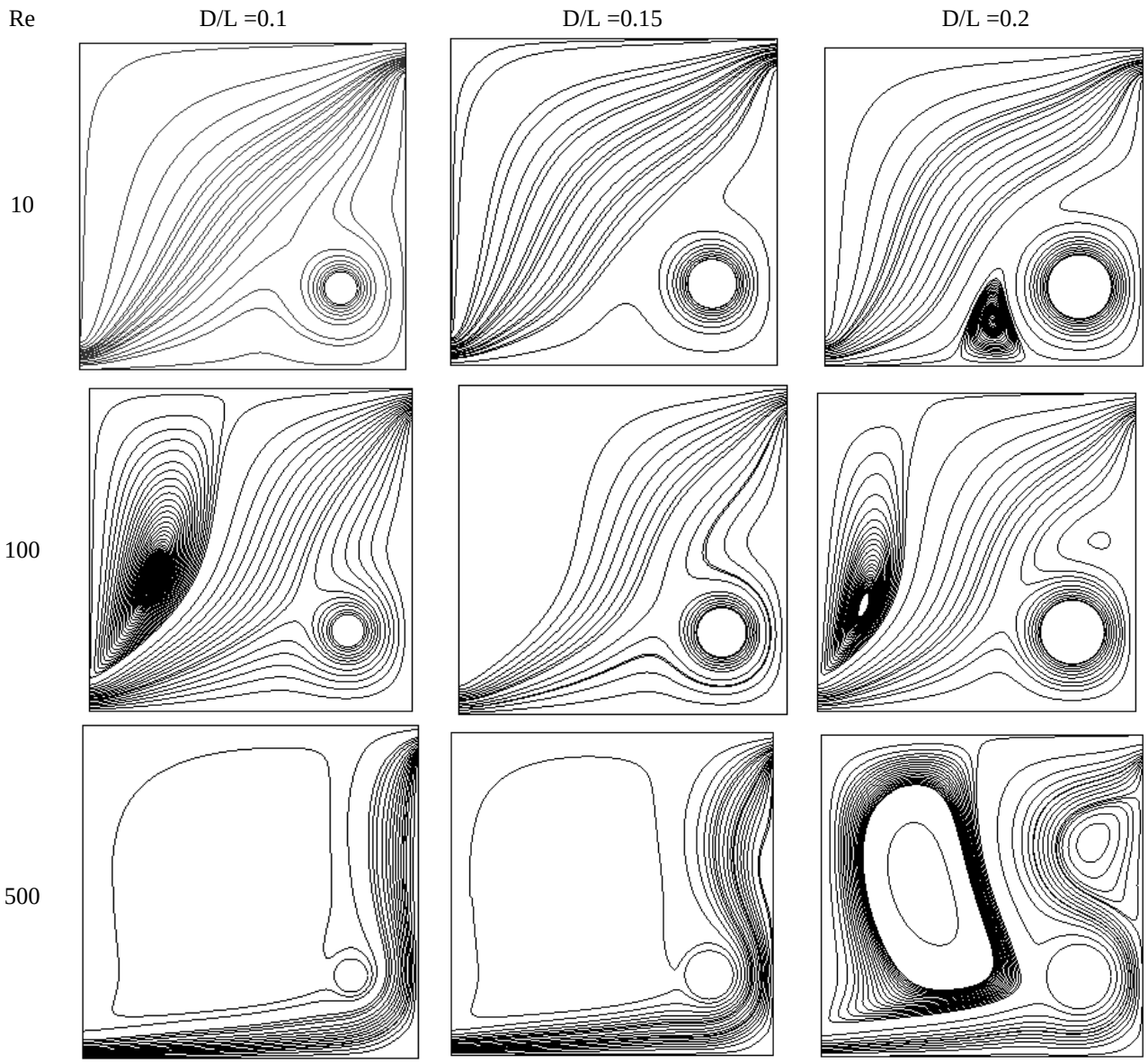

Figure 5.3.7: Heat lines inside ventilated cavity for different non-dimensional cylinder diameter of the rotating cylinder (ξ =1.0; X_c = 0.8, Y_c = 0.25) at Ri = 0.1.

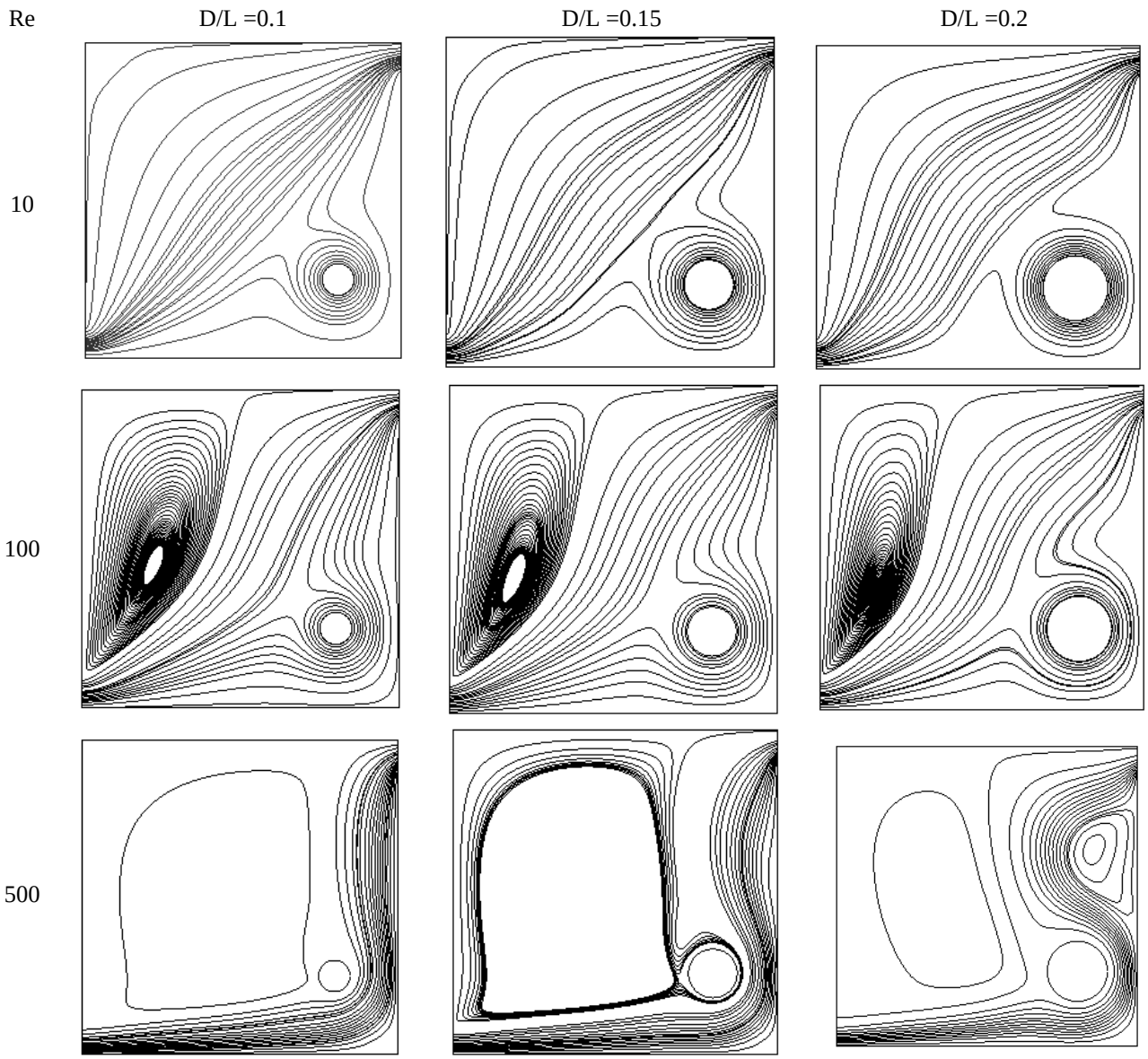

Figure 5.3.8: Heat lines inside ventilated cavity for different non-dimensional cylinder diameter of the rotating cylinder (ξ =1.0; X_c = 0.8, Y_c = 0.25) at Ri = 1.0.

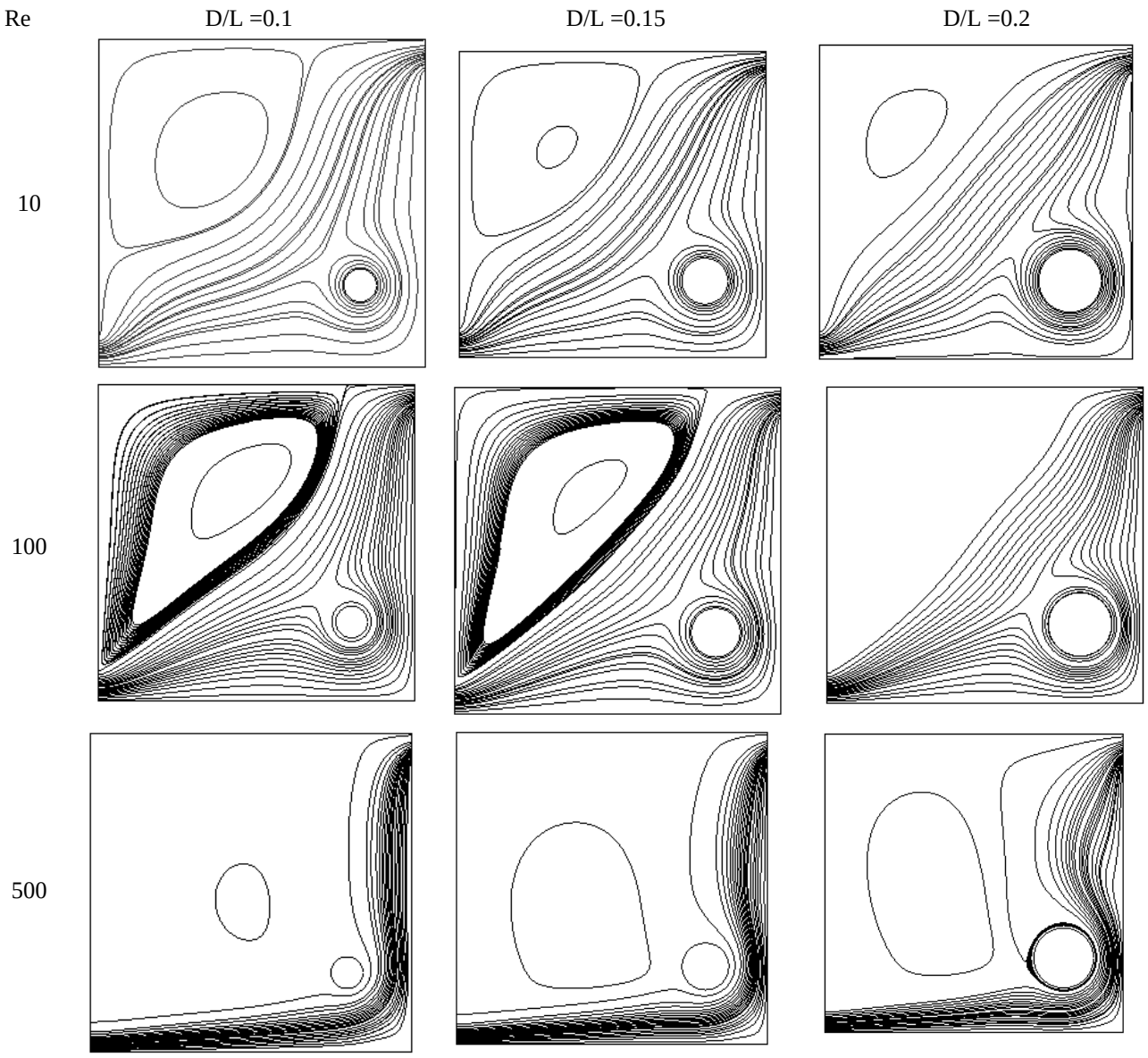

Figure 5.3.9: Heat lines inside ventilated cavity for different non-dimensional cylinder diameter of the rotating cylinder (ξ =1.0; X_c = 0.8, Y_c = 0.25) at Ri = 10.

5.3.4. Effect of size of the cylinder on the heat transfer rate

Figure 5.3.10 shows the variation of normalized heat transfer rate at *Re* = 10 with different Richardson number for different non-dimensional diameters. It is obvious from the figure that for all non-dimensional diameters the heat transfer rate at this *Re* is slightly better than when there is no cylinder. However, there is variation of the heat transfer rate with variation in *Ri*. The heat transfer rate decreased from that of when there is no cylinder for all non-dimensional diameters for higher *Ri*.

Figure 5.3.11 shows the variation of normalized heat transfer rate at *Re* = 50 with different Richardson number for different non-dimensional diameters. From the figure it is obvious that when the *D/L* = 0.1 the heat transfer rate is better than when there is no cylinder in the cavity for all *Ri*, although there is a variation for different *Ri*. The highest heat transfer rate is found for both the cases at *Ri* = 10. Larger diameter cylinder has low heat transfer rate than when there is no cylinder for all *Ri* and the lowest value is found at about *Ri* = 5. And in case of *D/L* = 0.15 the heat transfer rate is slightly better at low *Ri*, yet with increasing *Ri* the heat transfer rate decreases. At this *Re* the highest heat transfer rate is found at *D*/*L*= 0.2 and at *Ri* = 10.

Figure 5.3.12 shows the variation of normalized heat transfer rate at *Re* = 100 with different Richardson number for different non-dimensional diameters. It is obvious from the figure that for all diameters the heat transfer is better than when there is no cylinder for all *Ri* though there is variation of heat transfer rate with increasing *Ri*. The highest heat transfer rate is found at about *Ri* = 0.1 when the *D/L* = 0.1 at this *Re.*

Figure 5.3.13 shows the variation of normalized heat transfer rate at *Re* = 10 with different Richardson number for different non-dimensional diameters. It is obvious from the figure that for all non-dimensional diameters the heat transfer rate is better for all *Ri*. However, at this *Re* heat transfer rate is evident at *Ri* = 0.1 when the *D/L* = 0.1.

Figure 5.3.14 shows the variation of normalized heat transfer rate at *Re* = 10 with different Richardson number for different non-dimensional diameters. It is obvious from the figure that at this *Re* for all non-dimensional diameters the heat transfer rate is better and the highest value is found at *Ri* = 0.1 for *D/L* = 0.1.

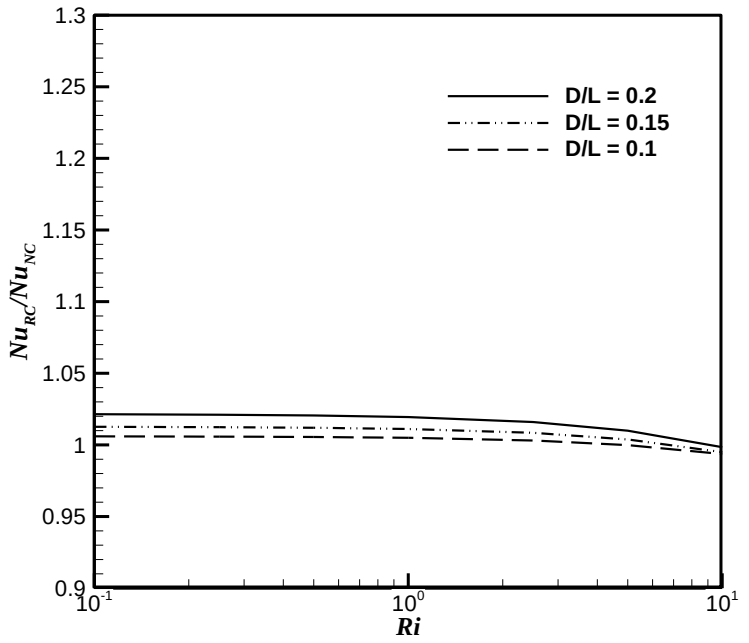

Figure 5.3.10: Normalized Nusselt No. variation with Richardson number (*Ri*) for different non-dimensional diameter (*D*/*L*) of the rotating cylinder (ξ =1.0; X_c = 0.8, Y_c = 0.25) at *Re* = 10

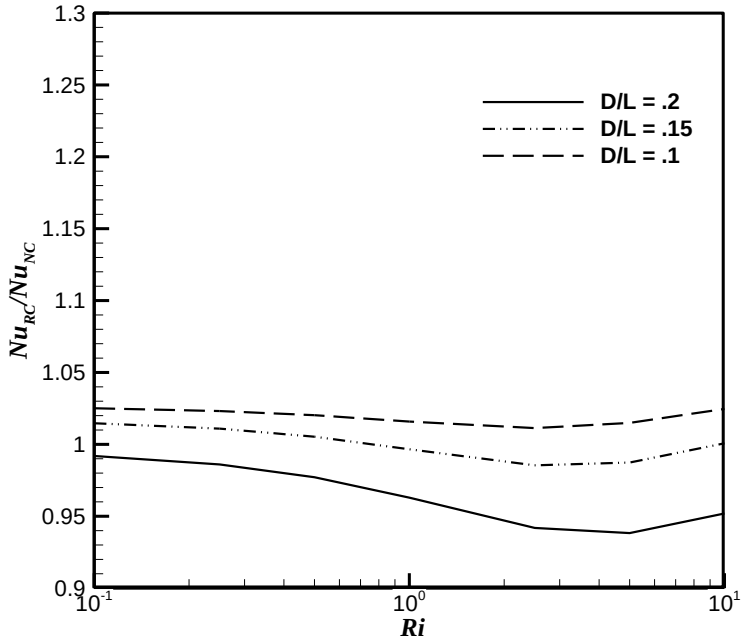

Figure 5.3.11: Normalized Nusselt No. variation with Richardson number (*Ri*) for different non-dimensional diameter (*D*/*L*) of the rotating cylinder (ξ =1.0; X_c = 0.8, Y_c = 0.25) at *Re* = 50

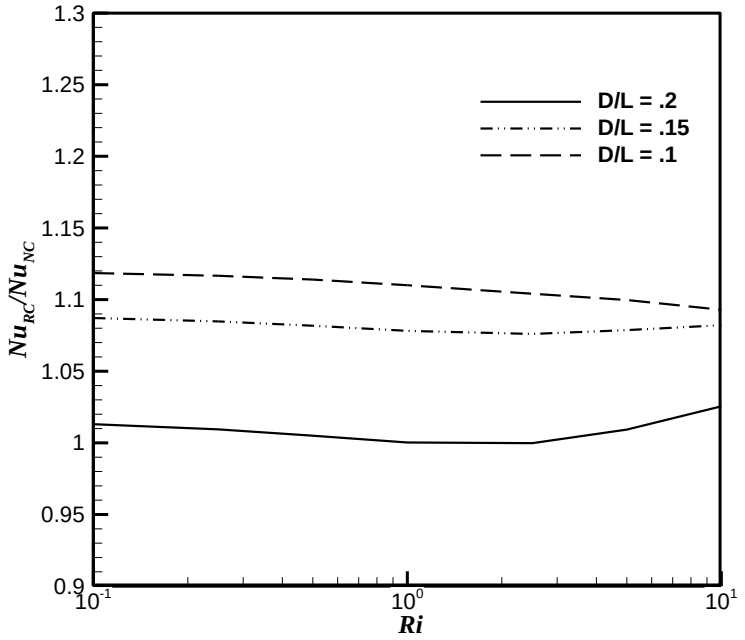

Figure 5.3.12: Normalized Nusselt No. variation with Richardson number (*Ri*) for different non-dimensional diameter (*D*/*L*) of the rotating cylinder (ξ =1.0; X_c = 0.8, Y_c = 0.25) at *Re* = 100

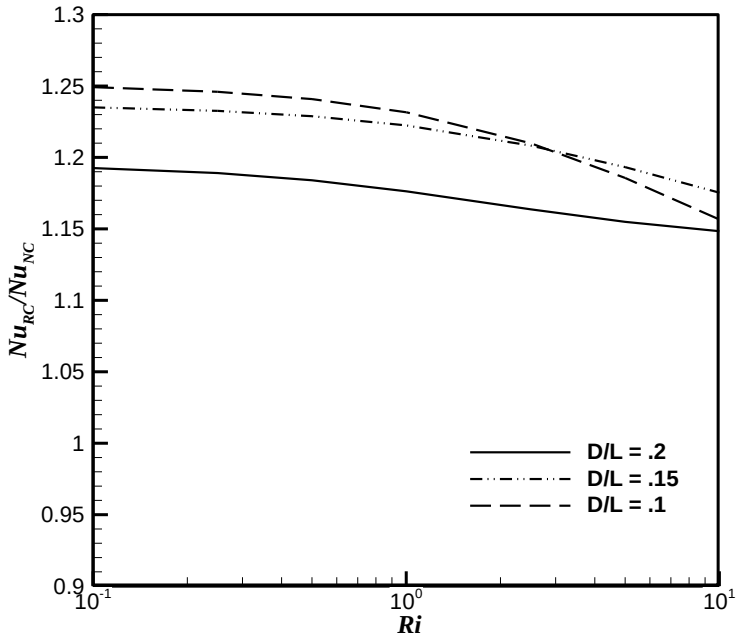

Figure 5.3.13: Normalized Nusselt No. variation with Richardson number (*Ri*) for different non-dimensional diameter (*D*/*L*) of the rotating cylinder (ξ =1.0; X_c = 0.8, Y_c = 0.25) at *Re* = 250

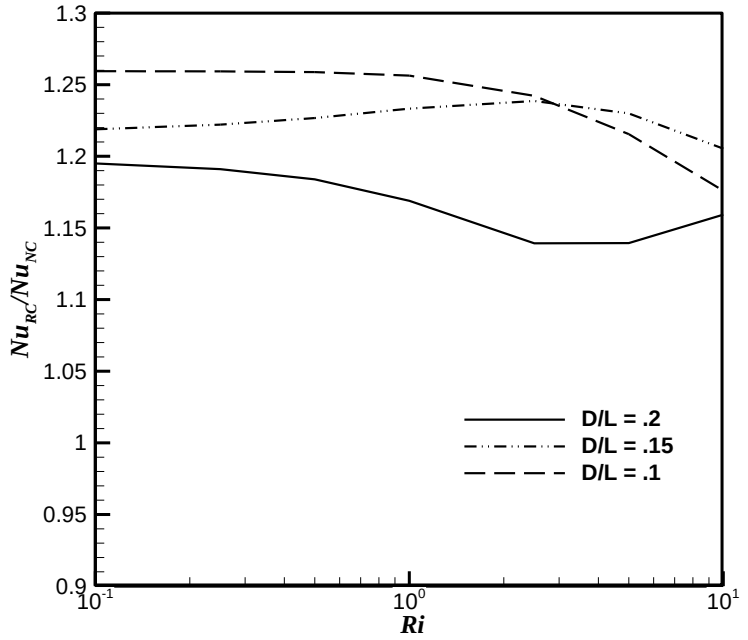

Figure 5.3.14: Normalized Nusselt No. variation with Richardson number (*Ri*) for different non-dimensional diameter (*D*/*L*) of the rotating cylinder (ξ =1.0; X_c = 0.8, Y_c = 0.25) at *Re* = 500

5.3.5. Effect of size of the cylinder on pumping power

Figure 5.3.15 shows the variation of % increase of pumping work at *Re* = 10 with different Richardson number for different non-dimensional diameters. From the figure, it is clear that for higher diameter cylinder the % increase of pumping work is higher and is also an increasing function of *Ri* while from Figure 5.3.10 it is evident that the heat transfer performance is low for higher diameters for higher *Ri*.

Figure 5.3.16 shows the variation of % increase of pumping work at *Re* = 100 with different Richardson number for different non-dimensional diameters. From the figure it is evident that for higher diameter cylinder the % increase of pumping work is higher although it is less than when *Re* = 10 and is also an increasing function of *Ri*. From Figure 5.3.12 it is clear that for *D/L* = 0.2 the heat transfer performance is highest at *Ri* = 0.1 which is at the expense of 1.1 % increase of pumping work.

Figure 5.3.17 shows the variation of % increase of pumping work at *Re* = 500 with different Richardson number for different non-dimensional diameters. In this case the % increase of pumping work is in the range of about 7.5% to 7.85% for *Ri* =0.1 and also an increasing function of *Ri*. Highest heat transfer performance can be achieved at *Ri* = 0.1 and *D/L* = 0.2 at the expense of about 7.85% increase of pumping work at this *Re*.

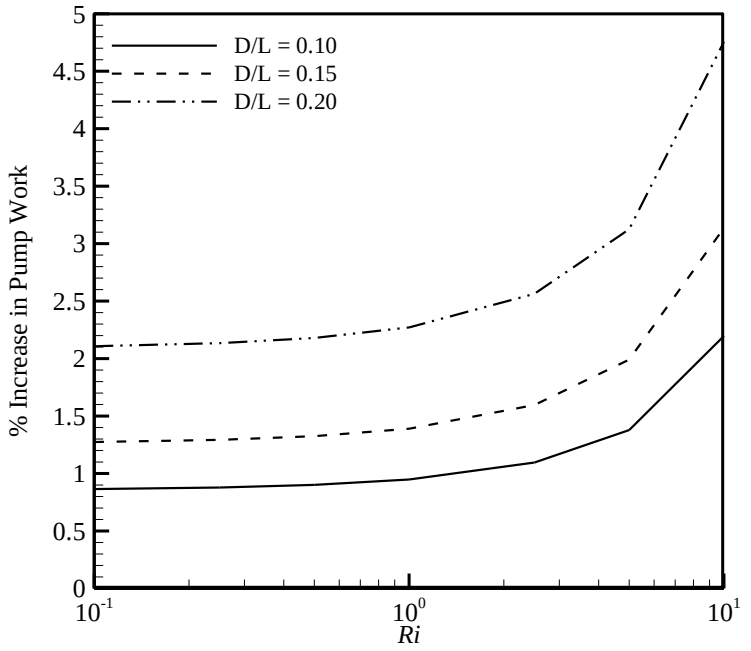

Figure 5.3.15: Variation of % increase of pumping work with Richardson No. (*Ri*) for different sizes of rotating cylinder (ξ = 1.0; X_c = 0.8; Y_c = 0.25) at *Re* = 10.

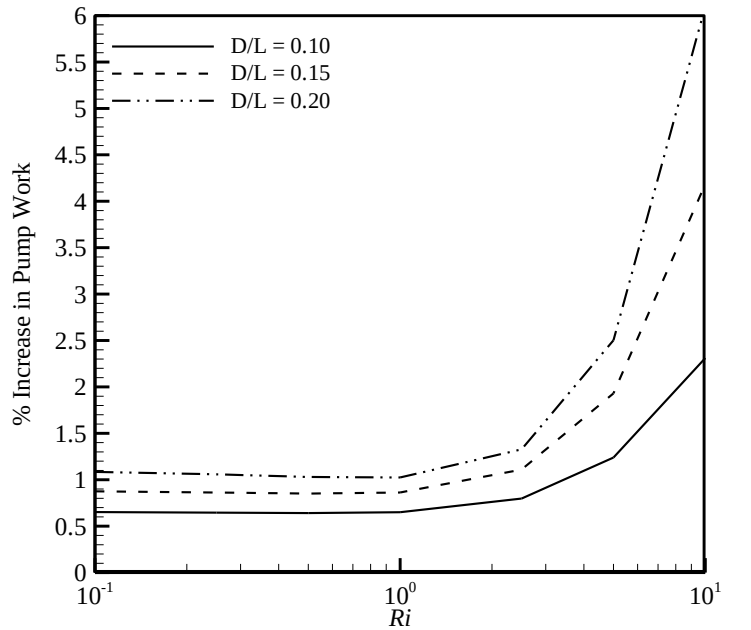

Figure 5.3.16: Variation of % increase of pumping work with Richardson No. (*Ri*) for different sizes of rotating cylinder (ξ = 1.0; X_c = 0.8; Y_c = 0.25) at *Re* = 100.

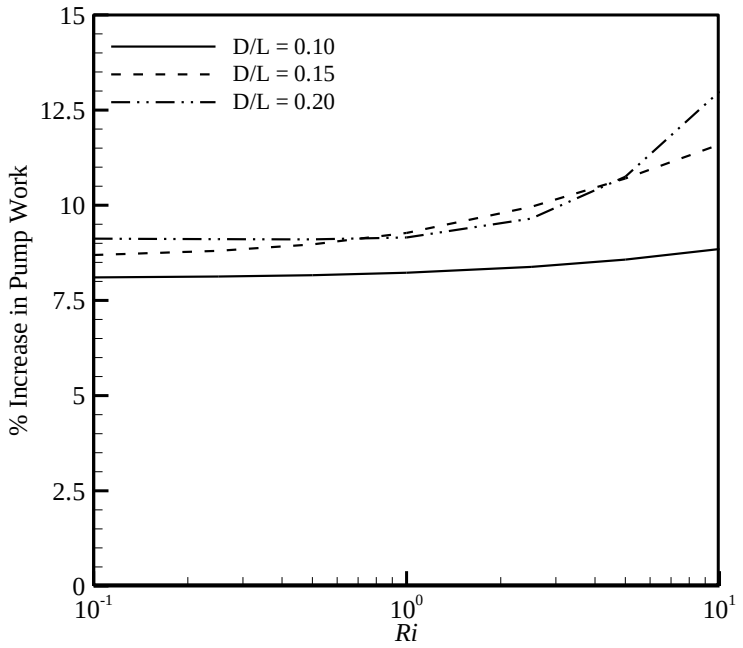

Figure 5.3.17: Variation of % increase of pumping work with Richardson No. (*Ri*) for different sizes of rotating cylinder (ξ = 1.0; X_c = 0.8; Y_c = 0.25) at *Re* = 500.

5.4. Effect of vertical location of the rotational cylinder inside ventilated cavity:

5.4.1. Effect of vertical position of the cylinder on streamlines

The streamline pattern inside a ventilated cavity for different non-dimensional vertical position (Y_c) of the rotating cylinder(ξ = 1.0; X_c = 0.8; D/L = 0.1) at different Richardson number (Ri =0.1, 1 and 10) for different Reynolds number (Re = 10, 100 and 500) are shown in Figure 5.4.1 to Figure 5.4.3.

In Figure 5.4.1, streamline patterns for different Re and different non-dimensional vertical position at Ri = 0.1 is shown. The flow in the ventilated cavity, at Re = 10 and for Y_c = 0.25,is mostly diagonal streamline flow. However, with increasing vertical height distortions in the diagonal flow is visible and for higher vertical positions, a low strength vortex is present which indicates that flow separation occurs for these cases. With increasing height the streamlines gets more distorted around the cylinder. For, Re =100, there is a presence of counter clockwise circulation which is more strong at the center of the vortex for all vertical positions. It is also observed that, for all non-dimensional vertical positions a portion of the streamlines also distorts around the cylinder tangentially which increases with increase in height due to large direct intrusion in the flow path. In this case, the flow is also separating in the bottom and right wall. In case of higher Re (Re = 500), the span of the vortex increases and pushes the streamline flow towards the right sidewall for all non-dimensional vertical positions, though the strength of the vortex minimizes for Y_c = 0.25 and 0.45 and increases for Y_c = 0.65 in the boundary region of the vortex. However, when Y_c = 0.45two small vortices have formed inside the large vortex due to the position of the cylinder and for Y_c = 0.65 the two small vortices seems to merge together due to the influence of the rotating cylinder at this position. Flow separation is also taking place at the bottom right corner for higher vertical positions.

In Figure 5.4.2, streamline patterns for different Re and different non-dimensional vertical positions of the rotating cylinder at Ri = 1 is shown. For Re = 10, the flow in the ventilated cavity is almost same as it was for Ri =0.1. For, Re = 100, like before, there is also a presence of counter clockwise circulation along with fine streamline flow, however the vortex for Y_c = 0.25 and Re = 100 has less strength. From the figure it is evident that flow separation is taking place

for all non-dimensional vertical positions and *Re* = 100 which is an increasing function of the vertical position. In case of higher *Re* (*Re* = 500), similar trend of flow pattern observed that of in case of *Ri* = 0.1 is evident which is, the span of the vortex increases again and pushes the streamline flow towards the bottom right corner of the cavity and when Y_c = 0.45two small vortices have formed inside the large vortex due to the position of the cylinder and for Y_c = 0.65 the two small vortices seems to merge together due to the influence of the rotating cylinder at this position and the cylinder acts as a driving force for the streamline flow and flow separation is also occurring for higher vertical positions.

In Figure 5.4.3, streamline patterns for different *Re* and different vertical positions of the rotating cylinder at *Ri* = 10 is shown. It is evident from the figure that for *Ri* = 10 at low *Re* (*Re* = 10) there is a presence of counterclockwise vortex in the cavity for all non-dimensional vertical positions. The vortex strength increases with higher *Re* and the presence of the cylinder influences the flow field similarly like it did for the cases of lower *Ri*, however for *Re* = 100 the vortices for Y_c = 0.25and 0.65 have more strength in the boundary of the vortex which indicates that at the core of the vortex there is no flow and for Y_c = 0.45the vortex has less strength. At *Re* = 500, for *Ri* = 10 the streamlines follow similar trends as it was for lower *Ri*, however the inertia force of the cylinder is less dominant and flow separation only occurs for Y_c = 0.65.

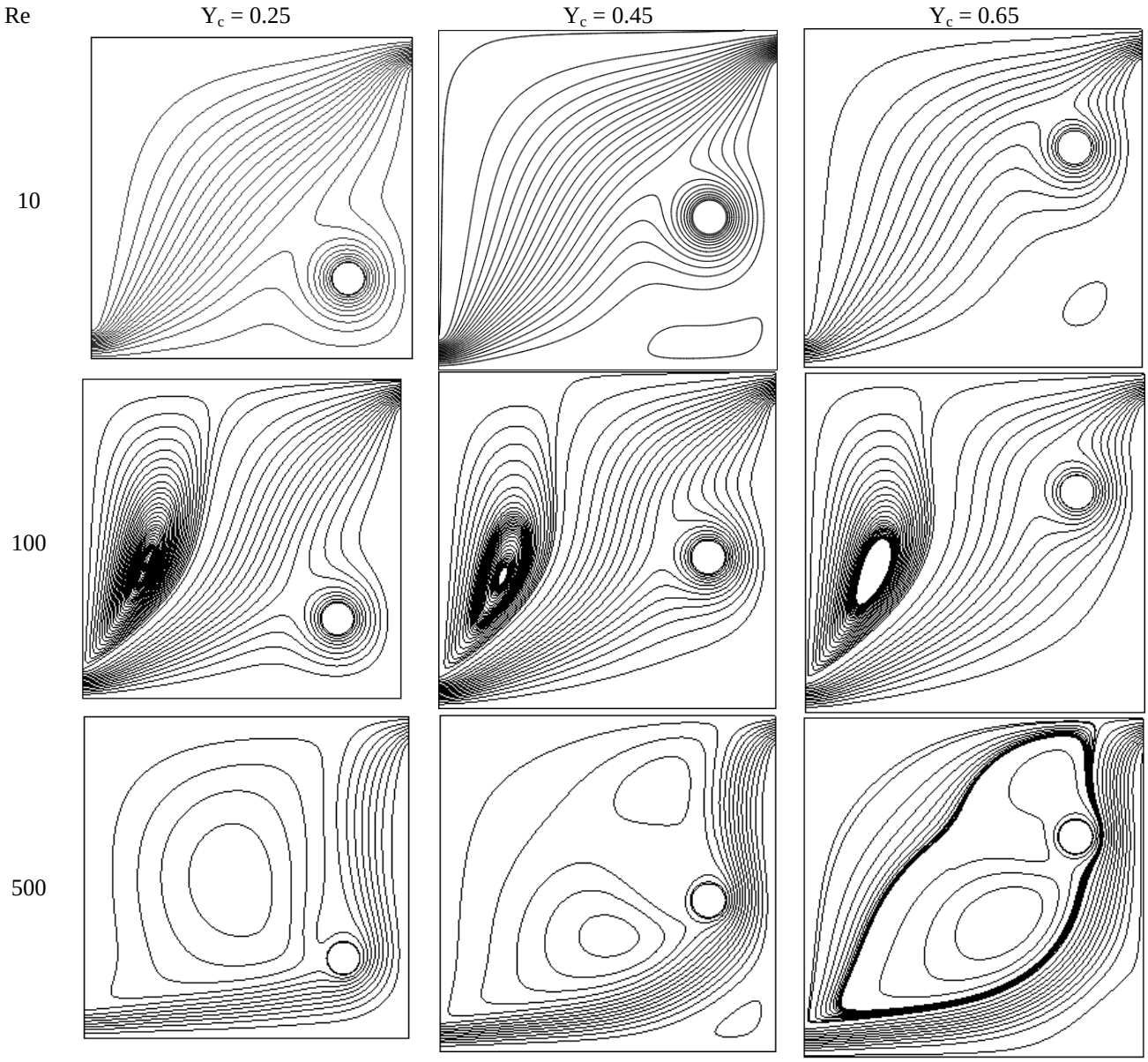

Figure 5.4.1: Streamline distribution inside ventilated cavity for different vertical position of the rotating cylinder (ξ = 1.0; X_c = 0.8; D/L = 0.1) at Ri = 0.1.

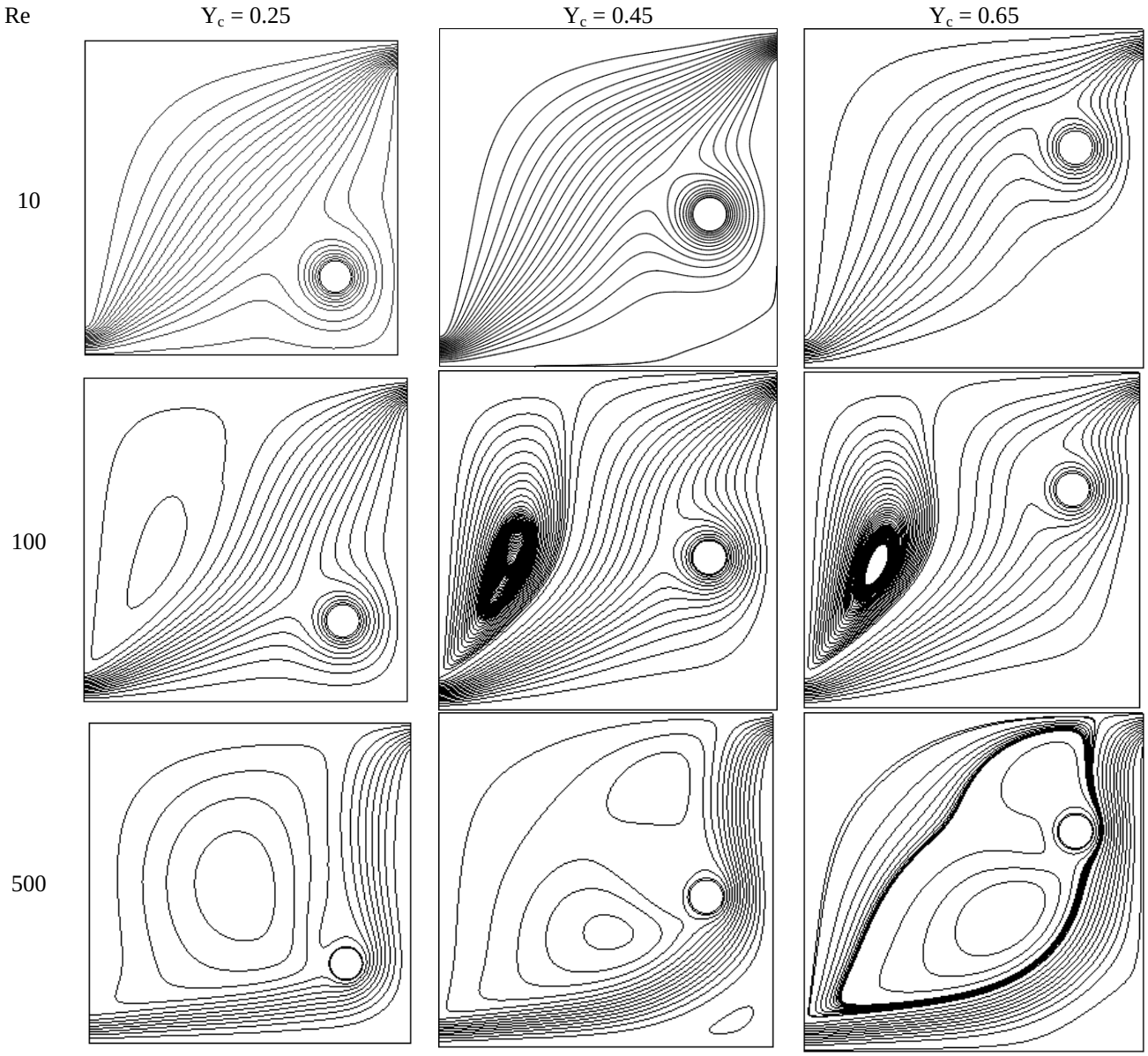

Figure 5.4.2: Streamline distribution inside ventilated cavity for different vertical position of the rotating cylinder (ξ = 1.0; X_c = 0.8; D/L = 0.1) at Ri = 1.0.

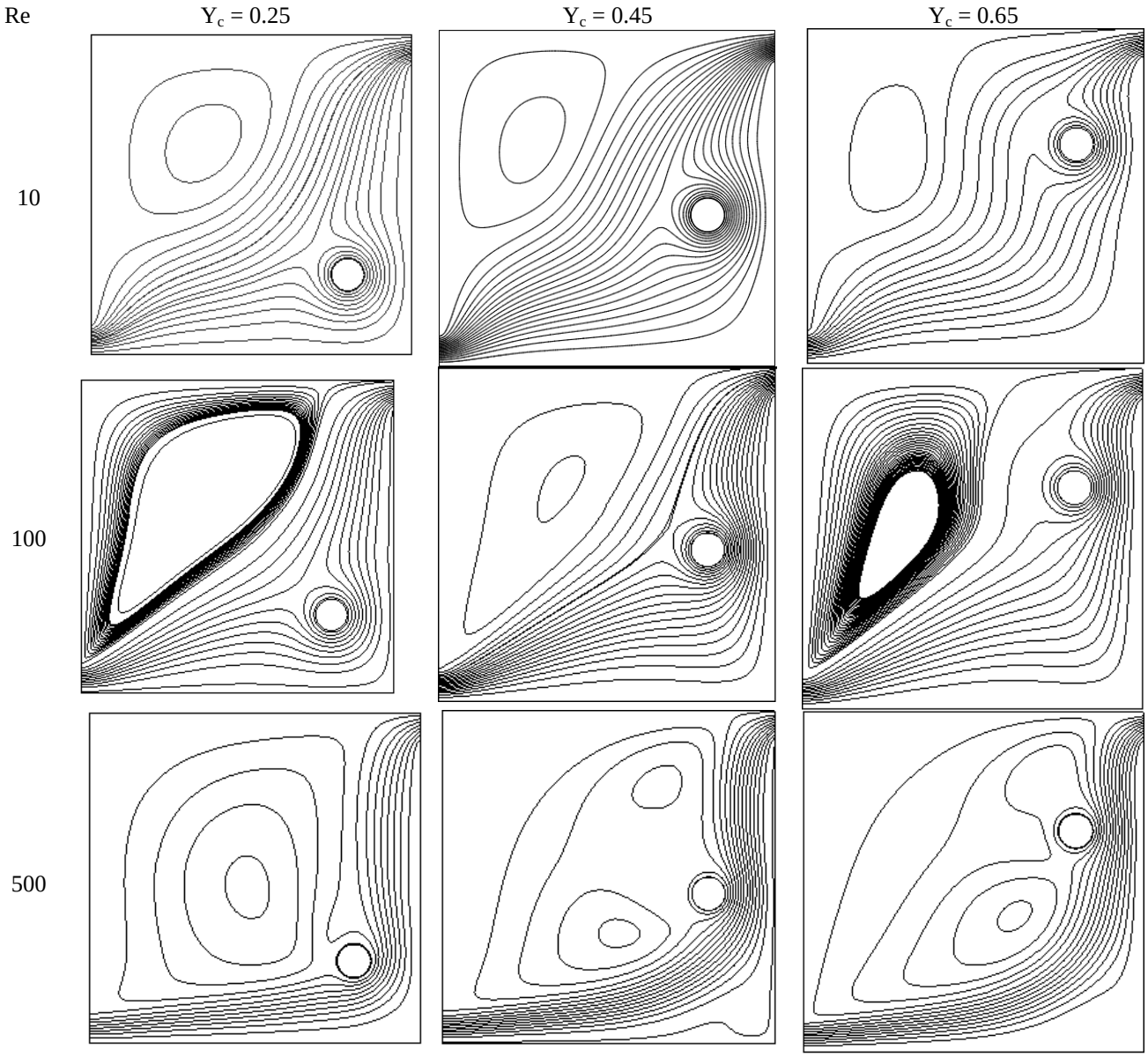

Figure 5.4.3: Streamline distribution inside ventilated cavity for different vertical position of the rotating cylinder (ξ = 1.0; X_c = 0.8; D/L = 0.1) at Ri = 10.0.

5.4.2. Effect of vertical position of the cylinder on isotherm contours

Figure 5.4.4 to Figure 5.4.6 show the isotherm contours inside a ventilated cavity for different non-dimensional vertical positions of the rotating cylinder at different Richardson number (*Ri* =0.1, 1 and 10) for different Reynolds number (*Re* = 10, 100 and 500). In Figure 5.4.4, isotherm contours for different *Re* and non-dimensional vertical positions at *Ri* = 0.1 is shown. It is evident from the Figure 5.4.4 that at *Ri* = 0.1 for low *Re* the isothermal contours are distributed throughout the cavity for all non-dimensional vertical positions. However, with increase in *Re* the isotherms are pushed to the right side of the cavity which indicates that most of the cavity is cold. Due to the presence of rotating cylinder the isotherms near the cylinder distorts where the cylinder is located. For *Re* = 500, the isotherms are more densely distributed near the right hot wall and near the cylinder the isotherms are more dense where in case of Y_c = 0.65the isotherms are more dense starting from the mid-section of the cavity to the cylinder position.

It is evident from the Figure 5.4.5 and 5.4.6 that at *Ri* = 1 and 10 for low *Re* the isothermal contours are distributed throughout the cavity for all non-dimensional vertical positions which is similar to the case of *Ri* = 0.1. Also, similar to *Ri* = 0.1, with increase in *Re* the isotherms are densely distributed in the right side of the cavity which indicates that most of the cavity is cold and the isotherms near the cylinder distorts for all vertical positions of the cylinder. Similarly, for *Re* = 500, the isotherms are also more densely distributed near the right hot wall and for Y_c = 0.45 and 0.65 for *Ri* = 10 a single isotherm line is visible, though the contour has low value, which reaches the left wall which is not visible for all other cases.

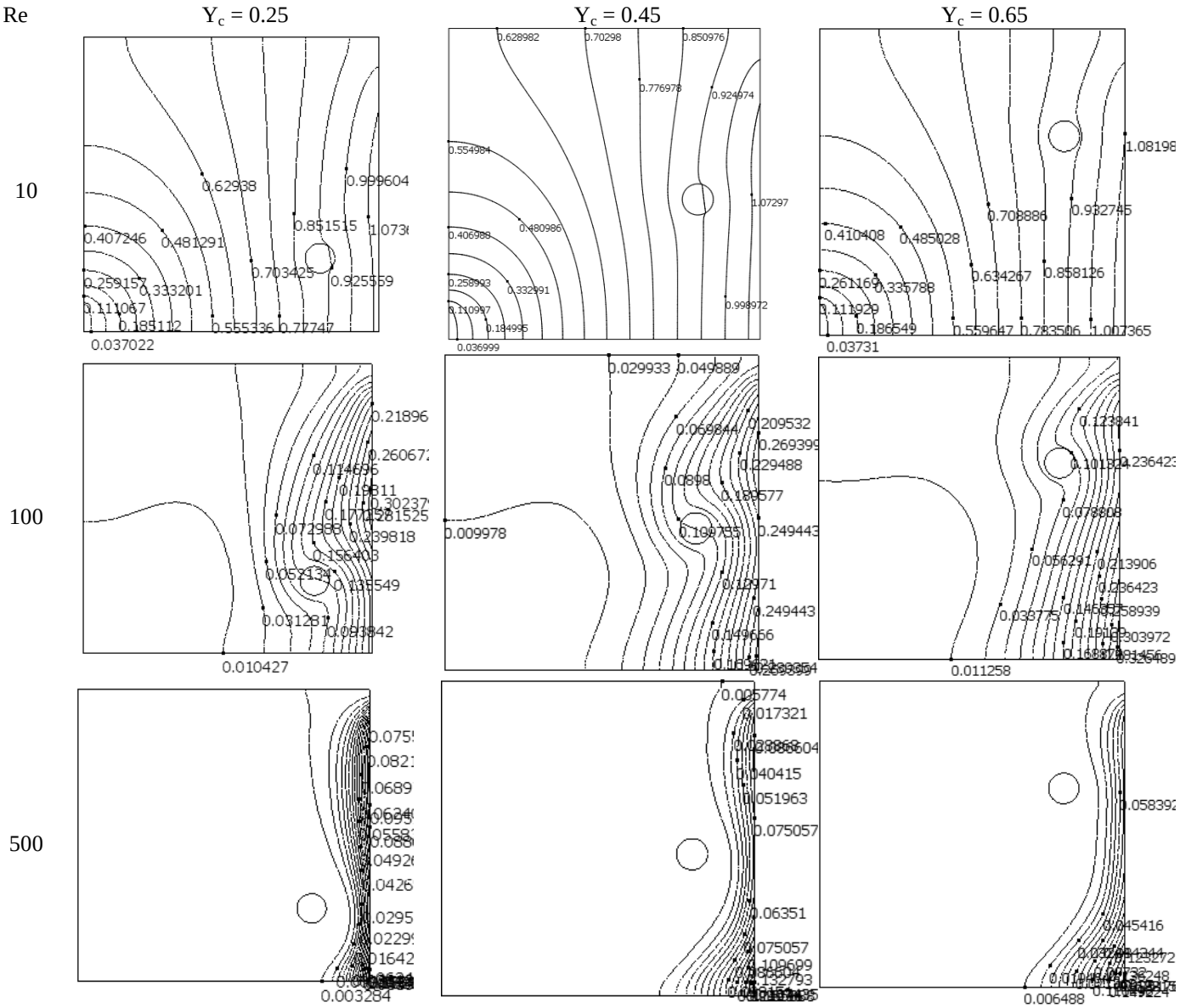

Figure 5.4.4: Thermal field inside ventilated cavity for different vertical position of the rotating cylinder (ξ = 1.0; X_c = 0.8; D/L = 0.1) at Ri = 0.1.

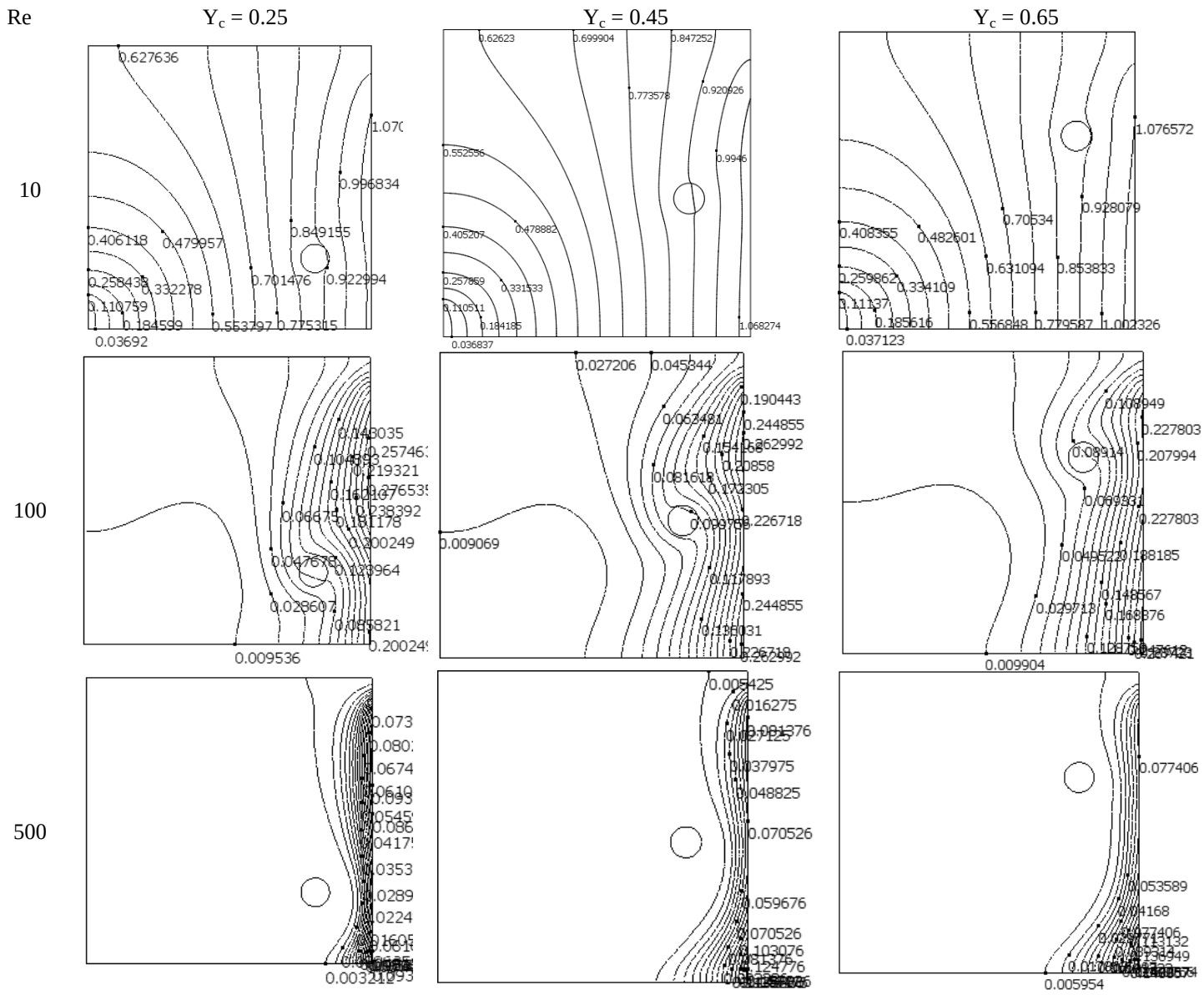

Figure 5.4.5: Thermal field inside ventilated cavity for different vertical position of the rotating cylinder (ξ = 1.0; X_c = 0.8; D/L = 0.1) at Ri = 1.0.

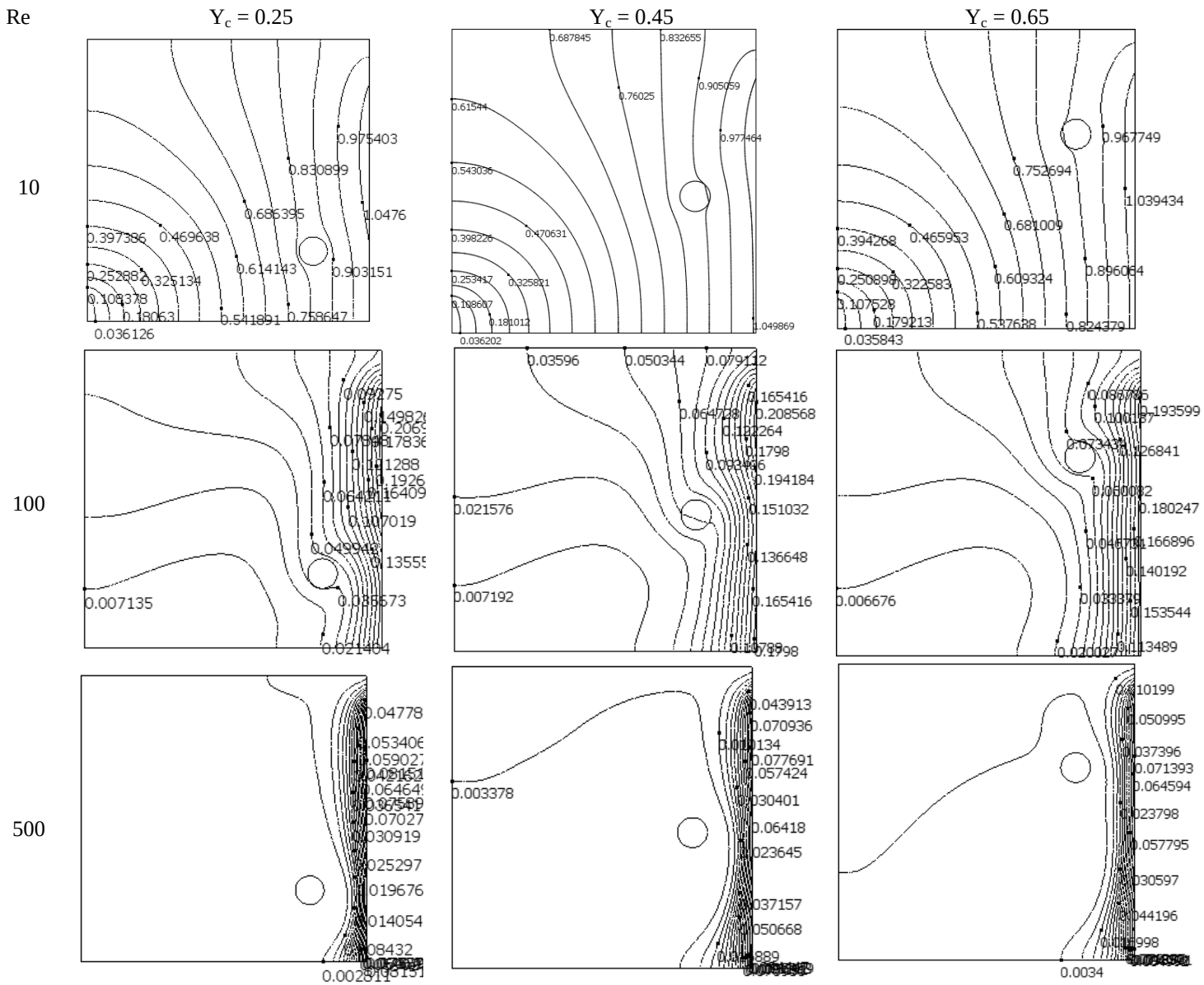

Figure 5.4.6: Thermal field inside ventilated cavity for different vertical position of the rotating cylinder (ξ = 1.0; X_c = 0.8; D/L = 0.1) at Ri = 10.0.

5.4.3. Effect of vertical position of the cylinder on heatlines

Figure 5.4.7 to Figure 5.4.9 show the heat line distribution inside a ventilated cavity for different non-dimensional vertical positions of the rotating cylinder at different Richardson number (*Ri* =0.1, 1 and 10) for different Reynolds number (*Re* = 10, 100 and 500). In Figure 5.4.7, heat line distributions for different *Re* and different vertical positions of the rotating cylinder at *Ri* = 0.1 is shown. The heat lines in the ventilated cavity, for all non-dimensional vertical positions, at *Re* = 10 is mostly diagonal straight lines which indicates that most of the heat flows diagonally, although distortions in the heat flow is visible in the upper triangle of the cavity and near the rotating cylinder for low vertical positions. However, at Y_c = 0.65 the heat flow is more distorted as the rotating cylinder is directly in the path of the heat flow.

For, *Re* =100, there is a presence of counter clockwise circulation whose strength is higher at the core along with finely distributed heat lines from the inlet to the outlet and like before distorted heat lines near the rotating cylinder. It is evident that, the vortices have the maximum strength near its core and flow separation at the right wall is evident for higher non-dimensional vertical positions due to larger inertia forces. In case of higher *Re* (*Re* = 500) the strength of the vortex decreases although the span increases and pushes the heat lines towards the bottom and right sidewalls for Y_c = 0.25 and 0.45. However, the strength of the distorted vortex is higher for Y_c = 0.65 the vortex is strong at its boundary region and for Y_c = 0.45 and 0.65 flow separation at the right hot wall is visible.

In Figure 5.4.8, heat line distributions for different *Re* and different non-dimensional vertical positions of the rotating cylinder at *Ri* = 1 is shown. For *Re* = 10 the flow in the ventilated cavity for all vertical positions is mostly same and flow separation is present which is not the case for *Ri* = 1. For, *Re* =100, like before, there is also a presence of counter clockwise circulation along with finely distributed heat lines except for Y_c = 0.25 the strength of the vortex lower than the others. In case of higher *Re* (*Re* = 500), similar trend of heat flow pattern is observed like that is in case of *Ri* = 0.1 which is, the span of the vortex increases at the cost of its strength and pushes the heat lines towards the bottom and right sidewalls for Y_c = 0.25 and 0.45 and for Y_c = 0.65 the vortex is strong at its boundary also flow separation occurs for Y_c = 0.45 and 0.65.

In Figure 5.4.9, heat line distributions for different *Re* and for different non-dimensional vertical positions of the rotating cylinder at *Ri* = 10 is shown. It is evident from the figure that for *Ri* = 10 at low *Re* (*Re* = 10) there is a presence of counterclockwise vortex in the cavity for all non-dimensional vertical positions which is very much unlikely for lower *Ri*. At *Re* = 100 the strength of the vortex is higher at the outer region for Y_c = 0.25 and higher at the core region for Y_c = 0.65 and for Y_c = 0.45 the vortex has less strength. However, at *Re* = 500 the strength of the vortices for Y_c = 0.25 and 0.65 decreased. However, for Y_c = 0.45 the vortex seemed to be distorted due to the cylinder position and the vortex has higher strength at the core though the boundary of the vortex is also bounding another region in where there seem to be no heat flow is occurring. No flow separation is taking place for this case.

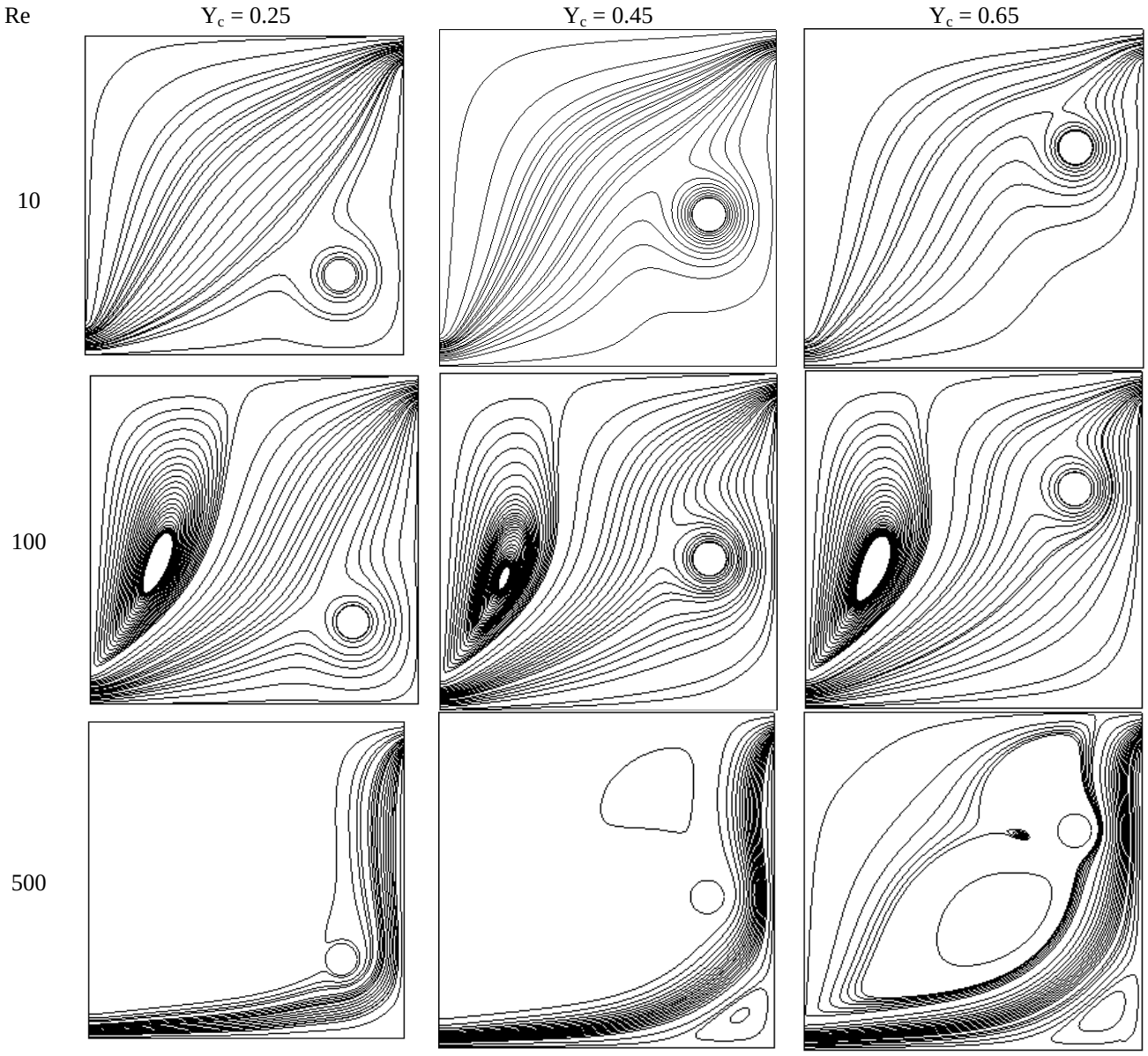

Figure 5.4.7: Heat lines inside ventilated cavity for different vertical position of the rotating cylinder (ξ = 1.0; X_c = 0.8; D/L = 0.1) at Ri = 0.1.

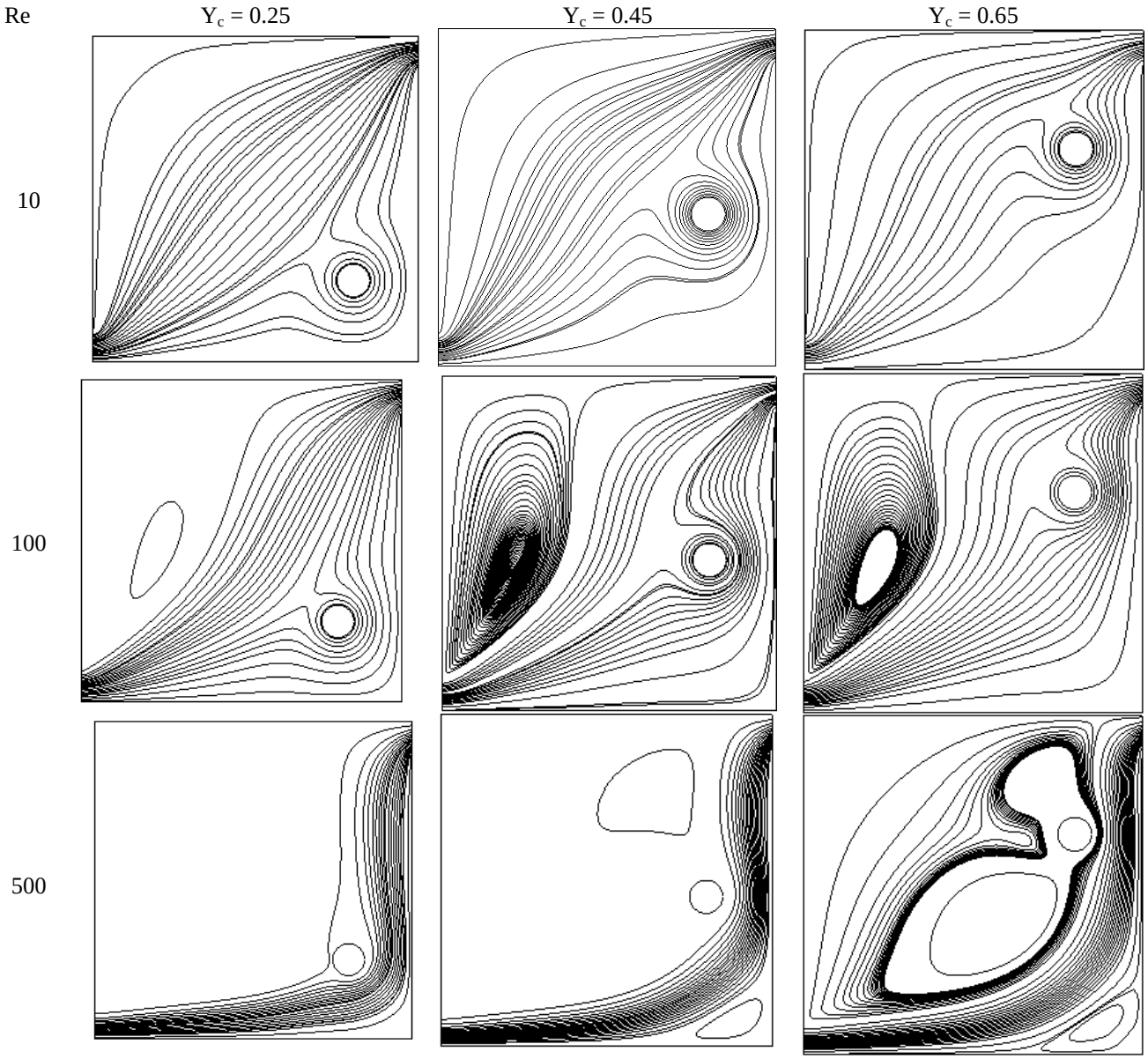

Figure 5.4.8: Heat lines inside ventilated cavity for different vertical position of the rotating cylinder (ξ = 1.0; X_c = 0.8; D/L = 0.1) at Ri = 1.0.

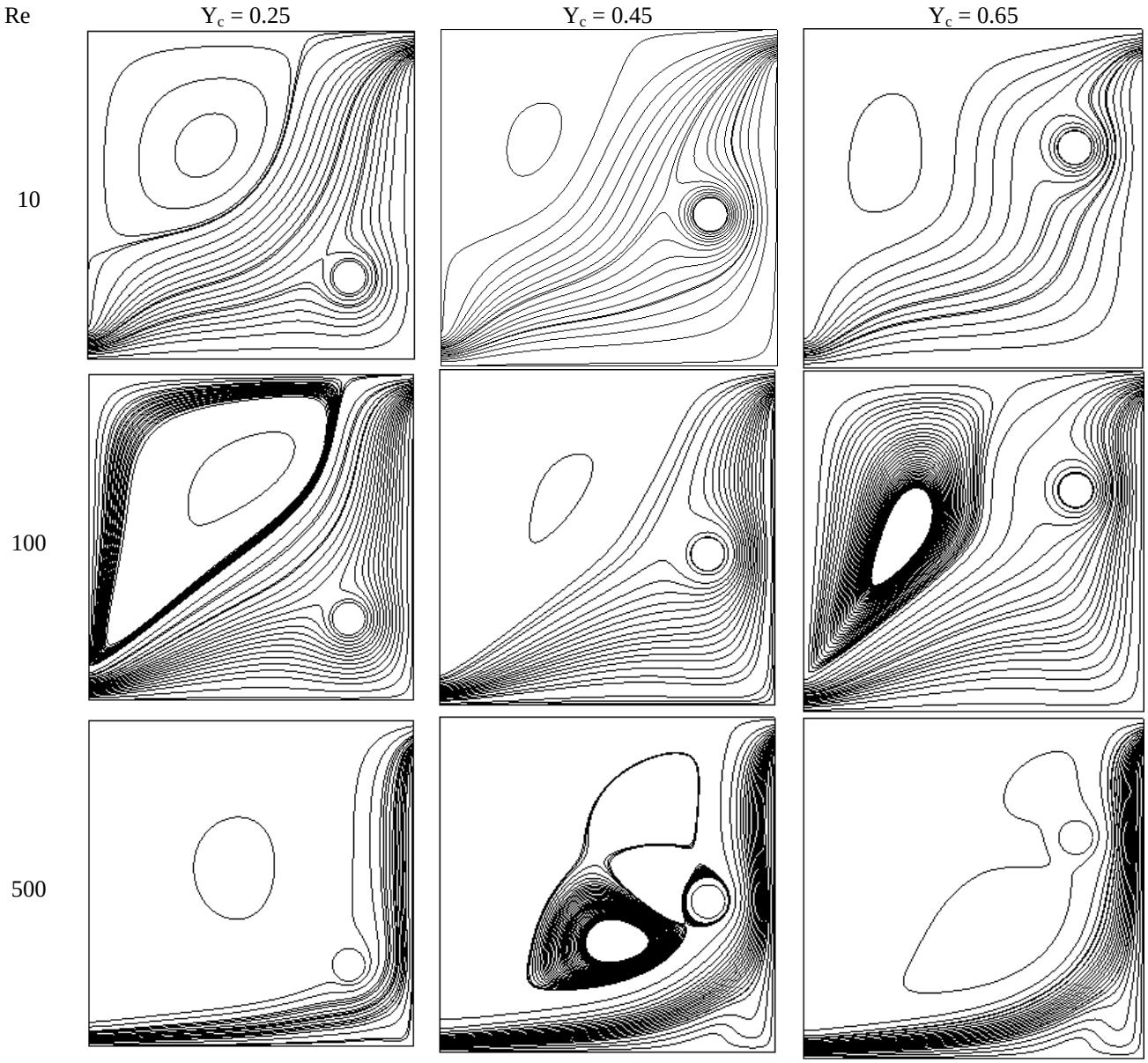

Figure 5.4.9: Heat lines inside ventilated cavity for different vertical position of the rotating cylinder (ξ = 1.0; X_c = 0.8; D/L = 0.1) at Ri = 10.0.

5.4.4. Effect of vertical position of the cylinder on the heat transfer rate

Figure 5.4.10 shows the variation of normalized heat transfer rate at *Re* = 10 with different Richardson number for different non-dimensional vertical positions. It is obvious from the figure that for all non-dimensional vertical positions the heat transfer rate at this *Re* is slightly better than when there is no cylinder and for all the positions the heat transfer rate is similar. However, there is variation of the heat transfer rate with variation in *Ri* .The heat transfer rate decreased from that of when there is no cylinder for all non-dimensional vertical positions for higher *Ri*.

Figure 5.4.11 shows the variation of normalized heat transfer rate at *Re* = 50 with different Richardson number for different non-dimensional vertical positions. From the figure it is obvious that when the Y_c = 0.25 the heat transfer rate is lower than when there is no cylinder in the cavity for all *Ri*, although there is a variation for different *Ri*. At Y_c = 0.45 and 0.65 there is higher heat transfer rate than when there is no cylinder for lower *Ri* and for with increasing *Ri* the heat transfer rate decreased and after reaching a lowest value at about *Ri* = 5 it again increases. The highest heat transfer rate is found for both the cases at *Ri* = 0.10.

Figure 5.4.12 shows the variation of normalized heat transfer rate at *Re* = 100 with different Richardson number for different non-dimensional vertical positions. It is obvious from the figure that for all vertical positions the heat transfer is better than when there is no cylinder for all *Ri* though there is variation of heat transfer rate with increasing *Ri*. The highest heat transfer rate is found at about *Ri* = 0.1 when Y_c = 0.25 at this *Re.*

Figure 5.4.13 shows the variation of normalized heat transfer rate at *Re* = 10 with different Richardson number for different non-dimensional vertical positions. It is obvious from the figure that for all non-dimensional vertical positions the heat transfer rate is better for all *Ri*. However, at this *Re* the highest heat transfer rate is also evident at *Ri* = 0.1 when the Y_c = 0.25.

Figure 5.4.14 shows the variation of normalized heat transfer rate at *Re* = 10 with different Richardson number for different non-dimensional vertical positions. It is obvious from the figure that at this *Re* for all non-dimensional vertical positions the heat transfer rate is better and the highest value is also found at *Ri* = 0.1 for Y_c = 0.25.

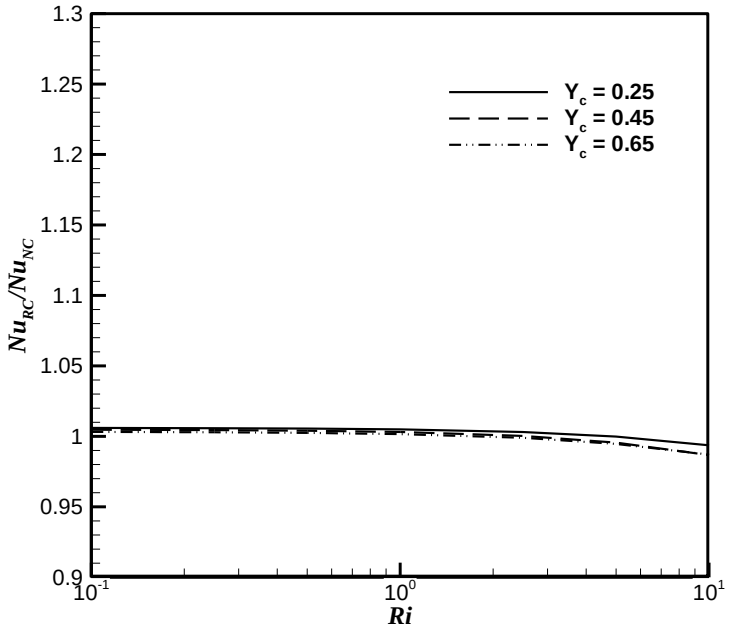

Figure 5.4.10: Normalized Nusselt No. variation with Richardson No. (*Ri*) for different non-dimensional vertical position of the rotating cylinder (ξ = 1.0; X_c = 0.8; D/L = 0.1) at *Re* = 10

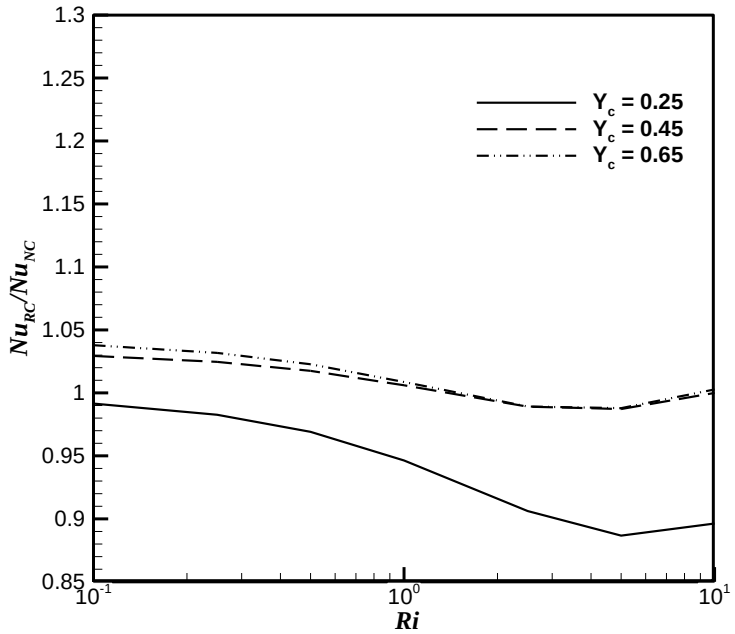

Figure 5.4.11: Normalized Nusselt No. variation with Richardson No. (*Ri*) for different non-dimensional vertical position of the rotating cylinder (ξ = 1.0; X_c = 0.8; D/L = 0.1) at *Re* = 50

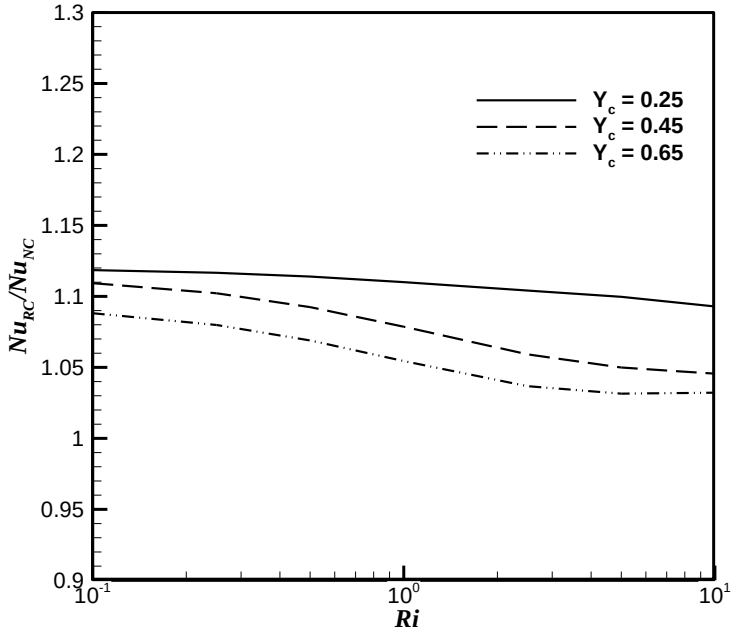

Figure 5.4.12: Normalized Nusselt No. variation with Richardson No. (*Ri*) for different non-dimensional vertical position of the rotating cylinder (ξ = 1.0; X_c = 0.8; D/L = 0.1) at *Re* = 100

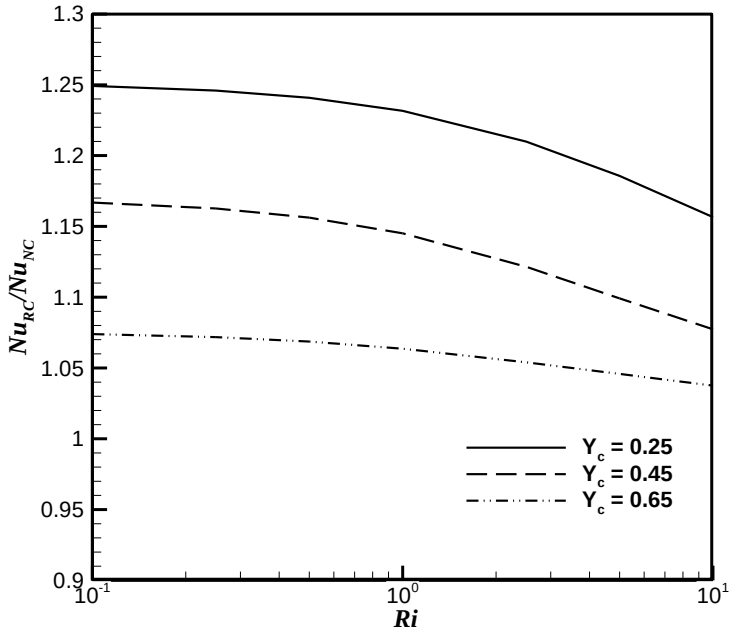

Figure 5.4.13 Normalized Nusselt No. variation with Richardson No. (*Ri*) for different non-dimensional vertical position of the rotating cylinder (ξ = 1.0; X_c = 0.8; D/L = 0.1) at *Re* = 250

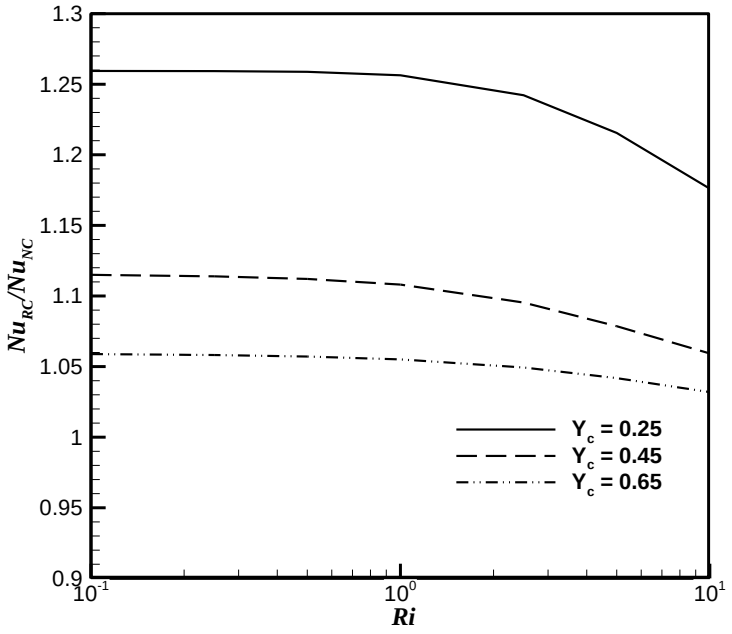

Figure 5.4.14: Normalized Nusselt No. variation with Richardson No. (*Ri*) for different non-dimensional vertical position of the rotating cylinder (ξ = 1.0; X_c = 0.8; D/L = 0.1) at *Re* = 500

Chapter 6: Conclusions and Recommendations

6.1. Conclusions

Numerical Study of mixed convection heat transfer in a ventilated square enclosure in presence of a rotating heat conducting cylinder has been performed in this analysis. In the analysis the Prandtl number of the fluid inside the cavity was fixed at 0.7 for all cases. The focus of this study is to show the effect physical and geometric parameters like diameter of the cylinder, speed ratio of the cylinder, vertical position of the cylinder on the flow field, temperature field, heat flow path and heat transfer rate. The temperature field, flow field and heat flow process visualization has been made by streamlines, isotherm lines and heatlines respectively. The heat transfer rate is analyzed in terms of normalized average Nusselt number over the heat transfer for different Richardson number and Reynolds number. From the analysis the following conclusion can be drawn:

1. The presence of the cylinder affects the heat transfer rate. When the cylinder is stationary the heat transfer rate decreases for all the cases except for when Re = 500 and the presence of rotating cylinder enhances the heat transfer rate for all Re conducted in the preset study.
2. The speed ratio of the rotating cylinder has a very strong effect on the heat transfer rate. At higher Re the heat transfer rate decreases with increasing speed ratio. Though heat transfer rate decreases with increasing Ri, the heat transfer rate is still higher than when there is no cylinder for higher Re. However, speed ratio of 1 produces the highest heat transfer rate at Ri = 0.1.
3. The variation of cylinder diameter affects the heat transfer performance significantly. The heat transfer rate increases with increasing Re; however, with increasing Ri the heat transfer rate decreases for all diameters of the cylinder. For small diameters of the cylinder higher heat transfer rate is observed with increasing Re. However, at low Re (Re = 10) larger diameter of the cylinder shows better performance than smaller diameter cylinders.

4. The variation of the cylinder vertical position affects the heat transfer similarly. With increase in the vertical height of the cylinder the heat transfer rate is found less than that is found in case of low vertical height. Except for the case when Re = 50, the heat transfer rate is better for Y_c = 0.25 for all other Re and Ri than the other positions.
5. With the increase of the diameter of the cylinder the pumping work also increases which is not desired as there is no significant change in performance with the variation of diameter of the cylinder. However, highest heat transfer rate is achieved at Ri = 0.1 and for D/L = 0.2;ξ = 1.0; X_c = 0.8; Y_c = 0.25 at the expense of about 7.85% increase of pumping work at Re = 500 which corresponds to the normalized Nusselt number of 1.26.

6.2. Recommendations

The analysis has a lot of potentials to be successively used in many heat transfer related problem. Hence it is imperative to carry the analysis further to get the full insight of the study. There are some recommendations in this regards as given below:

1. The study is based on the assumption of laminar flow regime which is not practical in many cases. So the analysis can be done for turbulent flow condition.
2. The analysis is also done for steady state which can be extended for unsteady case.
3. The analysis can also be done for different thermal and velocity boundary conditions.
4. Investigation of effect of various physical fields like magnetic field can also be carried out.
5. More ever any numerical investigation is incomplete without experimental verification. So the verification of the present study can be done by experimental testing of the study.

Bibliography

1. Lewis, R. W., Nithiarasu, P., and Seetharamu, K. N. Fundamentals of the Finite Element Method for Heat and Fluid Flow, 2004.
2. Cengel, Y. A., Ghajar, A. J., and Ma, H. (2011). *Heat and Mass Transfer: Fundamentals and Applications, 4e*. McGraw-Hill.
3. Munson, B. R., Young, D. F., and Okiishi, T. H. (1990). Fundamentals of fluid mechanics. *New York*, *3*, 4.
4. Çengel, Y. A., and Boles, M. A. (2015). *Thermodynamics: an engineering approach*. M. Kanoğlu (Ed.). McGraw-Hill Education.
5. Incropera, F., and DeWitt, D. (1985). Introduction to heat transfer.
6. Potter, M. C., and Somerton, C. W. (1993). *Schaum's outline of theory and problems of thermodynamics for engineers*. McGraw-Hill.
7. Falkovich, G. (2011). *Fluid mechanics: A short course for physicists*. Cambridge University Press.
8. Joye, D. D., Bushinsky, J. P., and Saylor, P. E. (1989). Mixed convection heat transfer at high Grashof number in a vertical tube. *Industrial and engineering chemistry research*, *28*(12), 1899-1903.
9. Kim, B. S., Lee, D. S., Ha, M. Y., and Yoon, H. S. (2008). A numerical study of natural convection in a square enclosure with a circular cylinder at different vertical locations. *International Journal of Heat and Mass Transfer*, *51*(7), 1888-1906.
10. Aminossadati, S. M., and Ghasemi, B. (2009). Natural convection cooling of a localized heat source at the bottom of a nanofluid-filled enclosure. *European Journal of Mechanics-B/Fluids*, *28*(5), 630-640.
11. Roslan, R., Saleh, H., Hashim, I., and Bataineh, A. S. (2014). Natural convection in an enclosure containing a sinusoidally heated cylindrical source. *International Journal of Heat and Mass Transfer*, *70*, 119-127.
12. Basak, T., Roy, S., Paul, T., and Pop, I. (2006). Natural convection in a square cavity filled with a porous medium: effects of various thermal boundary conditions. *International Journal of Heat and Mass Transfer*, *49*(7), 1430-1441.

13. Basak, T., Roy, S., Sharma, P. K., and Pop, I. (2009). Analysis of mixed convection flows within a square cavity with linearly heated side wall (s). *International Journal of Heat and Mass Transfer*, *52*(9), 2224-2242.
14. Oztop, H. F., and Dagtekin, I. (2004). Mixed convection in two-sided lid-driven differentially heated square cavity. *International journal of heat and mass transfer*, *47*(8), 1761-1769.
15. Moallemi, M. K., and Jang, K. S. (1992). Prandtl number effects on laminar mixed convection heat transfer in a lid-driven cavity. *International Journal of Heat and Mass Transfer*, *35*(8), 1881-1892.
16. Aydin, O. and Yang, W. J. (2000). Mixed convection in cavities with a locally heated lower wall and moving sidewalls. *Numerical Heat Transfer: Part A: Applications*, *37*(7), 695-710.
17. Guo, G., and Sharif, M. A. (2004). Mixed convection in rectangular cavities at various aspect ratios with moving isothermal sidewalls and constant flux heat source on the bottom wall. *International journal of thermal sciences*, *43*(5), 465-475.
18. Billah, M. M., Rahman, M. M., Saidur, R., and Hasanuzzaman, M. (2011). Simulation of mhd mixed convection heat transfer enhancement in a double lid-driven obstructed enclosure. *International Journal of Mechanical and Materials Engineering*, *6*(1), 18-30.
19. Bahlaoui, A., Raji, A., Hasnaoui, M., and Naïmi, M. (2016). Mixed Convection Heat Transfer Enhancement in a Vented Cavity Filled with a Nanofluid. *Journal of Applied Fluid Mechanics*, *9*(2).
20. Saedodin, S., Biglari, M., Esfe, M. H., and Noroozi, M. J. (2013). Mixed convection heat transfer performance in a ventilated inclined cavity containing heated blocks: effect of dispersing Al2O3 in water and aspect ratio of the block. *Journal of Computational and Theoretical Nanoscience*, *10*(11), 2663-2675.
21. Mehrizi, A. A., Farhadi, M., Afroozi, H. H., Sedighi, K., and Darz, A. R. (2012). Mixed convection heat transfer in a ventilated cavity with hot obstacle: effect of nanofluid and outlet port location. *International Communications in Heat and Mass Transfer*, *39*(7), 1000-1008.

22. Esfe, M. H., Niazi, S., Esforjani, S. S. M., and Akbari, M. (2014). Mixed convection flow and heat transfer in a ventilated inclined cavity containing hot obstacles subjected to a nanofluid. *Heat Transfer Research*, *45*(4).
23. Saha, S., Mamun, A. H., Hossain, M. Z., and Islam, A. K. M. S. (2008). Mixed convection in an enclosure with different inlet and exit configurations. *Journal of Applied Fluid Mechanics*, *1*(1), 78-93.
24. Raji, A., Hasnaoui, M., and Bahlaoui, A. (2008). Numerical study of natural convection dominated heat transfer in a ventilated cavity: Case of forced flow playing simultaneous assisting and opposing roles. *International Journal of Heat and Fluid Flow*, *29*(4), 1174-1181.
25. Mamun, M. A. H., Rahman, M. M., Billah, M. M., and Saidur, R. (2010). A numerical study on the effect of a heated hollow cylinder on mixed convection in a ventilated cavity. *International Communications in Heat and Mass Transfer*, *37*(9), 1326-1334.
26. Hinojosa, J. F., Rodríguez, N. A., and Xamán, J. (2016). Heat transfer and airflow study of turbulent mixed convection in a ventilated cavity. *Journal of Building Physics*, *40*(3), 204-234.
27. Doghmi, H., Abourida, B., Aelarche, I., Sannad, M., and Ouzaouit, M. Effect of the inlet opening on mixed convection inside a three-dimensional ventilated cavity.
28. Chamkha, A. J., Hussain, S. H., and Abd-Amer, Q. R. (2011). Mixed convection heat transfer of air inside a square vented cavity with a heated horizontal square cylinder. *Numerical Heat Transfer, Part A: Applications*, *59*(1), 58-79.
29. ElGhnam, R. I., Abdelaziz, R. A., Sakr, M. H., and Abdelrhman, H. E. (2012). An experimental study of freezing and melting of water inside spherical capsules used in thermal energy storage systems. *Ain Shams Engineering Journal*, *3*(1), 33-48.
30. Alam, M., Kamruzzaman, Ahsan, F., and Hasan, M. N. (2016, July). Mixed convection heat transfer inside a differentially heated square enclosure in presence of a rotating heat conducting cylinder. In *AIP Conference Proceedings* (Vol. 1754, No. 1, p. 050035). AIP Publishing.
31. Karimi, F., Xu, H., Wang, Z., Yang, M., and Zhang, Y. (2016). Numerical Simulation of Steady Mixed Convection around Two Heated Circular Cylinders in a Square Enclosure. *Heat Transfer Engineering*, *37*(1), 64-75.

32. Selimefendigil, F., and Öztop, H. F. (2014). Estimation of the mixed convection heat transfer of a rotating cylinder in a vented cavity subjected to nanofluid by using generalized neural networks. *Numerical Heat Transfer, Part A: Applications*, *65*(2), 165-185.

33. Costa, V. A. F., and Raimundo, A. M. (2010). Steady mixed convection in a differentially heated square enclosure with an active rotating circular cylinder. *International Journal of Heat and Mass Transfer*, *53*(5), 1208-1219.

34. Gupta, S. K., Chatterjee, D., and Mondal, B. (2015). Investigation of mixed convection in a ventilated cavity in the presence of a heat conducting circular cylinder. *Numerical Heat Transfer, Part A: Applications*, *67*(1), 52-74.

35. Hussain, S. H., and Hussein, A. K. (2011). Mixed convection heat transfer in a differentially heated square enclosure with a conductive rotating circular cylinder at different vertical locations. *International Communications in Heat and Mass Transfer*, *38*(2), 263-274.

36. Liao, C. C., and Lin, C. A. (2014). Mixed convection of a heated rotating cylinder in a square enclosure. *International Journal of Heat and Mass Transfer*, *72*, 9-22.

37. Ghaddar, N. K., and Thiele, F. (1994). Natural convection over a rotating cylindrical heat source in a rectangular enclosure. *Numerical Heat Transfer*, *26*(6), 701-717.